



TECHNISCHE UNIVERSITÄT MÜNCHEN

LEHRSTUHL FÜR ANALYTISCHE CHEMIE UND WASSERCHEMIE

INSTITUT FÜR KLINISCHE CHEMIE UND PATHOBIOCHEMIE

**Nanodiscs incorporating functional human beta-1 adrenergic
receptors as novel diagnostic approach for autoimmune dilated
cardiomyopathy**

Ruoyu Sun

Vollständiger Abdruck der von der Fakultät für Chemie der Technischen Universität München zur Erlangung des akademischen Grades eines

Doktors der Naturwissenschaften (Dr. rer. nat.)

genehmigten Dissertation.

Vorsitzender: Prof. Dr. Franz Hagn
Prüfer der Dissertation: 1. Prof. Dr. Reinhard Nießner
2. apl. Prof. Dr. Peter B. Lippa

Die Dissertation wurde am 08.03.2018 bei der Technischen Universität München eingereicht und durch die Fakultät für Chemie am 12.04.2018 angenommen.

Teile der vorliegenden Arbeit wurden bereits veröffentlicht unter:

Mak, S., Sun, R., Schmalenberg, M., Peters, C., & Lippa, P. B. (2017). Express incorporation of membrane proteins from various human cell types into phospholipid bilayer nanodiscs. *Biochem J*, 474(8), 1361-1371.

For my beloved parents and husband.

For your unconditional love and support, at all times.

I'm working on myself,

by myself,

for myself.

“In the midst of chaos, there is also opportunity.”

— Sun Tzu

Acknowledgement

Firstly, I would like to express my special appreciation and thanks to my advisor Prof. Dr. Luppá for the opportunity to join his research group and for his continuous support during the last three years. I want to thank him for the freedom he gave me to create and implement new ideas, for his immense knowledge, patience and motivation which encouraged my research and guided me to grow as a scientist. At the same time, I really appreciate his engagement to create a great working atmosphere. I really enjoyed our Christmas dinners, go-kart racings, jokes, funny facts and cartoons. I could not have imagined having a better advisor and mentor for my PhD study.

I also want to thank my advisor Prof. Dr. Nießner whole-hearted for his insightful comments and encouragement, but also for the hard questions which incited me to widen my research from various perspectives.

My PhD project couldn't have been done without my collaboration partners and institutes, here I want to thank Prof. Dr. Boege at the Central Institute of Clinical Chemistry and Laboratory Medicine, University of Düsseldorf, and his co-worker Birgit Hanzen for recruitment of heart failure patients as well as the intensive discussion about the autoimmune aspect of the disease. I would like to thank Prof. Dr. Schimke of Berlin Cures GmbH, and Dr. Wenzel for discussing and demonstrating the cardiomyocyte contraction assay.

Big thanks goes to our group leaders who survived me in the last three years: Dr. Alexander LeBlanc, Dr. Michael Schmalenberg and Dr. Andreas Poschenrieder, for initializing the nanodisc project, for their knowledge and patience in countless discussions and their ability to motivate me in every difficult stage of my project.

I also want to thank our "real doctors" Dr. med. Andreas Bietenbeck, Dr. med. Markus Thaler and Dr. med. Christof Winter for giving patient explanations of medical aspects during my whole PhD study, especially Dr. med. Andreas Bietenbeck who helped me a lot finding the red thread in the midst of data chaos.

Without the excellent support of our lab assistants Anita Schreiegg and Christine Grubmüller in all kinds of lab works, this thesis couldn't be done or will take at least another three years.

Special thanks to my lab mates Stefanie Mak, Christine Schönmann, Christopher Beaudoin, Janine Potreck, Dr. Heike Bittersohl and my undergrad student Stefanie Reisenauer for the great atmosphere, stimulating discussions and for being my healthy donors in the early stage of the assay

optimization. For all the fun we have had in the last three years, I will never forget all the birthday parties, BBQ, movie nights, creative baking experiments and conversation about everything, weird things among others. Special thanks go to Michael and Steffi for your patient proofreading and fruitful discussions, now we are finally done.

I also want to thank all colleagues at the Institute of Clinical Chemistry and Pathobiochemistry, TUM, especially the members of research groups of Prof. Dr. Ruland and of Prof. Dr. Groß for the shareconomy of lab equipments and scientific exchanges and discussions.

Special thanks to my parents Xiaoguang Yu and Guowang Sun, my friends, as well as all the members of my big family and my family-in-law. Words cannot express how grateful I am to have you always by my side and your support in every decision I made. I am always thankful that you never forget to show me all the other perspectives of this beautiful life. I also want to thank my beloved husband Dr. rer. nat. Mathias Hackl, for every second we spent, laughed and cried together, for all the nice places we have seen through each other's eyes, for all the countless hours talking about work, life, politic, literature and of course, for your unconditional love.

Eidesstattliche Erklärung

Ich erkläre hiermit ehrenwörtlich, dass ich die vorliegende Arbeit selbständig angefertigt habe. Die aus fremden Quellen direkt und indirekt übernommenen Gedanken sind als solche kenntlich gemacht. Ich weiß, dass die Arbeit in digitalisierter Form daraufhin überprüft werden kann, ob unerlaubte Hilfsmittel verwendet wurden und ob es sich – insgesamt oder in Teilen – um ein Plagiat handelt. Zum Vergleich meiner Arbeit mit existierenden Quellen darf sie in eine Datenbank eingestellt werden und nach der Überprüfung zum Vergleich mit künftig eingehenden Arbeiten dort verbleiben. Weitere Vervielfältigungs- und Verwertungsrechte werden dadurch nicht eingeräumt. Die Arbeit wurde weder einer anderen Prüfungsbehörde vorgelegt noch veröffentlicht.

Ort, Datum

Unterschrift

Table of contents

Table of contents.....	i
Abbreviations	iv
Figure index.....	vii
Table index	ix
1. Abstract	1
2. Zusammenfassung.....	3
3. Introduction	5
3.1. Dilated cardiomyopathy	5
3.1.1. DCM induced by AAB against beta-1 adrenergic receptor	6
3.2. Beta-1 adrenergic receptor	8
3.2.1. Signaling	9
3.2.2. Structure.....	10
3.3. Nanodisc technology	13
3.3.1. Structure of nanodiscs.....	14
3.3.2. Generation of nanodiscs	15
3.3.3. Applications of nanodisc technology	16
3.4. Aim of the thesis	18
4. Experimental Section	19
4.1. Materials	19
4.1.1. Chemicals	19
4.1.2. Buffers, media and solutions.....	20
4.1.3. Antibodies	23
4.1.4. Cultured human cell lines.....	23
4.1.5. Kits.....	24
4.1.6. Consumables	24
4.1.7. Instruments	24

4.1.8.	Software	25
4.2.	Methods	26
4.2.1.	Determination of protein concentration	26
4.2.2.	Cell culture	26
4.2.2.1.	Splitting and counting	27
4.2.2.2.	Harvest and lysis.....	27
4.2.3.	Isolation of cell membrane using Dounce homogenization.....	27
4.2.4.	Nanodisc generation	28
4.2.5.	Size exclusion chromatography.....	28
4.2.6.	Pull-down experiments	28
4.2.6.1.	Alprenolol Magnetic Beads	28
4.2.6.2.	GFP-Trap Magnetic Beads	29
4.2.6.3.	Co-Immunoprecipitation using GFP-Trap Magnetic Beads.....	29
4.2.7.	SDS-PAGE and Western Blot	30
4.2.8.	Enzyme-linked immunosorbent assay.....	30
4.2.9.	Surface plasmon resonance spectroscopy	31
4.2.10.	Optical Methods.....	32
4.2.10.1.	Fluorescence determination with ESE Quant Tube Scanner.....	32
4.2.10.2.	Fluorescence spectroscopy	32
4.2.10.3.	Electron microscopy	32
4.2.11.	Patient assignment.....	33
4.2.12.	Statistics	33
5.	Results and Discussion	34
5.1.	Characterization of applied human cell lines.....	34
5.2.	Characterization of the generated nanodiscs	37
5.2.1.	Size exclusion chromatography.....	37
5.2.2.	Electron microscopy	40

5.2.3.	Optimization of the nanodisc generation protocol.....	40
5.2.3.1.	Detergent	40
5.2.3.2.	Membrane Scaffold Protein	42
5.2.3.3.	PEG-PE	43
5.2.3.4.	Bio-Beads.....	45
5.2.3.5.	Component-to-volume ratio	46
5.2.3.6.	Reaction time	46
5.2.3.7.	Membrane preparation.....	48
5.2.4.	Scale up approaches.....	50
5.2.5.	Storage conditions.....	52
5.3.	Verification of β 1AR incorporation in nanodiscs	55
5.3.1.	Functional characterization of the β 1AR using Alprenolol Beads	56
5.4.	Interaction of AABs and incorporated beta-1 adrenergic receptors in nanodiscs.....	58
5.4.1.	Interaction assay with GFP-Trap Beads.....	58
5.4.2.	SPR assay	60
5.4.2.1.	Affinity measurements.....	63
5.4.2.2.	Kinetic measurements.....	64
5.5.	ELISA assay with human serum samples.....	66
5.5.1.	Optimization.....	66
5.5.1.1.	Plate, Blocking Solution and Wash Buffer	66
5.5.1.2.	Antibodies and β 1AR nanodiscs	67
5.5.2.	Standard ELISA set-up with GFP-Trap as capture antibody	68
5.5.2.1.	Characterization of subjects measured with nanodisc ELISA.....	74
5.5.2.2.	Statistical analysis of IgG concentration determined with the nanodisc ELISA	76
6.	Conclusion and Outlook	79
7.	References.....	82

Abbreviations

7TMD	seven transmembrane domain
AAB	autoantibody
AC	adenylyl cyclase
ApoA1	apolipoprotein A1
APS	ammonium persulfate
b1AR	beta-1 adrenergic receptor
BE	beads equilibration
BRK	Bayerisches Rotes Kreuz
BSA	bovine serum albumin
cAMP	cyclic adenosine monophosphate
CFP	cyan fluorescent protein
CMC	critical micelle concentration
CV	coefficient of variation
Da	Dalton
DCM	dilated cardiomyopathy
DDM	n-dodecyl- β -D-maltoside
DMEM	Dulbecco's modified Eagle medium
DMPC	1,2-dimyristoyl-sn-glycero-3-phosphorylcholine
DMSO	dimethyl sulfoxide
DPBS	Dulbecco's phosphate-buffered saline
DPPC	1,2-dipalmitoyl-sn-glycero-3-phosphorylcholine
E	elution
EC	extracellular
EDC	1-ethyl-3-(3-dimethylaminopropyl)carbodiimide hydrochloride
EDTA	ethylenedinitrilotetraacetic acid disodium salt dehydrate
EKG	electrocardiogram
ELISA	enzyme-linked immunosorbent assay
EM	electron microscopy
FACS	fluorescence-activated cell sorting
FAM	carboxyfluorescein
FBS	fetal bovine serum
Fig	figure

FPLC	fast protein liquid chromatography
FRAP	fluorescence recovery after photo-bleaching
FRET	fluorescence resonance energy transfer
FT	flow-through
GDP	guanosine diphosphate
GFP	green fluorescent protein
GOÄ	Gebührenordnung für Ärzte
GTP	guanosine triphosphate
h	hour
HDL	high-density lipoprotein
HEK293	human embryonic kidney cells 293
HEPES	4-2-hydroxyethylpiperazine-1-ethanesulfonic acid
HF	heart failure
HRP	horseradish peroxidase
IC	intracellular
ICM	ischemic cardiomyopathy
iDCM	idiopathic dilated cardiomyopathy
IgG	immunoglobulin G
IP	immunoprecipitation
LOD	limit of detection
LOQ	limit of quantification
LTCC	L-type Ca ²⁺ -channel
min	minute
MS	mass spectrometry
MSP	membrane scaffold protein
MT-CO2	Mitochondrially Encoded Cytochrome C Oxidase II
MW	molecular weight
ND	nanodisc
NEG	negative
NHS	N-hydroxysuccinimide
NMR	nuclear magnetic resonance spectroscopy
OG	octyl-β-D-glucopyranoside
PDB	protein data bank
PEG-PE	1,2-distearoyl- <i>sn</i> -glycero-3-phospho-ethanolamine-N-[methoxy-polyethylene

	glycol-2000]
PKA	protein kinase A
PLN	phospholamban
POPC	1-palmitoyl-2-oleoyl-sn-glycero-3-phosphocholin
POS	positive
PVDF	polyvinylidene difluoride
RAAS	renin–angiotensin–aldosterone system
RT	room temperature
RyR	ryanodine receptor
s	second
SD	standard deviation
SDS	sodium dodecyl sulphate
SDS-PAGE	sodium dodecyl sulfate polyacrylamide gel electrophoresis
SEC	size exclusion chromatography
SNS	sympathetic nerve system
SPR	surface plasmon resonance spectroscopy
TEM	transmission electron microscopy
TEMED	tetramethylethylenediamine
TEV	Tobacco Etch Virus
TMB	3,3',5,5'-tetramethylbenzidine
TMD	transmembrane domain
W	wash
WB	western blot
WT	wild type
YFP	yellow fluorescent protein
β1AR	beta-1 adrenergic receptor
β2AR	beta-2 adrenergic receptor
βAR	β-adrenergic receptor

Figure index

Figure 1: Illustrated morphology of a DCM and a normal heart.....	5
Figure 2: Prevalence of anti- β 1AR antibodies in DCM and ICM patients, as well as healthy controls	6
Figure 3: Human β 1-adrenergic receptor.....	9
Figure 4: β 1AR signaling pathways in cardiomyocytes	10
Figure 5: Crystal structures of the turkey β 1AR with stabilizing mutations and truncations	11
Figure 6: Illustration of a nanodisc and conformation models of MSP molecules in nanodiscs	14
Figure 7: Schematic illustration of nanodisc generation according to the original protocol.....	15
Figure 8: Resolved protein structures using nanodisc technology	17
Figure 9: Transmission light microscopy and fluorescence microscopy images of HEK293 cell lines ..	35
Figure 10: Fluorescence spectroscopy measurements of cell lysates	36
Figure 11: Fluorescence imaging of HEK293 cells overexpressing β 1AR-YFP.	36
Figure 12: Gel filtration chromatograms of generated nanodiscs.....	38
Figure 13: Calibration curve used for MW calculation of nanodiscs	38
Figure 14: Characterization of nanodiscs generated according to the standard protocol	39
Figure 15: Negative stain TEM image of nanodiscs generated from HEK293 cells.....	40
Figure 16: Gel filtration chromatograms of nanodiscs generated with DDM or digitonin	41
Figure 17: Gel filtration chromatograms of nanodiscs generated using MSP1D1 and MSP1E3D1	43
Figure 18: Impact of PEG-PE on nanodisc generation.....	44
Figure 19: Impact of Bio-Beads amount on nanodisc generation.....	45
Figure 20: Impact of component-to-volume ratios on nanodisc generation.....	46
Figure 21: Impact of reaction time on nanodisc generation.....	47
Figure 22: Fluorescence intensity of protein-containing fractions during the membrane isolation process	48
Figure 23: Nanodisc generation from cell lysate and isolated cell membrane.....	50
Figure 24: Gel filtration chromatograms of scale up approaches.....	51
Figure 25: Evaluation of storage conditions for nanodiscs	54
Figure 26: Characterization of β 1AR incorporated in nanodiscs.....	55
Figure 27: Functional characterization of β 1AR-nanodiscs using alprenolol beads	57
Figure 28: Affinity purification of β 1AR-YFP NDs using magnetic beads coupled with GFP-Trap	58
Figure 29: Co-IP of anti- β 1AR antibodies using β 1AR-YFP NDs coated on GFP-Trap Magnetic Beads.	59
Figure 30: Immobilization of GFP-Trap on the CM5 sensor surface by amine coupling.....	61
Figure 31: Binding of antibodies to β 1AR-YFP NDs captured on the sensor chip via GFP-Trap.	62

Figure 32: Stability of immobilized GFP-Trap and captured β 1AR-YFP-NDs on the sensor surface	63
Figure 33: Binding affinity of huMAB23-6-7 to β 1AR-YFP nanodisc	64
Figure 34: Binding kinetics of huMAB23-6-7 to β 1AR-YFP nanodisc	65
Figure 35: Impact of Blocking Solution on ELISA measurements.....	66
Figure 36: Impact of GFP-Trap amount and combination of GFP-Trap and β 1AR-NDs amount on ELISA measurements	68
Figure 37: Schematic illustration of the standard ELISA set-up for patient sample measurements	69
Figure 38: Schematic illustration and normalized ELISA signal of control experiments compared with the standard ELISA set-up	70
Figure 39: ELISA read-out of huMAB23-6-7 in serial dilution measured with the standard set-up	71
Figure 40: Impact of sample conditions on ELISA measurement.....	71
Figure 41: Inter-assay variance of applied standards and human serum samples, as well as β 1AR expression level and nanodisc concentration in 15 ELISA plates measured.....	73
Figure 42: Age and sex distribution of cardiomyopathy patients measured with the ELISA assay	74
Figure 43: Patients splitted into subgroups based on diagnosis of cardiomyopathy	75
Figure 44: Frequency of sampling at different time points	75
Figure 45: Calculated concentration of anti- β 1AR antibodies in human samples measured with the standard ELISA set-up	77

Table index

Table 1: High resolution structures of β 1AR in its ligand-bound conformation	12
Table 2: Physical and chemical properties of DDM and digitonin	41
Table 3: Physical and chemical properties of MSP1E3D1 and MSP1D1	42
Table 4: Results of scale up approaches	52
Table 5: Proportion of anti- β 1AR antibody-positive subjects in each subgroup considering defined cut-offs	78
Table 6: Cost calculation for ELISA assay with β 1AR-YFP nanodiscs	80

1. Abstract

Dilated cardiomyopathy is a common cause of severe heart failure with a prevalence of 1:2500. The five-year survival rate after diagnosis is only 60% due to its association with high cardiovascular morbidity and mortality. Among genetic, metabolic and toxic factors inducing dilated cardiomyopathy, the presence of potentially disease-driving anti- β 1-adrenergic receptor autoantibodies was estimated as 25% to 75% in dilated cardiomyopathy patients. However, these autoantibodies could also be found in 10% of healthy controls and ischemic cardiomyopathy patients. The association of anti- β 1AR autoantibodies with the disease progression was proven by a large number of analyses and *in vivo* animal testing. Diverse therapeutic studies have shown that the removal of anti- β 1AR antibodies as well as the interruption of the antibody-antigen interaction leads to a prolonged improvement of heart function in dilated cardiomyopathy patients.

However, to apply treatments targeting the autoantibody- β 1AR interaction, the presence and impact of anti- β 1AR autoantibodies in dilated cardiomyopathy patients must be examined. Until now, a reliable, standardizable diagnostic method is still not available. Approaches using fragments or linear peptides for antigen presentation showed no satisfying results since pathologically relevant anti- β 1AR antibodies only bind to the correctly folded 3-dimensional conformational epitope of the receptor. Cell-based functional interaction assays, as well as bioassays performed with isolated and cultivated rat cardiomyocytes, are hard to standardize and to introduce into routine diagnostics due to the need of living cells and the complexity of the instrumentation.

The aim of this thesis was therefore the development of an *in vitro* diagnostic assay to support the diagnosis of anti- β 1AR autoantibody-induced dilated cardiomyopathy. To enable the presentation of the native 3-dimensional conformational epitope, the β 1-adrenergic receptor was overexpressed in human HEK293 cells and reconstituted into lipid bilayer nanodiscs. Nanodiscs are round slides of phospholipid bilayers stabilized by synthetic membrane scaffold proteins with a well-defined monodisperse and reproducible particle size. They provide a native-like membrane environment for the incorporation of the β 1-adrenergic receptor, which stabilizes this G-protein coupled membrane protein in aqueous solution for measurements with standard immunological techniques. Advantages of this technology are easy handling, high protein stability and full accessibility to both intra- and extracellular protein domains. To fulfill the requirements of a routine diagnostic assay, the nanodisc generation was optimized to the β 1AR. At the same time, the generation process was simplified regarding reaction time, hands-on time and use of specific equipment.

With the β 1AR-nanodisc construct, immunoassays in enzyme-linked immunosorbent assay (ELISA) and surface plasmon resonance spectroscopy (SPR) assay formats have been developed and optimized for the detection of anti- β 1AR antibodies in human serum. SPR measurements allow a label-free and deep insight into the binding event between anti- β 1AR antibodies and β 1AR-nanodiscs captured on the sensor surface. Binding affinity and binding kinetics were further evaluated with the SPR assay. With the β 1AR-nanodisc ELISA, simultaneous measurement of up to 40 samples in duplicate is possible. In total, 435 samples from 207 cardiomyopathy patients, as well as 90 samples from 90 healthy controls, were measured with the optimized β 1AR-nanodisc ELISA. The established ELISA assay allows a differentiation between anti- β 1AR autoantibody-positive and anti- β 1AR autoantibody-negative subjects in the analyzed patient collective. An inter-assay variance of 24%, as well as an intra-assay variance of 5% was determined. For the optimized β 1AR-nanodisc ELISA, the limit of detection was determined as 0.64 ng/mL and the limit of quantification as 1.26 ng/mL.

2. Zusammenfassung

Die dilatative Kardiomyopathie ist eine häufige Ursache für schwere Herzinsuffizienz mit einer Prävalenz von 1:2500. Die Fünfjahresüberlebensrate nach der Diagnose beträgt aufgrund der hohen kardiovaskulären Morbidität und Mortalität nur 60%. Neben den genetischen, metabolischen und toxischen Faktoren, die eine dilatative Kardiomyopathie induzieren, wurde das Vorhandensein von potenziell krankheitsauslösenden Anti- β 1-adrenergen Rezeptor-Autoantikörpern bei dilatativen Kardiomyopathie-Patienten auf 25% bis 75% geschätzt. Diese Autoantikörper konnten jedoch auch bei 10% der gesunden Kontrollpersonen und ischämischen Kardiomyopathie-Patienten gefunden werden. Die Assoziation zwischen Anti- β 1AR-Autoantikörpern und dem Krankheitsverlauf wurde durch eine große Anzahl von Analysen und *in-vivo*-Tierversuchen nachgewiesen. Diverse Therapiestudien haben gezeigt, dass sowohl das Entfernen von Anti- β 1AR-Antikörpern als auch die Unterbrechung der Antikörper-Antigen-Interaktion bei dilatativen Kardiomyopathie-Patienten zu einer anhaltenden Verbesserung der Herzfunktion führt.

Um jedoch Behandlungen anwenden zu können, die auf die Autoantikörper- β 1AR-Interaktion abzielen, muss das Vorhandensein und der Einfluss von Anti- β 1AR-Autoantikörpern bei Patienten mit dilatativer Kardiomyopathie untersucht werden. Eine zuverlässige, standardisierbare Diagnosemethode steht bis heute nicht zur Verfügung. Ansätze, die Fragmente oder lineare Peptide für die Antigenpräsentation verwenden, zeigten keine befriedigenden Ergebnisse, da pathologisch relevante Anti- β 1AR-Antikörper nur an das korrekt gefaltete 3-dimensionale Konformationsepitop des Rezeptors binden. Zellbasierte funktionelle Interaktionsassays sowie Bioassays, die mit isolierten und kultivierten Rattenkardiomyozyten durchgeführt werden, sind aufgrund der Notwendigkeit lebender Zellen und der Komplexität der Messausrüstung schwer zu standardisieren und sind für die Routine-Diagnostik ungeeignet.

Das Ziel dieser Dissertation war daher die Entwicklung eines *in-vitro*-Diagnostikassays zur Unterstützung der Diagnose einer durch Anti- β 1AR-Autoantikörper induzierten dilatativen Kardiomyopathie. Um die Präsentation des nativen 3-dimensionalen Konformationsepitops zu ermöglichen, wurde der β 1-adrenerge Rezeptor in menschlichen HEK293-Zellen überexprimiert und in Lipid-Doppelschicht-Nanodisks rekonstituiert. Nanodisks sind durch synthetische Membrane-Scaffold-Proteine stabilisierte runde Scheiben aus Phospholipid-Doppelschichten mit genau definierter monodisperser und reproduzierbarer Partikelgröße. Sie bieten eine native Membrenumgebung für den Einbau von G-Protein-gekoppelten Membranproteinen, die in wässriger Lösung für Messungen mit immunologischen Standardtechniken stabilisiert werden. Vorteile dieser

Technologie sind einfache Handhabung, hohe Proteinstabilität und vollständige Zugänglichkeit der intra- als auch der extrazellulären Proteindomänen. Um die Anforderungen eines routinemäßigen diagnostischen Tests zu erfüllen, wurde die Nanodisc-Generierung auf den β 1AR optimiert. Gleichzeitig wurde der Generierungsprozess in Bezug auf die Reaktionszeit, die Hands-on-Zeit und die Verwendung spezifischer Geräte vereinfacht.

Mit dem β 1AR-Nanodisk-Konstrukt wurden Immunoassays in Enzyme-linked Immunosorbent Assay- (ELISA) und Oberflächenplasmonresonanzspektroskopie- (SPR) testformaten entwickelt und optimiert für den Nachweis von Anti- β 1AR-Antikörpern in humaner Serummatrix. SPR-Messungen ermöglichen einen markierungsfreien und tiefen Einblick in das Bindungsereignis zwischen Anti- β 1AR-Antikörpern und β 1AR-Nanodisks, die auf der Sensoroberfläche präsentiert werden. Bindungsaffinität und Bindungskinetik wurden mit dem SPR-Assay bestimmt. Mit dem β 1AR-Nanodisc-ELISA ist eine simultane Messung von bis zu 40 Proben in technischen Duplikaten möglich. Insgesamt wurden 435 Proben von 207 Kardiomyopathie-Patienten sowie 90 Proben von 90 gesunden Kontrollpersonen mit dem optimierten β 1AR-Nanodisc-ELISA gemessen. Der etablierte ELISA-Assay erlaubt eine Differenzierung zwischen Anti- β 1AR-Autoantikörper-positiven und Anti- β 1AR-Autoantikörper-negativen Subgruppen im analysierten Patientenkollektiv. Es wurde eine Inter-Assay-Varianz von 24% sowie eine Intra-Assay-Varianz von 5% bestimmt. Für den optimierten β 1AR-Nanodisc-ELISA wurde die Nachweisgrenze auf 0,64 ng/mL und die Quantifizierungsgrenze auf 1,26 ng/mL bestimmt.

3. Introduction

3.1. Dilated cardiomyopathy

Chronic heart failure (HF) is a common disease worldwide with high morbidity and premature mortality. The prevalence of HF in the US has risen from 5.7 million (2009 to 2012) to 6.5 million (2011 to 2014) with 2.04% increase (year 2014), the five-year survival after diagnosis is estimated as 61% (year 2010). In the US, there are 960000 new cases reported annually, one in 8 deaths has heart failure mentioned on the death certificate (Benjamin et al., 2017). Cardiomyopathy represents a diverse group of heart (cardio) muscle (myo) diseases (pathy), whereas over 80% of cardiomyopathies are classified as dilated (Schonberger & Seidman, 2001).

Dilated cardiomyopathy (DCM, ICD-10 Code I42.0) is characterized by ventricular dilation and contractile dysfunction increasing the left ventricular end-diastolic and end-systolic blood volumes gradually. The prevalence is estimated to be 1:2500 (Maron et al., 2006) and it is the most common cardiomyopathy type among children (Benjamin et al., 2017). In DCM, both mass and volume of heart muscle are increased while the heart wall appears thinner and distended (Fig 1). The heart becomes enlarged and is unable to pump blood efficiently into the body. The ejection fraction of blood is reduced continuously. Various risk factors are reported to be associated with DCM, including metabolic and toxic factors like smoking and alcohol intake, infections (viral myocarditis), autoimmune causes as well as genetic mutations (Benjamin et al., 2017). However, the underlying pathology is not known for many cases and therefore, these cases with unknown cause are classified as idiopathic DCM (iDCM). The diagnosis of DCM is primarily based on results of 2-dimensional echocardiography by examining the heart chambers and pump function. Other clinical tests such as chest X-ray, electrocardiogram (EKG) and blood tests also help diagnosing DCM.

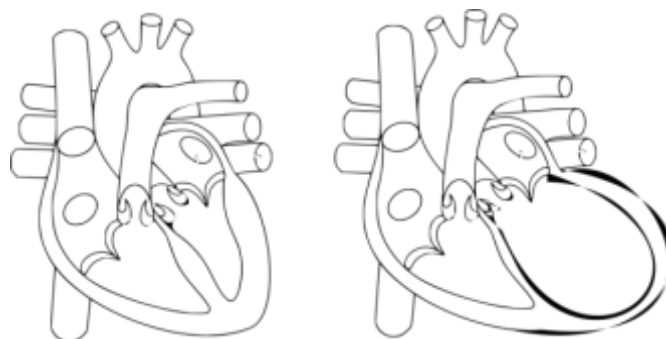


Figure 1: Illustrated morphology of a DCM (right) and a normal heart (left). Left ventricular end-diastolic and end-systolic volumes are increased in DCM with thinning of the heart wall, indicated as thicker lines.

3.1.1. DCM induced by AAB against beta-1 adrenergic receptor

β ARs play a major role in heart failure, the survival of heart failure patients correlates inversely with pronounced activation of the sympathetic system. The expression level of β 1AR is downregulated in heart failure while the remaining receptors are desensitized by uncoupling from stimulating Gs protein (Lohse et al., 1996; Lohse et al., 2003). Experiments performed with transgenic mouse model overexpressing cardiac β 1AR showed the association between β 1AR expression level and hypertrophy, fibrosis and heart failure (Bisognano et al., 2000; Engelhardt et al., 1999). Furthermore, rats immunized against the EC2 loop of β 1AR develop anti- β 1AR antibodies which induce cardiac dilatation and dysfunction. Isogenic transfer of these antibodies induce DCM in healthy animals (Buval et al., 2007; Jahns et al., 2006). Isolated anti- β 1AR antibodies showed a positive chronotropic effect on rat cardiomyocytes (Magnusson et al., 1994) and inotropic effect on purkinje fibers (Stavrakis et al., 2011). The chronic overstimulation of agonistic anti- β 1AR antibodies leads to β 1AR desensitization, downregulation and thereby the cardiac remodeling (Freedman & Lefkowitz, 2004).

According to different studies, the prevalence of anti- β 1AR antibodies in DCM varies from 25% to 75% (Jahns et al., 1999; Jane-wit et al., 2007; Patel & Hernandez, 2013; San Martín et al., 2002; Wallukat et al., 2014; Wallukat & Schimke, 2014). However, anti- β 1AR antibodies are also found in about 10% of healthy controls (Dandel et al., 2012) and ischemic cardiomyopathy (ICM) patients (Patel & Hernandez, 2013) (Fig 2). In DCM patients, more severe heart failure symptoms were found in anti- β 1AR antibody-positive patients (Deubner et al., 2010; Iwata et al., 2001; Stork et al., 2006).

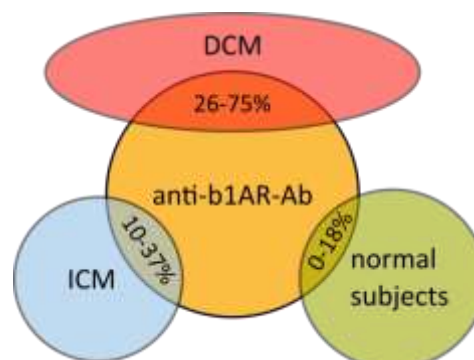


Figure 2: Prevalence of anti- β 1AR antibodies in DCM and ICM patients, as well as healthy controls, modified from Patel & Hernandez, 2013.

Selective and non-selective extracorporeal immunoadsorption of anti- β 1AR antibodies leads to a prolonged improvement of heart function in DCM patients (Dandel et al., 2015; Dandel et al., 2013; Felix et al., 2002; Mobini et al., 2003; Trimpert et al., 2010). A detailed clinical overview is issued in Patel & Hernandez, 2013. In addition, pathological effects of anti- β 1AR antibodies could be neutralized with aptamers binding to the β 1AR (Haberland et al., 2011; Wallukat et al., 2016) or

epitope mimicking peptides binding to antibodies (Münch et al., 2012) to inhibit the antibody-antigen interaction. The cyclic COR-1 peptide inhibiting the binding of agonist-like autoantibodies (AABs) against β 1AR is currently tested in a randomized, double-blind phase-2 pilot study (Störk et al., 2016).

However, to apply immunoabsorption or other treatments targeting the antibody- β 1AR interaction, DCM patients must be classified into anti- β 1AR antibody-positive and anti- β 1AR antibody-negative subgroups. A reliable standard diagnostic method is not available yet (Bornholz et al., 2014). Approaches using fragments or linear peptides for antigen presentation in enzyme-linked immunosorbent assays (ELISA) (Jahns et al., 1999) showed no satisfying results since anti- β 1AR antibodies only bind to the 3-dimensional conformational epitope of the receptor (Bornholz et al., 2016; Bornholz et al., 2014). A functional interaction assay using fluorescence resonance energy transfer (FRET) to detect ligand binding-induced conformational rearrangement is being developed by Bornholz et al., 2016. The binding events of antibodies to β 1AR overexpressed in HEK293 cells could be recorded by fluorescence-activated cell sorting (FACS). Another functional assay measuring β 1AR-induced increase of cytosolic cAMP level using a highly sensitive cAMP FRET sensor in living HEK293 cells is also available (Nikolaev et al., 2007). In the functional bioassay established by Wallukat & Nissen, 2001, cardiomyocytes are isolated from rat embryos and cultivated, the binding event of antibodies to β 1AR is then measured by the contraction rate. Despite of the specific read-outs of functional assays, they are hard to standardize and to introduce into routine diagnostics due to the need of living cells and the complexity of instrumentation (Bornholz et al., 2016).

3.2. Beta-1 adrenergic receptor

β -adrenergic receptors (β ARs) belong to class A of the superfamily of G protein-coupled receptors (GPCRs) with characteristic seven transmembrane domains (7TMD). This family includes over 800 members (Fredriksson et al., 2003) and is characterized by the 7TMD configuration with N-terminus on the extracellular (EC) surface, C-terminus in the intracellular (IC) space, three EC and three IC loops. While the superposition of the seven transmembrane domains shows a strong similarity in their conformation embedded in the phospholipid bilayer, the IC and EC loops vary in their structural motifs in order to induce diverse downstream signaling pathways. GPCRs comprise the largest family of integral membrane proteins currently known and include receptors for many hormones, neurotransmitters, chemokines as well as sensory stimuli (Rosenbaum et al., 2009). They are responsible for about 80% of signal transduction across the cell membrane (Millar & Newton, 2010) and are the most common target of therapeutic drugs with a very important role in clinical medicine and pharmacology (Pierce et al., 2002).

The human β 1-adrenergic receptor (β 1AR, ADRB1, Uniprot P08588) presents the most prominent β AR in the heart and is encoded by an intronless gene on chromosome 10q25.3. It consists of 477 amino acids with a molecular weight of 51.3 kDa (Fig 3). β 1AR is mainly responsible for positive chronotropic (heart rate), dromotropic (conduction speed) and inotropic (muscle contraction) effects of catecholamines epinephrine and norepinephrine (Lohse et al., 2003), which are released from the sympathetic nerve system (SNS). Therefore, the β 1AR is the main target of receptor antagonists, the so called β -blockers, which are particularly used for the management of cardiac arrhythmias, cardioprotection after myocardial infarction (Freemantle et al., 1999) and hypertension (Cruickshank, 2010). In acute heart failure, β 1AR agonists are applied to improve the positive inotropic effect. Beside the moderation of cardiac functions, β 1AR controls tightly the renin release and thereby also regulates the blood pressure via the renin–angiotensin–aldosterone system (RAAS).

The human β 1AR is N-glycosylated (GlcNAc) at amino acid 15. The intracellular C-terminus is anchored to the cell membrane by S-palmitoylation of the cysteine residual at amino acid position 392. Moreover, the β 1-adrenergic receptor contains three phosphorylation sites of protein kinase A (PKA) at serines in the third IC loop (amino acid position 312) and the cytoplasmic C-terminus (amino acid positions 412 and 428). Two disulfide bonds occur between cysteines 131-216 and 209-215. Several natural variants are reported for the β 1-adrenergic receptor. Polymorphisms in the extracellular N-terminal loop (amino acid position 26, 29, 31 and 49) and in the intracellular C-terminus (amino acid position 389, 399 and 405) may possibly alter the accessibility of the binding pocket or the interaction with intracellular interaction partners (Ahles & Engelhardt, 2014). The

expression level of β 1AR is very low with no more than 50 fmol/mg to 70 fmol/mg membrane protein (3 ng to 4 ng β 1AR in 1 mg membrane protein) in cardiomyocytes of most species (Lohse et al., 2003).

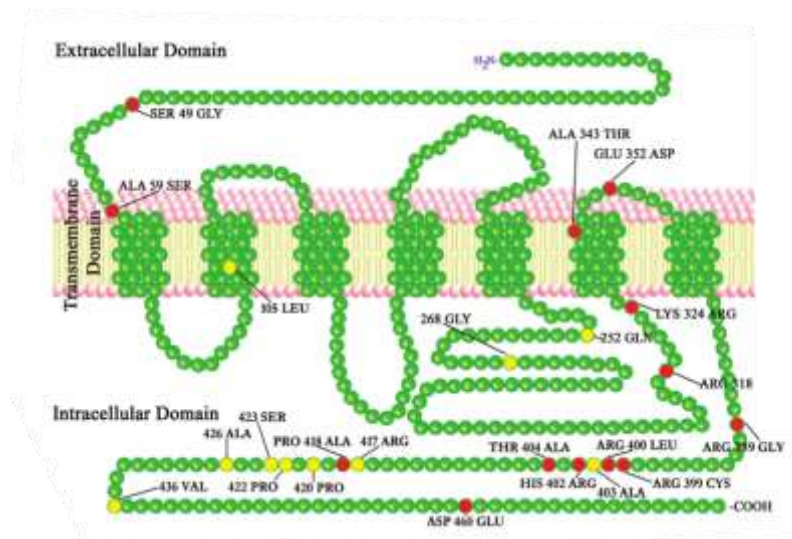


Figure 3: Human β 1-adrenergic receptor, modified from Taylor & Bristow, 2004. Amino acid residues without reported polymorphisms in green, silent polymorphisms in yellow (different nucleotide, same amino acid) and polymorphisms with exchanged amino acid in red.

3.2.1. Signaling

β ARs play an important role for regulation of the sympathetic nervous system. They transduce signals from the outside of the cell to the cytoplasm. Stimulation of the β 1AR by the endogenous catecholamines epinephrine and norepinephrine induces a conformational rearrangement of the receptor which subsequently activates the stimulatory G_s protein. The α subunit of the G_s protein binds guanosine diphosphate (GDP) and is associated with the subunit G_β and G_γ in its inactive state. Upon activation, GDP is replaced by guanosine triphosphate (GTP) and the $G_{\beta\gamma}$ heterodimer is dissociated from the G_α subunit (Fig 4). Thereby, the membrane-embedded adenylyl cyclase (AC) is activated and leads to the generation of the second messenger cyclic adenosine monophosphate (cAMP) in the IC space and the activation of the cAMP-dependent PKA (Fig 4). PKA phosphorylates numerous cellular proteins such as phospholamban (PLN), ryanodine receptors (RyR), L-type Ca^{2+} -channels (LTCC) and troponin I in cardiomyocytes as well as the β ARs themselves (Lohse et al., 2003; Wallukat, 2002). The resulting Ca^{2+} increase in cytosol through LTCC activation stimulates the calcium-induced calcium release in cardiac muscle cells which leads to cardiac contraction.

Dysfunction, overexpression and downregulation of β ARs are associated with diverse diseases like obesity, hypertension, heart failure and diabetes mellitus (Bristow et al., 1985; Chang et al., 2005; Masuo, 2010; Reihnsaus et al., 1993; Scognamiglio et al., 1998). Chronic stimulation of β 1AR causes

hypertrophy in cultured rat ventricular myocytes (Schafer et al., 2000), which was also shown in transgenic mouse model overexpressing β 1AR in cardiomyocytes (Engelhardt et al., 1999).

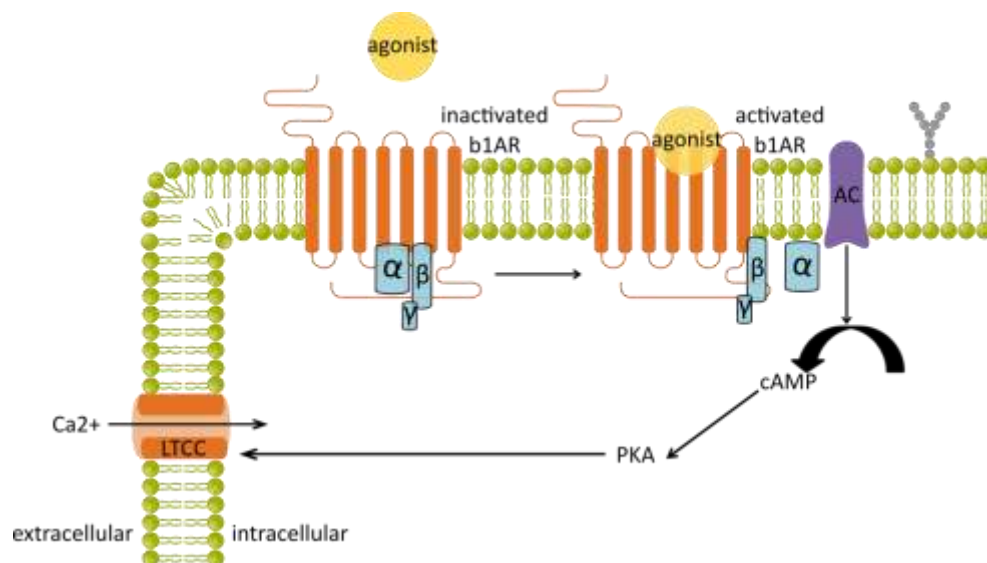


Figure 4: β 1AR signaling pathways in cardiomyocytes, modified from Lohse et al., 2003; Machuki et al., 2017; Sondek & Siderovski, 2001 and Tang & Insel, 2004.

3.2.2. Structure

The determination of the β AR structure is essential for understanding how agonists and antagonists bind to the receptors and change the receptor conformation. The determination of high resolution crystal structures of β ARs has been the goal of research for almost 30 years (Blois & Bowie, 2009; Strader et al., 1988). The native β 1AR is unstable in detergent (Serrano-Vega & Tate, 2009) and the structure determination of the active state was only possible with thermostabilized mutations and additional stabilizing modifications (Warne et al., 2011; Warne et al., 2008). The high resolution structure of β 1AR was finally solved using X-ray diffraction of protein crystals with antibody, agonist or antagonist stabilization in the last years (Fig 5) (Warne et al., 2011; Warne et al., 2008).

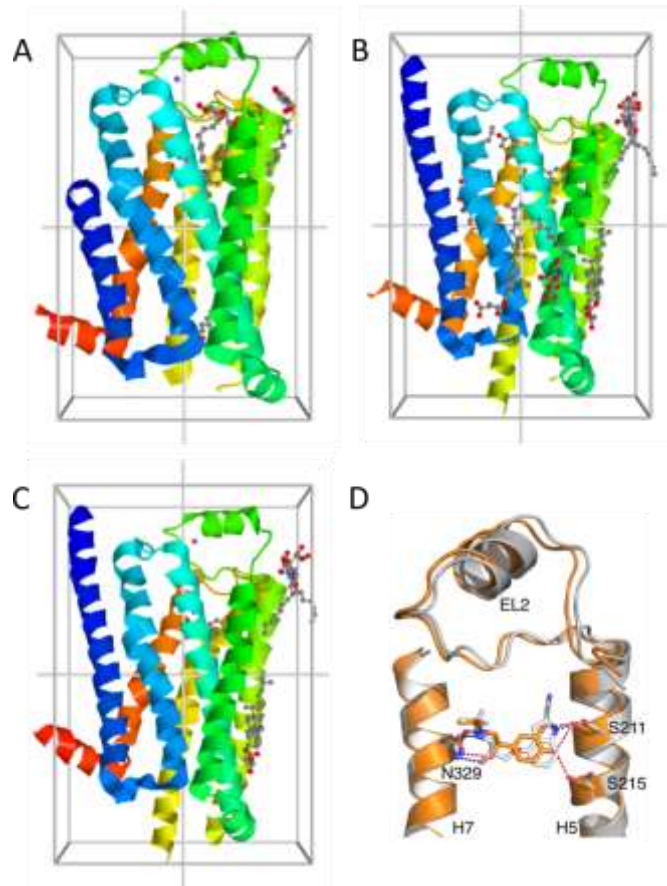


Figure 5: Crystal structures of the turkey β 1AR with stabilizing mutations and truncations at the N-terminus, IC loop 3 and C-terminus. Antagonist cyanopindolol (A, PDB ID 2VT4, (Warne et al., 2008)), partial agonist dobutamine (B, PDB ID 2Y01, (Warne et al., 2011)) and full agonist isoprenaline (C, PDB ID 2Y03, (Warne et al., 2011)) are co-crystallized and shown as a ball and stick model in the ligand binding pocket. D: Ligand binding pocket of antagonist- (cyanopindolol, grey) and full agonist- (isoprenaline, orange) bound β 1AR, modified from (Warne et al., 2011). All structures are taken from Protein Data Bank (PDB) and were generated using the JSmol software.

Structure determination of β 1AR in its agonist- and antagonist-bound conformations provides a better understanding of the ligand-induced conformational change of the receptor, a selection of ligand-bound crystal structures of turkey β 1AR, expressed in *trichoplusia ni*, is listed in Table 1.

Table 1: High resolution structures of β 1AR in its ligand-bound conformation.

PDB ID	Year	Mutations	Ligand	Reference
5F8U	2015	38	4-([(2S)-3-(tert-butylamino)-2-hydroxypropyl]oxy)-3H-indole-2-carbonitrile	Leslie, Warne, & Tate, 2015
5A8E	2015	11	7-methylcyanopindolol	Sato et al., 2015
4BVN	2014	11	cyanopindolol	Miller-Gallacher et al., 2014
3ZPQ	2013	8	4-(piperazin-1-yl)-1h-indole	Christopher et al., 2013
3ZPR	2013	8	4-methyl-2-(piperazin-1-yl) quinoline	Christopher et al., 2013
2Y03	2011	36	isoprenaline	Warne et al., 2011
2Y00	2011	36	dobutamine	Warne et al., 2011
2VT4	2008	8	cyanopindolol	Warne et al., 2008

The ligand binding is mediated by polar and hydrophobic contact residues from TMD 3, 5, 6, 7 (Rosenbaum et al., 2009), whereas the extracellular loop 2 (EC2) is reported to be involved in the ligand binding process by forming a lid over the binding pocket (Venkatakrisnan et al., 2013; Warne et al., 2008). The EC2 region contains a short two-turn α -helix and is stabilized by disulfide bonds between cysteines 131-216 and 209-215 (Warne et al., 2011; Warne et al., 2008). Agonist binding induces rotamer conformation changes of side chains Ser211 (TMD 5) and Ser215 (TMD 5) as well as a 1 Å contraction of the catecholamine-binding pocket relative to the antagonist-bound receptor (Fig 3D). Full agonists can form hydrogen bonds with two conserved serine residues in transmembrane helix 5 (Ser211, Ser215), while partial agonists only interact with Ser211 (Warne et al., 2011).

Homo- as well as hetero-dimerization is reported to be a general phenomenon for GPCRs (Ferre & Franco, 2010). Specific but instable interactions between β 1AR monomers were discovered using fluorescence recovery after photo-bleaching (FRAP) experiments (Dorsch et al., 2009; Lohse, 2010), differently from the large and static oligomeric complexes formed by β 2AR monomers. The X-ray crystal structure of β 1AR in a ligand-free basal state shows the packing of β 1AR oligomers with two alternating dimer interfaces, which are sensitive to ligand binding (Huang et al., 2013).

Taken together, the stabilization and handling of β 1AR still remain challenging. The novel nanodisc technology could be the problem-solving approach to reconstitute and solubilize β 1AR for diagnostic purposes.

3.3. Nanodisc technology

In the 1990s, the first notion of preparing nanometer-size phospholipid bilayer particles by mimicking the properties of high-density lipoproteins (HDL) was proposed by S. Sligar and his fellow researchers (Bayburt et al., 1998; Carlson et al., 1997). Until now, nanodisc technology has been applied to reconstitute and characterize various membrane proteins for analytical approaches with a broad spectrum of biochemical and biophysical methods.

Membrane proteins represent the largest target class for over 60% of all known drugs (Arinaminpathy et al., 2009; Overington et al., 2006), even though they only make up 20% to 30% of the human proteome (Wallin & von Heijne, 1998). However, due to their amphipathic nature, membrane proteins are easily denatured and aggregated in absence of the native membrane surroundings. Therefore, they are strongly underrepresented regarding biophysical investigations, structure determination and other *ex vivo* studies.

Different amphipathic methods have been developed in the last decades to facilitate interrogation of membrane proteins, such as using detergent solubilization, micelles, bicelles or liposomes (Seddon et al., 2004). In general, the presence of detergent during the solubilization process can irreversibly denature membrane proteins (Garavito & Ferguson-Miller, 2001). Detergent-protein-lipid micelles are used widely for solubilization and characterization of membrane proteins. However, micelles are spherical particles which don't mimic biological lipid bilayer. In addition, reconstitution into micelles is not optimal for optical techniques due to absorbance and light scattering of the micellar phase. Liposomes are only suitable for approaches if either the intracellular or the extracellular side of the membrane protein is required. In addition, liposomes are unstable and the generation of precisely defined particle size is difficult (T. H. Bayburt & Sligar, 2010). Taken together, none of these classical methods provide a native-like lipid bilayer with easy handling, protein stability and full accessibility to both intra- and extracellular protein domains (Mak et al., 2017).

In contrast, nanodiscs generate a biomimetic phospholipid bilayer environment for incorporating membrane proteins, which stabilizes the membrane protein in aqueous solution for measurements with standard techniques. Additionally, both the intra- and the extracellular sides of membrane proteins are accessible for analytical measurements as well as interactions with binding partners. The particle size of nanodiscs shows a monodisperse and reproducible distribution and in solution, nanodiscs are robust and stable in different conditions (Nath et al., 2007).

3.3.1. Structure of nanodiscs

Nanodiscs are round slices of a phospholipid bilayer enveloped by two identical copies of α -helical, amphipathic membrane scaffold proteins (MSP) (Bayburt et al., 2002). MSP is genetically modified from apolipoprotein A1 (ApoA1), the major protein component of high-density lipoprotein (HDL) in blood. The hydrophobic part of MSP faces to the inside of the nanodisc, interacting with the aliphatic residues of lipids while the hydrophilic part is directed outwards and interacts with surrounding molecules in the aqueous solution. The thickness of the phospholipid bilayer is estimated as 5.7 nm (Bayburt et al., 2002). Based on the MSP variants (commercially available: MSP1D1 and MSP1E3D1) used for the generation of nanodiscs, the diameter of the disc varies from 8 nm to 17 nm (Bayburt & Sligar, 2010; Denisov et al., 2004) and contains about 150 lipid molecules per disc (Bayburt et al., 2002).

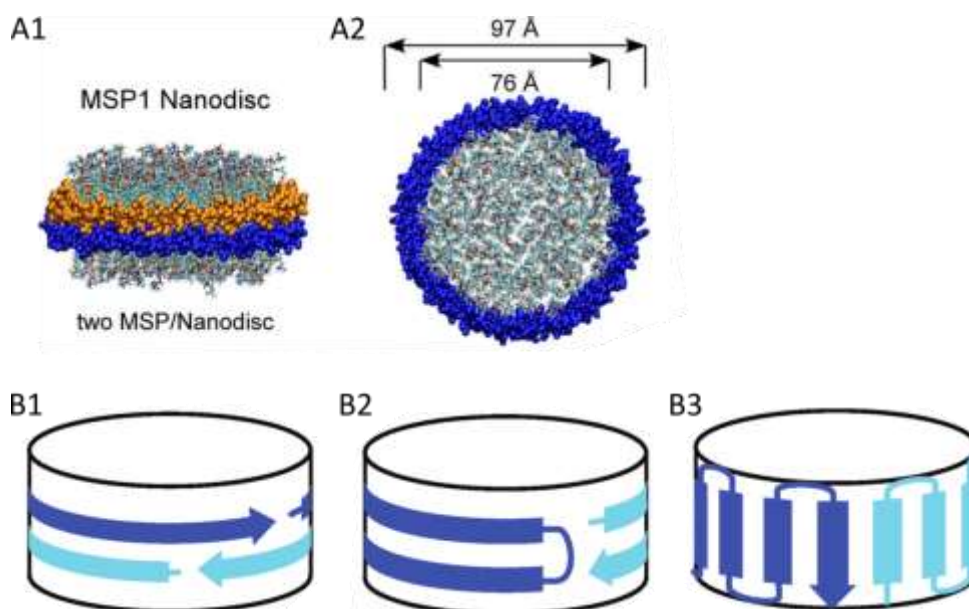


Figure 6: Illustration of a nanodisc and conformation models of MSP molecules in nanodiscs. The nanodisc without incorporated membrane proteins is shown in side view (A1) and top view (A2). The nanodisc is composed of phospholipid and MSP1D1 (orange and blue), modified from Bayburt & Sligar, 2010. Three possible conformation models of MSP molecules in nanodiscs are shown in B: the belt model (B1), the hairpin model (B2), and the picket fence (B3), modified from Nath et al., 2007.

The structure dynamics of nanodiscs were analyzed with hydrogen exchange mass spectrometry (MS) (Morgan et al., 2011), whereas the lipid order and protein dynamics in nanodiscs were characterized with solid-state nuclear magnetic resonance spectroscopy (NMR) (Mors et al., 2013). With the same method, the conformation of MSP molecules in nanodiscs was discussed between the picket fence model, the hairpin model and the belt model (Fig 6B) (Nath et al., 2007), whereas the belt model is strongly supported by the structural data (Li et al., 2006).

Depending on specific needs, MSP has also been modified in different lengths and with different affinity tags (e.g. His, FLAG, Cys). A large number of MSP variants is listed in (Ritchie et al., 2009). A controlled size of nanodiscs is generated by deletion and insertion of amino acid sequences of the applied MSP molecule (Denisov et al., 2004). Extremely short MSP variants were generated by (Hagn et al., 2013) resulting nanodiscs with a diameter of 3 nm. Lately, an ApoA1-mimetic peptide with no sequence homology to endogenous ApoA1 was designed to use nanodiscs as vaccines for personalized cancer immunotherapy (Kuai et al., 2017).

3.3.2. Generation of nanodiscs

The original protocol of nanodisc generation (Bayburt et al., 2002) has been extensively developed and adapted for different membrane proteins of various origins (Bayburt & Sligar, 2010). According to the original protocol, membrane proteins are expressed in overexpression systems, isolated, purified and solubilized in detergent. Afterwards, phospholipids and MSPs are added into the reaction mixture and the self-assembly process of nanodiscs is induced by removal of detergent using dialysis or hydrophobic adsorbents (Fig 7).

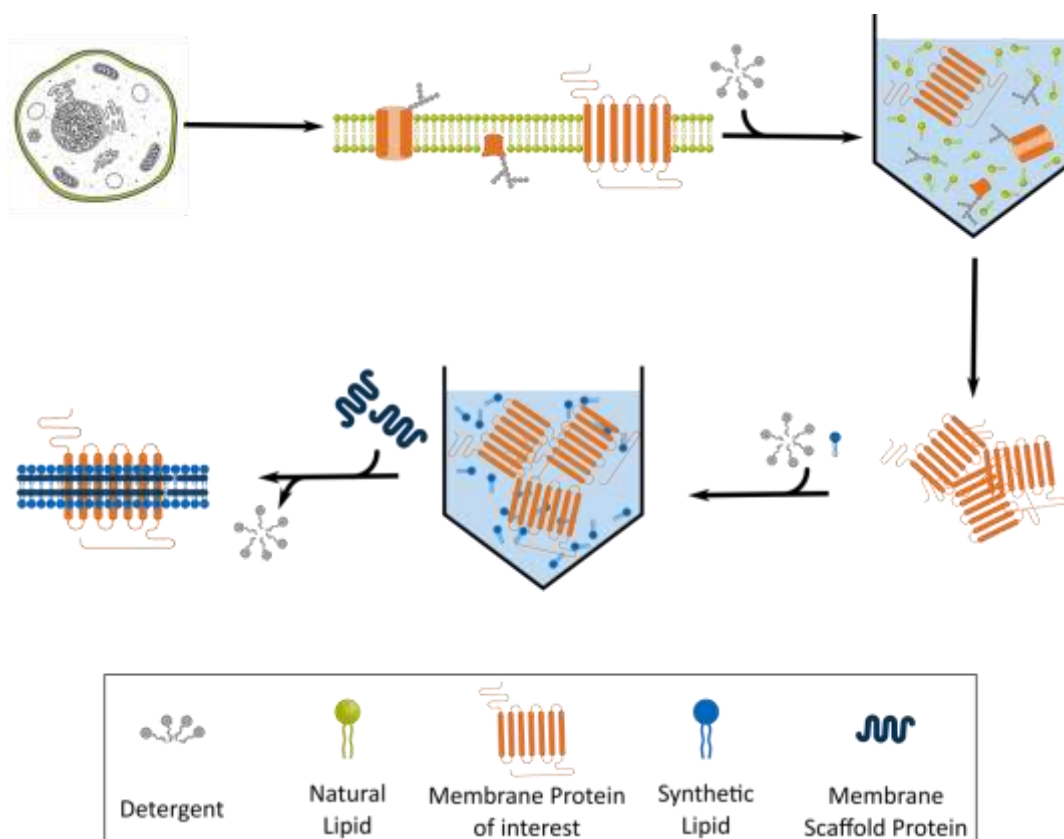


Figure 7: Schematic illustration of nanodisc generation according to the original protocol. Cells used for protein overexpression are lysed and the plasma membrane is isolated. The membrane protein of interest is purified and solubilized in detergent. Phospholipids and MSPs are added into the reaction mixture in the next step, the self-assembly process of nanodiscs is induced by removal of detergent.

The membrane protein of interest could either be isolated directly from animal (Mak et al., 2017) or plant cells (Pandit et al., 2011), expressing the protein of interest naturally, or produced in recombinant expression systems. Recombinant production of membrane proteins in bacterial (e.g. *E. coli*) and insect cell (e.g. *Sf9*) systems is widely used due to the high expression rate and easy handling (Shirzad-Wasei et al., 2015). In addition, first approaches using cell-free expression systems for protein expression and incorporation into nanodiscs were already carried out (Lyukmanova et al., 2012). To obtain the correct posttranslational modifications and native folding of membrane proteins of human origin, human cell cultures (e.g. HEK293) are also utilized as expression system (Leitz et al., 2006; Mak et al., 2017; Mitra et al., 2013). However, an additional, time-consuming step of membrane isolation is applied if human cell lines were used as expression system.

The choice of detergent as well as of additional phospholipids is dependent on properties of the membrane protein of interest and is widely discussed in the literature (Chattopadhyay et al., 2015; Goddard et al., 2015; Seddon et al., 2004). Our previous publication presented a new approach using natural phospholipids of the plasma membrane to fill the nanodiscs without addition of synthetic lipids (Mak et al., 2017). At the same time, the solubilization step is kept as short as possible to reduce incubation time of membrane proteins in detergent. In respect of applying nanodisc technology for routine diagnostics, the nanodisc generation process is speeded up and modified for the use of only conventional laboratory equipment.

3.3.3. Applications of nanodisc technology

The classical application of nanodisc technology remains the stabilization and reconstitution of membrane proteins for characterization and structure determination in aqueous solution. A large number of membrane proteins from different protein families with various numbers of transmembrane domains were already successfully incorporated into nanodiscs and analyzed, e.g. protective antigen (PA) (Akkaladevi et al., 2015), enzyme cytochrome P450 3A4 (CYP3A4) (Baas et al., 2004), virulence-related outer membrane protein X (OmpX) (Hagn et al., 2013), neurotensin receptor 1 (NTS1) (Inagaki et al., 2013), anthrax toxin pore (Vernier et al., 2009), light-harvesting complexes (LHC) (Pandit et al., 2011) and bacteriorhodopsin (bR) (Orwick-Rydmark et al., 2012), just to name a few. By variation of the MSP length, nanodiscs could be either used for single-pass transmembrane proteins (e.g. CD4) (Gluck et al., 2011) as well as for large multimeric membrane protein complexes (e.g. NOMPC) (Jin et al., 2017) (Fig 8).

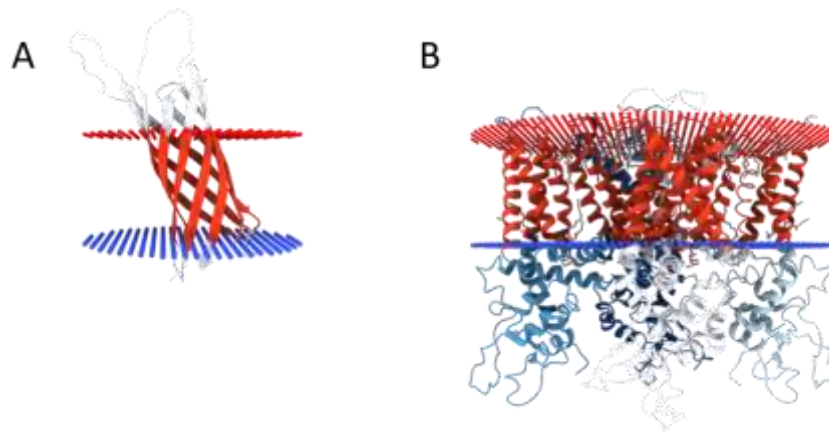


Figure 8: Resolved protein structures using nanodisc technology. A: 16-kDa OmpX from *Escherichia coli*, structure determination with NMR (PDB ID 2M06) (Hagn et al., 2013). B: 302-kDa TRPV1 from *Rattus norvegicus*, with EM (PDB ID 5IRZ) (Gao et al., 2016).

A large number of interaction studies and kinetic analysis were performed with membrane proteins incorporated into nanodisc and their binding partners, for example SecYEG channel (Alami et al., 2007), human adenosine (A2A) receptor (Bocquet et al., 2015), cholera toxin binding to glycolipid receptor GM1 (Borch et al., 2008) and binding of monoclonal antibodies to CD4 (Gluck et al., 2011).

This technology was also applied to generate a drug screening platform for cytochrome P450 3A3 (Das, Zhao, Schatz, Sligar, & Van Duyne, 2009), a membrane protein library from *E. coli* (Marty et al., 2013) and mammalian cells (Roy et al., 2015).

Two novel, innovative approaches regarding drug discovery were reported. (Sheng et al., 2010) tested acetylcholine receptor (AChR) incorporated into nanodiscs to adsorb autoantibodies in myasthenia gravis *in vivo*. First experiments were performed in mice models with intravenous injection of nanodiscs with no obvious organ toxicity observed. The second approach is to use nanodiscs as formulation for vaccines in personalized cancer immunotherapy, which is also already successfully tested *in vivo* in a mice model (Kuai et al., 2017).

Various analytical methods for structural and functional elucidation such as nuclear magnetic resonance spectroscopy (Hagn et al., 2013; Mors et al., 2013), electron microscopy (Akkaladevi et al., 2015; Pandit et al., 2011; Vernier et al., 2009), mass spectrometry (Marty et al., 2013; Roy et al., 2015), surface plasmon resonance spectroscopy (Bocquet et al., 2015; Borch et al., 2008; Gluck et al., 2011), analytical ultracentrifugation (Alami et al., 2007; Inagaki et al., 2013), dynamic light scattering (Inagaki et al., 2013; Vernier et al., 2009), single molecule fluorescence spectroscopy (Nath et al., 2008; Whorton et al., 2007) and single-molecule force spectroscopy (Zocher et al., 2012) have been successfully applied to nanodiscs.

3.4. Aim of the thesis

The aim of this PhD thesis was the development of *in vitro* diagnostic assays to quantitatively estimate anti- β 1AR autoantibodies in patients with diagnosis of dilative cardiomyopathy. The biggest challenge in detection of pathological autoantibodies binding and stimulating the beta-1 adrenergic receptor in human samples is the presentation of the native conformational epitope of the receptor. This difficulty could be circumvented with the nanodisc technology, which reconstitutes and stabilizes the beta-1 adrenergic receptor in a biomimetic membrane environment.

Within this scope, the standard nanodisc generation protocol with purified, recombinant proteins overexpressed in *E. coli* (Sligar lab) should be adapted and optimized for cell lysate directly from HEK293 cell lines without membrane isolation or further purification steps. Process optimization regarding choice of detergent, MSP variant, PEG-PE concentration, amount of Bio-Beads and other reaction components should be performed and verified. In respect of a possible application of nanodisc technology in the routine autoantibody diagnostics, this protocol should also be time- and cost- optimized. Nanodiscs generated according to a sophisticated protocol should be characterized using different analytical methods. First approaches concerning scale up and storage should be carried out.

In the second part of the thesis, nanodiscs should be generated according the optimized protocol established in the first part, incorporating beta-1 adrenergic receptor directly from human HEK293 cells. Generated nanodiscs and more importantly the incorporated receptor should be further analyzed and characterized, especially regarding the folding and the functionality of the receptor to achieve a native-like and stable presentation of the conformational epitope for autoantibody binding. Assay development should be carried out with β 1AR-nanodiscs in different assay formats, binding affinity and kinetics should be further characterized. With the final assay set-up, recruited patient samples with dilated cardiomyopathy as well as healthy controls should be measured. Estimated results should be analyzed statistically and evaluated clinically regarding a possible standardization and reliability for clinical diagnostic testing in the future. The specificity and sensitivity of the assay should be discussed by analyzing the clinical metadata of involved individuals. Correlation analysis should be done between the nanodisc assay and other assays detecting anti- β 1AR antibodies.

4. Experimental Section

4.1. Materials

4.1.1. Chemicals

Chemical	Manufacturer
1,2-distearoyl- <i>sn</i> -glycero-3-phospho-ethanolamine-N-[methoxy-(polyethylene glycol)-2000] (PEG-PE)	Avanti POLAR LIPIDS (Alabasta, AL, USA)
1,4-Dithiothreitol (DTT)	Sigma-Aldrich (St. Louis, MO, USA)
3,3',5,5'-Tetramethylbenzidine (TMB)	Sigma-Aldrich (St. Louis, MO, USA)
Acrylamid/Bis Solution 37.5:1, 40%	Bio-Rad (Hercules, CA, USA)
Alprenolol hydrochloride	Sigma-Aldrich (St. Louis, MO, USA)
Alprenolol-agarose	CellMosaic (Woburn, MA, USA)
Amersham Full-range rainbow molecular weight marker	GE Healthcare (Little Chalfont, GB)
Ammonium acetate	Sigma-Aldrich (St. Louis, MO, USA)
Ammonium persulfate (APS)	Roth (Karlsruhe, Germany)
Ampicillin sodium salt	Roth (Karlsruhe, Germany)
Bio-Beads SM-2 adsorbent	Bio-Rad (Hercules, CA, USA)
Bovine serum albumin (BSA)	Sigma-Aldrich (St. Louis, MO, USA)
Brilliant blue R	Sigma-Aldrich (St. Louis, MO, USA)
Digitonin	Sigma-Aldrich (St. Louis, MO, USA)
Dimethyl sulfoxide (DMSO)	Sigma-Aldrich (St. Louis, MO, USA)
Disodium hydrogen phosphate (Na ₂ HPO ₄)	Sigma-Aldrich (St. Louis, MO, USA)
Dulbecco's modified Eagle medium (DMEM), high glucose, GlutaMAX™ supplement, pyruvate	Thermo Fisher Scientific (Waltham, MA, USA)
D-Sorbitol	Sigma-Aldrich (St. Louis, MO, USA)
Dulbecco's phosphate-Buffered saline (DPBS)	Sigma-Aldrich (St. Louis, MO, USA)
Ethanol	Sigma-Aldrich (St. Louis, MO, USA)
Ethylenedinitrilotetraacetic acid disodium salt dehydrate (EDTA, Titriplex III)	Merck (Darmstadt, Germany)
Fetal bovin serum (FBS)	Thermo Fisher Scientific (Waltham, MA, USA)
GFP-Trap (uncoupled protein)	ChromoTek GmbH, (Planegg-Martinsried, Germany)
GFP-Trap Magnetic Beads	ChromoTek GmbH, (Planegg-Martinsried, Germany)
Glycerol	Sigma-Aldrich (St. Louis, MO, USA)
Glycine	Merck (Darmstadt, Germany)
Hydrochloric acid (HCl), 37%	Sigma-Aldrich (St. Louis, MO, USA)
Magnesium chloride hexahydrate (MgCl ₂ x 6 H ₂ O)	Merck (Darmstadt, Germany)

Membrane scaffold protein 1D1 (MSP1D1)	Sigma-Aldrich (St. Louis, MO, USA)
Membrane scaffold protein 1E3D1 (MSP1E3D1)	Sigma-Aldrich (St. Louis, MO, USA)
n-Dodecyl- β -D-maltoside (DDM)	Thermo Fisher Scientific (Waltham, MA, USA)
Potassium carbonate (K_2CO_3)	Merck (Darmstadt, Germany)
Potassium chloride (KCl)	Roth (Karlsruhe, Germany)
Potassium dihydrogen phosphate (KH_2PO_4)	Merck (Darmstadt, Germany)
Potassium sulfate (K_2SO_4)	Merck (Darmstadt, Germany)
Protease inhibitor mini tablets, EDTA-free	Thermo Fisher Scientific (Waltham, MA, USA)
PureCube Alprenolol-agarose	Cube Biotech (Monheim, Germany)
Puromycin	InvivoGen (San Diego, CA, USA)
Quick start Bradford 1x dye reagent	Bio-Rad (Hercules, CA, USA)
Restore western blot stripping buffer	Thermo Fisher Scientific (Waltham, MA, USA)
Roti-Blue quick	Roth (Karlsruhe, Germany)
Skim milk powder	Sigma-Aldrich (St. Louis, MO, USA)
Sodium acetate (CH_3COONa)	Sigma-Aldrich (St. Louis, MO, USA)
Sodium chloride (NaCl)	Merck (Darmstadt, Germany)
Sodium dodecyl sulphate (SDS)	Sigma-Aldrich (St. Louis, MO, USA)
Sodium hydrogen carbonate ($NaHCO_3$)	Merck (Darmstadt, Germany)
Sodium hydroxide pellets (NaOH)	Merck (Darmstadt, Germany)
Tetramethylethylenediamine (TEMED)	Bio-Rad (Hercules, CA, USA)
Tris(hydroxymethyl)aminomethane (Tris)	Merck (Darmstadt, Germany)
Tris(hydroxymethyl)aminomethane hydrochloride	Merck (Darmstadt, Germany)
Trypan blue (0.4%)	Thermo Fisher Scientific (Waltham, MA, USA)
Tween-20	Sigma-Aldrich (St. Louis, MO, USA)

4.1.2. Buffers, media and solutions

Buffer	Concentration	Chemical
Cell Lysis Buffer, pH 7.5	50 mM	Tris/HCl
	300 mM	NaCl
	1% (w/v)	DDM
	1 tablet for 10 mL	Protease Inhibitor Mini Tablet
DMEM+++	1 x	DMEM high glucose, GlutaMAX™ Supplement, pyruvate
	10%	FBS
	100 units/mL	Penicillin
	100 μ g/mL	Streptomycin
EM Buffer, pH 7.5	10 mM	Tris/HCl
	150 mM	NaCl
	0.5 mM	EDTA

FPLC Running Buffer, pH 7.4	10 mM	Na ₂ HPO ₄ /HCl
	150 mM	NaCl
PBS Buffer, pH 7.4	10 mM	Na ₂ HPO ₄ /HCl
	2.6 mM	KCl
	138 mM	NaCl
	1.8 mM	KH ₂ PO ₄
PBS-T, pH 7.4	1x	PBS Buffer
	0.05% (v/v)	Tween-20
Sonication Buffer, pH 7.2	340 mM	Sorbitol
	10 mM	HEPES
	1 tablet for 10 mL	Protease Inhibitor Mini Tablet
Alprenolol Magnetic Beads Affinity Purification		
Wash Buffer, pH 7.4	10 mM	Tris/HCl
	100 mM	NaCl
	50 μM	DTT
Elution Buffer, pH 7.4	1x	Wash Buffer
	20 mM	Alprenolol
Dounce Homogenization		
Dounce Buffer, pH 7.6	10 mM	Tris/HCl
	0.5 mM	MgCl ₂
	1 tablet for 10 mL	Protease Inhibitor Mini Tablet
Hypotonic Buffer, pH 8.0	5 mM	KH ₂ PO ₄
Tonicity Restoration Buffer, pH 7.6	10 mM	Tris/HCl
	0.5 mM	MgCl ₂
	600 mM	NaCl
ELISA		
PBS-T, pH 7.4	1x	PBS Buffer
	0.05% (v/v)	Tween-20
Blocking Buffer	1x	PBS Buffer
	5% (w/v)	Skim Milk Powder

GFP-Trap Magnetic Beads Affinity Purification, Co-IP	Concentration	Chemical
GFP-Trap Wash Buffer, pH 7.5	10 mM	Tris/HCl
	150 mM	NaCl
	0.5 mM	EDTA
GFP-Trap Elution Buffer, pH 2.5	0.2 mM	Glycine/HCl
GFP-Trap Neutralisation, pH 10.4	1 M	Tris/HCl

SDS-PAGE	Concentration	Chemical
Loading Buffer (3x), pH 6.8	30% (w/v)	Glycerol
	6% (w/v)	SDS
	0.03% (w/v)	Brilliant blue R
	187.5 mM	Tris/HCl
	150 mM	1,4-Dithiothreitol
Upper Buffer (for Stacking Gel), pH 6.7	500 mM	Tris/HCl
	0.4% (w/v)	SDS
Lower Buffer (for Running Gel), pH 8.8	1.5 mM	Tris/HCl
	0.4% (w/v)	SDS
SDS Running Buffer	25 mM	Tris
	192 mM	Glycine
	1% (w/v)	SDS

SPR	Concentration	Chemical
Immobilization Buffer, pH 5.5	10 mM	Sodium acetate
Running Buffer, pH 7.4	1x	FPLC Buffer
	0.05%	Tween-20
Regeneration Solution 1, pH 1.5	100 mM	Glycine/HCl
Regeneration Solution 2, pH 13	50 mM	NaOH
	1 M	NaCl

Western Blot	Concentration	Chemical
Transfer Buffer	25 mM	Tris
	192 mM	Glycine
	0.0001%	SDS
	20%	Methanol
TBS-T	20 mM	Tris
	500 mM	NaCl
	0.2%	Tween-20
Blocking Buffer	5% (w/v)	Skim Milk Powder in TBS-T

4.1.3. Antibodies

Antigen	ID	Species	Clonality	Modification	Manufacturer
β 1AR	Ab3442	rabbit	polyclonal		Abcam (Cambridge, MA, USA)
β 1AR	MAB23-6-7	mouse	monoclonal		Research Group of Prof. Jahns, Department of Internal Medicine I, Universitätsklinikum Würzburg (Würzburg, Germany)
β 1AR	huMAB23-6-7	mouse	monoclonal	humanization	Research Group of Prof. Jahns, Department of Internal Medicine I, Universitätsklinikum Würzburg (Würzburg, Germany)
GFP	Ab290	rabbit	polyclonal		Abcam (Cambridge, MA, USA)
GFP	Ab32146	rabbit	monoclonal [E385]		Abcam (Cambridge, MA, USA)
GFP	JL-8	mouse	monoclonal		Clontech (Mountain View, CA, USA)
His-Tag	THE His-Tag Antibody	mouse	monoclonal	HRP	Genscript (Piscataway, NJ, USA)
human CD147	MAB972	mouse	monoclonal		R&D Systems (Minneapolis, MN, USA)
Human IgG	P0214	rabbit	polyclonal	HRP	Dako (Glostrup, Denmark)
mouse IgG	P1318HRP	goat	polyclonal	HRP	Acris (Rockville, MD, USA)
mouse IgG	Ab97023	goat	polyclonal	HRP	Abcam (Cambridge, MA, USA)
MT-CO2	Ab91317	rabbit	polyclonal		Abcam (Cambridge, MA, USA)
PEG	THE PEG Antibody	mouse	monoclonal		Genscript (Piscataway, NJ, USA)
Penta-His	34660	mouse	monoclonal		Qiagen (Hilden, Germany)
rabbit IgG	Ab16284	donkey	polyclonal	HRP	Abcam (Cambridge, MA, USA)
testosterone	BM2076	mouse	monoclonal		Acris (Rockville, MD, USA)

4.1.4. Cultured human cell lines

Cell line	Manufacturer
HEK293, ACC 305	DSMZ (Braunschweig, Germany)
HEK293: β 1AR-YFP	construct from Research Group of Prof. Boege, Central Institute of Clinical Chemistry and Laboratory Medicine, Heinrich Heine University Düsseldorf
HEK293: β 1AR-YFP/CFP	construct from Research Group of Prof. Boege, Central Institute of Clinical Chemistry and Laboratory Medicine, Heinrich Heine University Düsseldorf

4.1.5. Kits

Kit	Manufacturer
Amine coupling kit	GE Healthcare (Little Chalfont, GB)
1-Ethyl-3-(3-dimethylaminopropyl)carbodiimide hydrochloride (EDC)	
N-Hydroxysuccinimide (NHS)	
Ethanolamine-HCl	
BIA maintenance kit	GE Healthcare (Little Chalfont, GB)
High MW gel filtration calibration kit	GE Healthcare (Little Chalfont, GB)
Quick Start BSA standard set	Bio-Rad (Hercules, CA, USA)
SuperSignal West Dura Extended duration substrate	Thermo Fisher Scientific (Waltham, MA, USA)

4.1.6. Consumables

Consumable	Manufacturer
96-well tissue culture test plate	TPP (Trasadingen, Switzerland)
Amicon ultra centrifugal filters (10k, 30k)	Merck Millipore (Darmstadt, Germany)
Carestream SO-163 film	Kodak (Rochester, NY, USA)
Immobilon-P transfer membrane, PVDF	Merck Millipore (Darmstadt, Germany)
Luminescence spectroscopy cells	PerkinElmer (Waltham, MA, USA)
Mobicol classic	MoBiTec (Goettingen, Germany)
Mobicol Filter 90 µm pore size	MoBiTec (Goettingen, Germany)
Neubauer counting chamber	Brand (Wertheim, Germany)
Nunc MaxiSorp flat-bottom 96 well plate	Thermo Fisher Scientific (Waltham, MA, USA)
Polycarbonate centrifuge tubes	Beckman Coulter (Brea, CA, USA)
Quartz SUPRASIL Ultra-micro Cuvette	PerkinElmer (Waltham, MA, USA)
Sensor chip CM5	GE Healthcare (Little Chalfont, GB)
Superdex 200 increase 10/300	GE Healthcare (Little Chalfont, GB)
T75 tissue culture flask	TPP (Trasadingen, Switzerland)

4.1.7. Instruments

Equipment	Manufacturer
Alpha 1-4 freeze dryer	Martin Christ (Osterode am Harz, Germany)
Amersham ÄKTA FPLC P-920	GE Healthcare (Little Chalfont, GB)
UPC-900 monitor	
P-920 pump system	
Frac-900 fraction collector	
Analytic Balance AC 120 S	Sartorius (Göttingen, Germany)
Basic pH meter PB-11-P11	Sartorius (Göttingen, Germany)
Biacore X100	GE Healthcare (Little Chalfont, GB)

BioTek ELx808 absorbance reader	Biotek (Bad Friedrichshall, Germany)
Centrifuge 5415 R	Eppendorf (Hamburg, Germany)
CO ₂ Incubator C150 (E2)	Binder (Tuttlingen, Germany)
DM IL LED microscope	Leica Microsystems (Wetzlar, Germany)
Dounce grind tube, Pestle A and B	Kimble Chase (Vineland, NJ, USA)
DynaMag magnet	Thermo Fisher Scientific (Waltham, MA, USA)
Electron microscope JEM 100CX	JEOL (Tokyo, Japan)
ESE Quant Tube Scanner	Qiagen (Hilden, Germany)
EVOS FL fluorescent microscope	Thermo Fisher Scientific (Waltham, MA, USA)
Flextight X5 scanner	Hasselblad (Gothenburg, Sweden)
Intas advanced western blot imager	Intas Science Imaging Instruments
LS 50 B luminescence spectrometer	PerkinElmer (Waltham, MA, USA)
Mini-PROTEAN tetra cell system	Bio-Rad (Hercules, CA, USA)
Mini trans tank blotting system	
Mr. Frosty cryo freezing container	Thermo Fisher Scientific (Waltham, MA, USA)
NanoDrop 2000 spectrophotometer	Thermo Fisher Scientific (Waltham, MA, USA)
Optima Max ultracentrifuge	Beckman Coulter (Brea, CA, USA)
RCT Basic magnetic stirrer	IKA (Staufen im Breisgau, Germany)
Rotina 360R centrifuge	Hettich (Tuttlingen, Germany)
Thermomixer comfort	Eppendorf (Hamburg, Germany)
Ultrasound sonicator Sonorex Super 10P	Bandelin (Berlin, Germany)
Vortex-Genie 2	Scientific Industries (Bohemia, NY, USA)
Waterbath WNB 10	Memmert (Schwabach, Germany)

4.1.8. Software

Software	Manufacturer
Biacore X100 control software	GE Healthcare (Little Chalfont, GB)
Biacore X100 evaluation software	GE Healthcare (Little Chalfont, GB)
ChemoStar imager	Intas Science Imaging Instruments (Göttingen, Germany)
FL WinLab	PerkinElmer (Waltham, MA, USA)
Gen5	Biotek (Bad Friedrichshall, Germany)
Image Studio Lite V4.0	LI-COR Biosciences (Lincoln, NE, USA)
Inkscape	Free Software Foundation (Boston, MA, USA)
NanoDrop 2000/2000c software	Thermo Fisher Scientific (Waltham, MA, USA)
OriginPro 8.5.1	Origin (Northampton, MA, USA)
Fluorescence SpectraViewer	Thermo Fisher Scientific (Waltham, MA, USA)
Tube Scanner Studio	Qiagen (Hilden, Germany)
Unicorn 4.0	GE Healthcare (Little Chalfont, GB)

4.2. Methods

4.2.1. Determination of protein concentration

Protein concentration of cell lysates was determined via Bradford Assay according to the manufacturer's protocol. Prior to the measurement, the impact of used detergent in the Lysis Buffer was determined by measurement of the blank sample without protein component. 5 μ L of cell lysates (typically in 1:5 or 1:10 dilutions with water), as well as the BSA standard, were pipetted in duplicate into 96-well plates. 250 μ L of Quick Start Bradford 1x Dye Reagent were added to the sample and BSA standard. After incubation of 5 min at RT, the signal was measured with the BioTek ELx808 Absorption Reader at 595 nm and the protein concentration was calculated with the Gen5 software.

NanoDrop 2000 was used to determine the concentration of isolated IgGs from patient serum. The absorbance was measured at 280 nm, as well as at 260 nm to examine the sample purity (A260/A280 ratio). The IgG concentration was calculated with the NanoDrop 2000/2000c software using pre-configured method for IgG sample.

4.2.2. Cell culture

HEK293 cells, as well as HEK293: β 1AR-YFP cells and HEK293: β 1AR-YFP/CFP cells, were cultured in DMEM+++ medium (DMEM (1x) + GlutaMAX-I, 10% fetal bovine serum (FBS), 100 units/mL penicillin, 100 μ g/mL streptomycin) under 5% CO₂ atmosphere at 37 °C. For overexpression cell lines, 0.4 g/mL puromycin was used for selection.

To unfreeze cells from liquid nitrogen, the cryo tube was thawed on ice. After slowly adding 1 mL of medium, the cell suspension was transferred into a 15-mL falcon tube, filled to 5 mL with medium and centrifuged (400 x *g*, 5 min, 20 °C). The supernatant containing DMSO was removed, the pellet resuspended and transferred into a T75 flask. The medium was changed 24 h later. For overexpression cell lines, the selection antibiotic puromycin was added one week after thawing.

To freeze cells for further use, the cryo freezing container was pre-cooled at 4 °C. Three parts of DMEM+++ were mixed with one part FBS and one part DMSO. The freezing solution was prepared freshly and stored on ice till use. Cells were counted as described below and pelleted at 400 x *g* for 5 min and resuspended in DMEM+++ according to the cell number to achieve a cell number of 5 million in 250 μ L medium. 250 μ L freezing solution were added to the cells in medium and mixed by pipetting. Cryo tubes containing cells were placed into the cryo freezing container and stored at -80 °C overnight. The cryo tubes were transferred into container with liquid nitrogen 24 h later.

To examine the morphology as well as the expression level of YFP-tagged β 1AR, cells were routinely checked under light microscope and fluorescence microscope.

4.2.2.1. Splitting and counting

Cells were split with a ratio of 1:3 to 1:7 according to the confluence of cells, which was estimated by light microscopy. The old cell medium was carefully discarded and the cells were washed with 10 mL DPBS. After removing DPBS, the cells were resuspended in fresh DMEM+++ by pipetting the medium up and down and thus detaching the cells from the coated surface of the flask by shearing forces. Trypsin was not used to detach the cells in order to reduce possible proteolysis of membrane proteins. Required volume of the cell suspension, according to the splitting rate, was transferred to a new cell culture flask with fresh DMEM+++.

Cell number in the cell suspension was determined using a Neubauer counting chamber. Cells were stained 1:2 or 1:4 with 0.4% Trypan Blue and pipetted into the counting chamber. Four of the big squares were counted using the light microscope. The total cell number in the sample was calculated considering the dilution rate and the chamber volume.

4.2.2.2. Harvest and lysis

To harvest HEK 293 cells, culture medium was removed 48 h after splitting and the cell layer was washed once with DPBS. Cells were completely detached by resuspension in fresh medium and spun down for 5 min at 4 °C and 500 x *g*. The resulting cell pellet was washed with DPBS and recentrifuged. Subsequently, the cell pellet was used for either membrane isolation or directly for nanodisc generation.

Cell Lysis Buffer was complemented with protease inhibitor tablet (1 tablet/10 mL) and DDM (10 mg/mL). The cell pellet was resuspended in 500 μ L Cell Lysis Buffer per 10 million cells. The suspension was transferred into an Eppendorf tube and incubated for 10 min on ice with occasional inversion. After incubation, unlysed cells as well as DNA and cell organelles were removed by centrifugation (16000 x *g*, 15 min, 4 °C) and the supernatant containing the target proteins was collected.

4.2.3. Isolation of cell membrane using Dounce homogenization

10 million HEK293 cells were pelleted and resuspended in 3 mL ice-cold Dounce Buffer and incubated on ice for 10 min. The cell suspension was then transferred to a Dounce grind tube and mechanically lysed by stroking 15 times with pestle A and 25 times with pestle B. 1 mL Tonicity Restoration Buffer was added to the cell lysate. Nuclei and non-destroyed cells were pelleted at 500 x *g* at 4 °C for

15 min and 40 μL of 0.5 M EDTA (pH 8) were added to the collected supernatant. Afterwards, the supernatant was transferred to polycarbonate centrifuge tubes and ultracentrifuged in an Optima Max ultracentrifuge at 100000 $\times g$ at 4 $^{\circ}\text{C}$ for 45 min. The membrane pellet was resuspended with 125 μL Lysis Buffer for each tube. Insoluble fractions were pelleted with 16000 $\times g$ for 15 min at 4 $^{\circ}\text{C}$ and the supernatant was used for nanodisc preparation.

4.2.4. Nanodisc generation

30 mg SM-2 adsorbent Bio-Beads were equilibrated in 800 μL FPLC Buffer or EM Buffer while shaking at RT for at least 2 h in glass tubes. The buffer was then carefully discarded from the pre-incubated bio-beads. PEG-PE was dried with nitrogen and vacuum, and then dissolved in 6% OG to a final concentration of 10 mg/mL.

For nanodisc preparation directly from whole cells, the cell pellet was incubated in Lysis Buffer for 10 min on ice. After the incubation, the cell lysate was centrifuged for 15 min at 4 $^{\circ}\text{C}$ and 16000 $\times g$. The protein concentration in the supernatant was determined photometrically by use of the Bradford assay against a BSA standard. 20 μg of cell lysate or isolated cell membranes were mixed with 50 μg MSP and 40 μg PEG-PE as stabilizing agent (corresponding to a ratio of 20 PEG-PE molecules per nanodisc), then filled up with Lysis Buffer to a final volume of 60 μL . The reaction mixture was incubated with Bio-Beads for 3 h at 4 $^{\circ}\text{C}$ under gentle agitation, thereby removing the detergent and inducing the self-assembly of the nanodiscs.

4.2.5. Size exclusion chromatography

SEC was performed using an Amersham ÄKTA FPLC P-920 system with a Superdex 200 Increase 10/300 GL column using FPLC Buffer or EM Buffer with a flow rate of 0.75 mL/min. The protein absorbance was monitored at 280 nm with the integrated UV-900 detector. For calibration and estimation of molecular weight, the high molecular weight gel filtration calibration kit was used. For further examination, SEC fractions were concentrated with Amicon Ultra-0.5 mL Centrifugal Filters MWCO 10kDa.

4.2.6. Pull-down experiments

4.2.6.1. Alprenolol Magnetic Beads

To isolate bioactive β1AR -nanodiscs from the reaction mixture, 200 μL PureCube Alprenolol Magnetic Beads (resin bed volume 50 μL) were washed three times with 150 μL Wash Buffer and magnetically separated for 3 min, the supernatant was collected (fraction BE: Beads Equilibration). Nanodiscs were diluted with Wash Buffer to a final volume of 150 μL , mixed with the pre-washed Alprenolol

Beads and incubated on an end-over-end mixer for 30 min at RT. Non-bound particles were removed from the beads by magnetic separation for 3 min (fraction FT: Flow-Through). Afterwards, the beads were washed three times with 150 μ L Wash Buffer (fraction: W1, W2 and W3) and active β 1AR-nanodiscs were eluted twice with 150 μ L Elution Buffer by end-over-end mixing for 20 min at RT (fraction: E1 and E2). For the complete removal of particles from the magnetic beads, 150 μ L SDS Loading Buffer (3x) were added to the beads and heated for 10 min at 95 $^{\circ}$ C to denature protein components (fraction: SDS). Collected fractions were analyzed with fluorescence spectroscopy and afterwards concentrated using Amicon Ultra-0.5 mL Centrifugal Filters MWCO 30kDa and analyzed via SDS-PAGE and WB.

4.2.6.2. GFP-Trap Magnetic Beads

β 1AR-nanodiscs with YFP- as well as YFP/CFP-Tag could be purified with GFP-Trap Magnetic Beads. 50 μ L of bead slurry (bed volume: 25 μ L) were equilibrated with 500 μ L ice-cold Wash Buffer and magnetically separated for 3 min (fraction BE). Generated β 1AR-nanodiscs were mixed with Wash Buffer to a final volume of 500 μ L and incubated with pre-equilibrated GFP-Trap beads on an end-over-end mixer for 90 min at RT. Beads were separated magnetically and the supernatant was collected (fraction FT). Afterwards, the beads were washed three times with 500 μ L Wash Buffer (fraction W1, W2 and W3) and eluted with 100 μ L Elution Buffer by constantly pipetting up and down for 30 s and shaking at RT for 10 min. The supernatant was transferred to a new tube and 10 μ L Neutralization Buffer were added (fraction E1). For the complete removal of particles from magnetic beads, 100 μ L SDS Loading Buffer (3x) were added to the beads and heated for 10 min at 95 $^{\circ}$ C (fraction SDS). Collected fractions were analyzed with size exclusion chromatography, fluorescence spectroscopy or WB considering downstream experiments.

4.2.6.3. Co-Immunoprecipitation using GFP-Trap Magnetic Beads

Beside the affinity purification of β 1AR-nanodiscs, the GFP-Trap Magnetic Beads could also be used for co-immunoprecipitation, in which the β 1AR-nanodiscs were coated on the surface of GFP-Trap Magnetic Beads to enable the immunoprecipitation of binding IgGs from human samples.

50 μ L (25 μ L bed volume) bead slurry were equilibrated with 500 μ L ice-cold Wash Buffer and magnetically separated for 3 min (fraction BE). Generated β 1AR-nanodiscs were mixed with Wash Buffer to a final volume of 500 μ L and incubated with pre-equilibrated GFP-Trap beads on an end-over-end mixer for 90 min at 4 $^{\circ}$ C. Beads were separated magnetically and the supernatant was collected (fraction FT1) and washed twice with 500 μ L Wash Buffer (fraction W1 and W2). 10 μ g of monoclonal antibody MAB23-6-7, 10 μ g of monoclonal antibody BM2067, 100 μ g of ProtA/G-purified

human IgG sample as well as 1:10-diluted human serum sample in a final volume of 500 μ L were added to the beads and incubate end-over-end for 30 min at RT. The beads were magnetically separated for 3 min, the supernatant consisting of non-bound antibodies was collected (fraction FT2). Beads were washed again three times (fraction W3, W4 and W5) and eluted with 100 μ L Elution Buffer by constantly pipetting up and down for 30 s (fraction E1). For the complete removal of all specific and unspecific bound particles from the magnetic beads, 100 μ L SDS Loading Buffer (3x) were added to the beads and heated for 10 min at 95 °C and 600 rpm (fraction SDS). Collected fractions were concentrated with Amicon Ultra-0.5 mL Centrifugal Filters MWCO 30 kDa to a final volume of 50 μ L and further analyzed with fluorescence spectroscopy and Western Blot.

4.2.7. SDS-PAGE and Western Blot (WB)

SDS-PAGE was performed by use of a Mini-PROTEAN Tetra Cell system with 3% stacking gels and 10% to 15% separation gels. Samples were mixed with 3x Loading Buffer and heated up for 15 min at 95 °C. The run was carried out at 100 V until the protein front reached the border between stacking and running gel. Then, the voltage was turned up to 120 V and the proteins were separated until the separation in the desired molecular weight range was achieved.

For WBs on polyvinylidene difluoride (PVDF) membranes, a Mini Trans Tank Blotting system was used according to the manufacturer's instruction. The transfer was carried out at 0.3 mA for 1.5 h. After transfer, the membranes were washed with TBS-T for 10 min and then blocked over night at 4 °C with Blocking Buffer. After blocking, the membranes were washed with TBS-T three times for 10 min and incubated with the primary antibody for two hours at RT, followed by another three washing steps. Afterwards, a secondary antibody with a horse radish peroxidase (HRP) tag was added for one hour. For detection, membranes were incubated with SuperSignal WestDura Extended Duration Substrate for 5 min and recorded using an Intas Advanced Western Blot Imager. Quantification of band intensity was performed with Image Studio Lite Ver. 4.0, LI-COR Biosciences with background noise correction.

4.2.8. Enzyme-linked immunosorbent assay

The wells of a Nunc MaxiSorp flat-bottom 96 well plate were coated with 100 μ L of GFP-Trap solution with a final amount of 0.3 μ g/well in PBS. The plate was covered with an adhesive plastic film and incubated for 1 h at RT. After the incubation, the coating solution was removed and the plate was washed four times by filling the wells with 300 μ L PBS-T. The solutions were removed by flicking the plate over a sink. The remaining drops were removed by patting the plate on a paper towel. The remaining protein-binding sites in the coated wells were blocked by adding 300 μ L Blocking Buffer

per well. The plate was covered with an adhesive plastic film and incubated overnight at 4 °C. The blocking solution was removed by the next day and the plate was washed four times with 300 µL PBS-T. 100 µL 1:4-diluted β 1AR-nanodiscs were added into the wells and incubated for 1 h at RT. After washing the plate for four times, standards (huMAB23-6-7 in different concentrations, samples P71 and K37 as reference samples) and 1:250-diluted patient serum samples were added into the wells and incubated for 1 h at RT. The plate was again washed and incubated with 100 µL of 1:1000-diluted secondary antibody P0214 in Blocking Solution for 1 h at RT. After washing the plate, 100 µL of the substrate solution TMB were dispensed into each well for a further 30 min incubation step in the dark. The reaction was stopped by adding 50 µL of Stopping Solution and the absorbance of each well was measured at 450 nm using the BioTek ELx808 Absorbance reader. The read-out was given in optical density (OD), which equals the decadic logarithm of the absorbance.

4.2.9. Surface plasmon resonance spectroscopy

All SPR experiments were performed with a Biacore X100 using CM5 sensor chips at 25 °C.

To immobilize the GFP-Trap on the sensor surface, GFP-Trap was diluted to 50 µg/mL in 10 mM sodium acetate with pH 5.5. To activate the surface, EDC and NHS were mixed 1:1 and added to both reference and active flow cells with a flow rate of 10 µL/min for 7 min. After the activation, diluted GFP-Trap was loaded for 7 min with a flow rate of 10 µL/min, a signal increase of about 3000 RU was induced by the immobilization. Other available binding sites were deactivated with ethanolamine for 7 min with the same flow rate. The running buffer used for the immobilization is deionized filtered water.

After the immobilization, the running buffer was changed to FPLC Buffer with additional 0.05% Tween-20 to reduce unspecific binding on the sensor surface. Generated β 1AR-nanodiscs were added to the active flow cell in different concentrations and with different flow rates (5 µL/min, 10 µL/min and 30 µL/min) for different flow durations considering the aim of each experiment.

For determination of binding events, samples (commercial antibodies, MAB23-6-7, huMAB23-6-7, isolated patient IgGs and patient serum samples) in different concentrations were added to the captured β 1AR-nanodiscs. After the binding event, the sensor surface was regenerated with the Regeneration Solution 1.

For the determination of binding kinetic and affinity, β 1AR-nanodiscs were captured with a flow rate of 5 µL/min for 600 s. After the injection, 1200 s were waited to generate a stable baseline for the antibody binding. To reduce the mass transfer effect, huMAB23-6-7 (diluted in steps of 1:3 from 300

nM to 3.7 nM) was injected with a high flow rate of 30 $\mu\text{L}/\text{min}$ for 180 s and the dissociation was monitored for further 600 s. To regenerate the surface efficiently, a two-step regeneration procedure with low pH (Regeneration Solution 1: 100 mM glycine, pH 1.5) and high pH (Regeneration Solution 2: 50 mM NaOH, 1 M NaCl, pH 13) for each 135 s with a flow rate of 10 $\mu\text{L}/\text{min}$ was performed. The affinity and kinetic parameters were calculated with the Biacore X100 Evaluation Software. For kinetic measurements, the 1:1-binding model was used to calculate kinetic parameters.

4.2.10. Optical Methods

4.2.10.1. Fluorescence determination with ESE Quant Tube Scanner

Fluorescence activity of the cell lysate was controlled prior to nanodisc generation with the Tube Reader. Samples were transferred to PCR reaction tubes with a minimum volume of 80 μl per tube. Fluorescence activity of the YFP-Tag attached to β1AR was measured using the pre-configured channel for fluorescence dye Carboxyfluorescein (FAM) by exciting the fluorophore at 494 nm and measuring the emission at 518 nm, which overlaps mostly the fluorescence spectrum of YFP (excitation at 485 nm, emission at 527 nm). Data was analyzed with the Tube Scanner Studio software.

4.2.10.2. Fluorescence spectroscopy

For measuring fluorescence activity after nanodisc generation with the fluorescence spectrometer (LS 50 B), a minimum sample volume of 100 μL was transferred into a quartz cuvette. The fluorophore YFP was excited at 485 nm, whereas the emission spectrum between 500 and 600 nm was scanned. CFP was excited at 350 nm, the emission spectrum between 375 and 545 nm was scanned. Fluorescence spectra were analyzed with the FL WinLab software.

4.2.10.3. Electron microscopy

Nanodiscs generated from HEK293 cell lysate in EM Buffer were adsorbed for 2 min onto carbon-coated grids that were glow discharged for 30 sec. Excess solution was blotted off, and the samples were stained negatively with uranyl acetate (5 μL 2% (w/v), 30 s). Electron micrographs were recorded at a nominal magnification of 50000 onto Carestream Kodak SO-163 film using a JEM 100CX electron microscope operated at 100 kV. Micrographs were digitized using a Flextight X5 Scanner. All TEM images were taken by Carsten Peters, Center for Integrated Protein Science Munich (CIPSM), Department Chemistry, TU München.

4.2.11. Patient assignment

Blood serum samples of cardiomyopathy patients were collected at the Heinrich Heine University Düsseldorf, Germany. Patient recruitment was approved by the human Ethics Committee of the medicine faculty, Heinrich Heine University Düsseldorf, Germany, with the registration ID 2016045065. The sample collection was performed in the division of cardiology, pulmonology and vascular Medicine, Medical Faculty, University Düsseldorf, Germany. Included were male and female patients of heart failure with a minimum age of 18 years, which undergo a treatment against heart failure. Excluded were patients with left ventricular assist device and patients after heart transplantation. An informed consent form was signed by each blood donor. Additionally to the routine blood sampling, 3 mL blood were gathered and used for further analysis. Information about previous medical history, medication and demographic data were acquired as well.

The control group used in this thesis is formed by healthy blood donors of the Bayerisches Rotes Kreuz (BRK).

4.2.12. Statistics

All data were analyzed with OriginPro 8.5.1, all results were presented as mean \pm SD if not stated otherwise. Statistical significance between groups was defined using one-way analysis of variance (ANOVA) and Pearson correlation analysis with p values < 0.05 .

5. Results and Discussion

In the first part of the section “Results and Discussion” genetically modified HEK293 cell lines which were used as expression systems for beta-1 adrenergic receptor fusion proteins were analyzed with transmission microscopy and fluorescence microscopy. Cell lysates were detected with fluorescence spectroscopy against the fluorescent Tags (**section 5.1.**).

The original nanodisc generation protocol with purified, recombinant proteins overexpressed in *E. coli* (Sligar lab) was simplified, adapted and optimized for cell lysate directly from HEK293 cell lines without membrane isolation or further purification steps (**section 5.2.**). Nanodiscs generated according to this optimized protocol were further characterized using different analytical methods. Results of first approaches concerning scale up and storage were analyzed and discussed.

In **section 5.3**, nanodiscs generated directly from human HEK293 cells overexpressing beta-1 adrenergic receptors were analyzed and characterized against the nanodisc generation itself and the folding and the functionality of the incorporated receptor.

Interactions between β 1AR-nanodiscs and antibodies were detected using different interaction assays. Antibody binding affinity and kinetics were further characterized with SPR (**section 5.4.**).

An ELISA assay was developed for the high throughput measurement of autoantibodies in human serum samples. With the optimized assay set-up, recruited patient samples with cardiomyopathy as well as healthy controls were detected against the autoantibody concentration, results and distributions were statistically analyzed and discussed regarding known clinical information about the patients (**section 5.5.**).

5.1. Characterization of applied human cell lines

Three HEK293 cell lines, wild type, β 1AR-YFP overexpression and β 1AR-YFP/CFP overexpression (β 1AR-FRET construct), were used as starting material for nanodisc generation. The overexpressing cell lines were kindly provided by the research group of Prof. Boege of the Central Institute of Clinical Chemistry and Laboratory Medicine, University of Düsseldorf. To generate the overexpressing cell lines, the fluorescence protein (YFP) was fused to the c-terminus of the human β 1AR. For the FRET-construct, an additional cyan fluorescence protein (CFP) was added into the third intracellular loop (IC3). These two fusion protein constructs were used to transfect HEK293 cells via the pMC plasmid. This resulted in an overexpression rate of 8 million β 1AR-binding sites/cell for YFP-fused receptor and 5 million binding sites/cell for YFP/CFP-fused construct (Bornholz et al., 2013). The morphology as

well as the expression level of β 1AR-constructs was routinely examined with light microscopy and fluorescence microscopy (Fig 9).

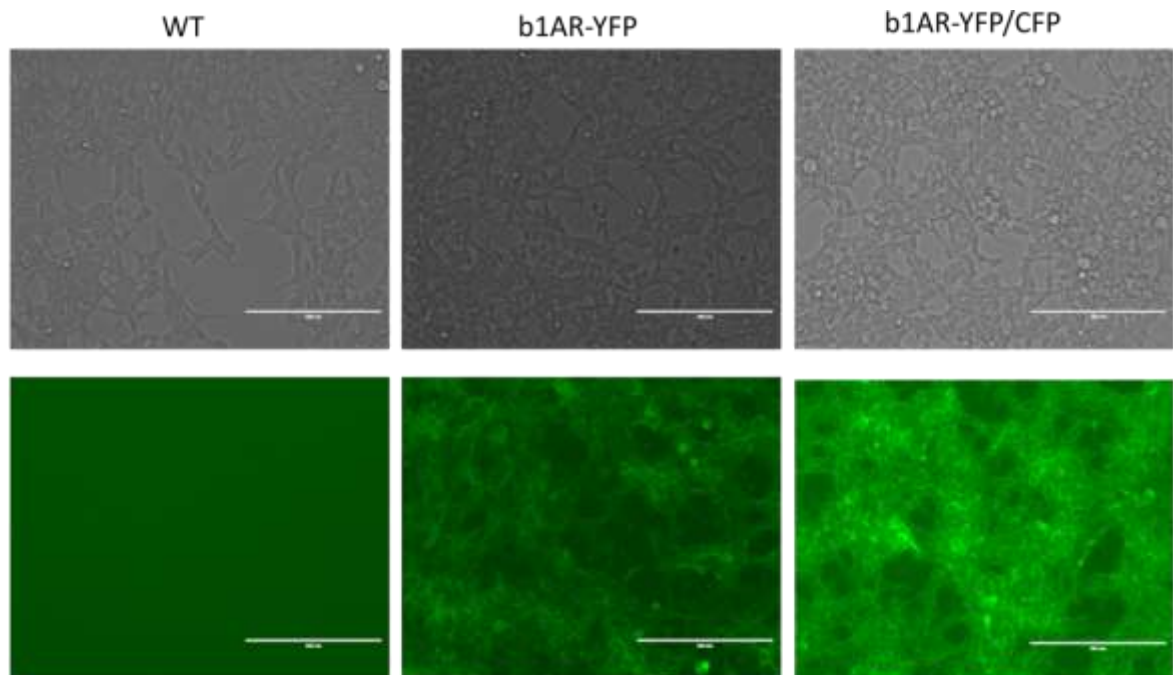


Figure 9: Transmission light microscopy (upper panel) and fluorescence microscopy (lower panel) images of applied HEK293 cell lines: wild type (WT), β 1AR-YFP overexpression and β 1AR-YFP/CFP overexpression cell lines. Images were taken in GFP channel with 20x objective, scale bar equals 200 μ m.

Once the cells were lysed, the soluble fraction of the cell lysate was analyzed with fluorescence spectroscopy detecting fluorophores CFP and YFP (fluorescence spectra in Fig 10A). For YFP detection, the fluorophore was excited at 485 nm, whereas the emission spectrum between 505 nm and 590 nm was scanned (Fig 10C). CFP was excited at 350 nm, the emission spectrum between 390 nm and 540 nm was scanned (Fig 10B). Cell lysate with overexpressed β 1AR-YFP/CFP could be detected in both YFP (emission peak at 527 nm) and CFP (emission peak at 480 nm) channels, whereas the β 1AR-YFP could only be observed in YFP channel, respectively.

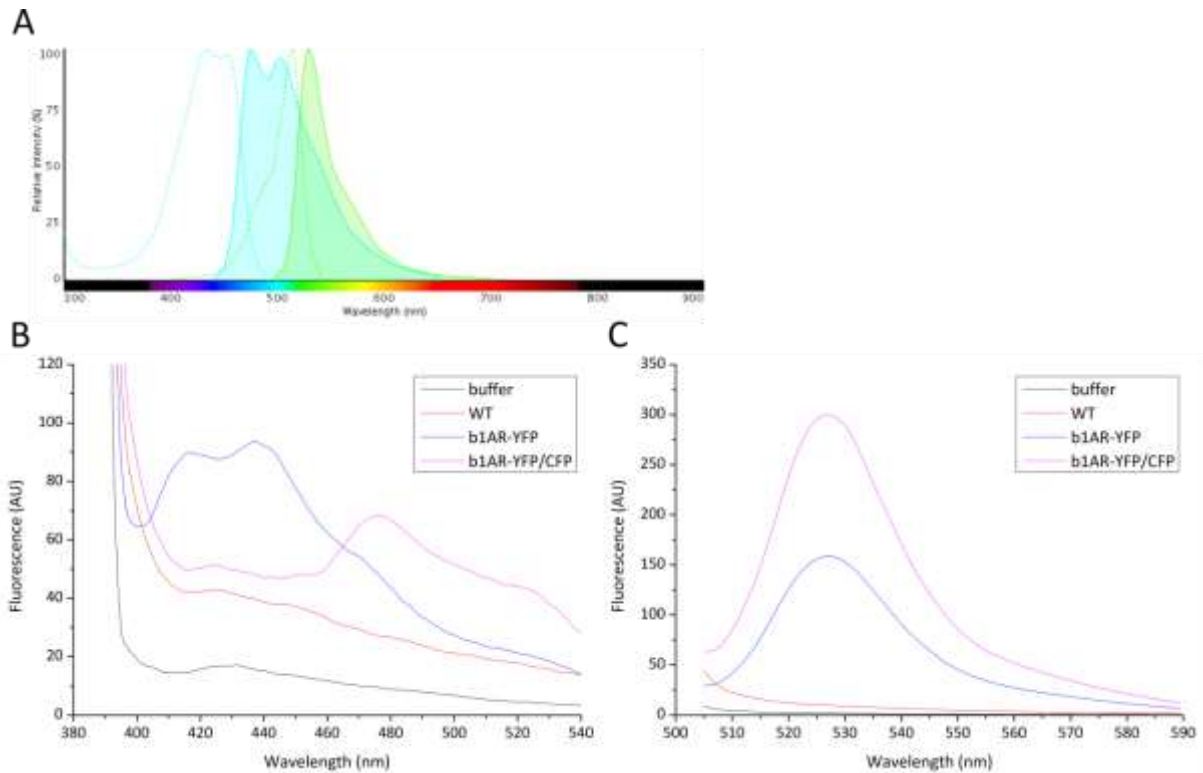


Figure 10: Fluorescence spectroscopy measurements of cell lysates. A: Excitation and emission spectra of CFP and YFP, generated with the software Fluorescence SpectraViewer. B: Fluorescence spectra of cell lysates in CFP channel. C: Fluorescence spectra of cell lysates in YFP channel.

Beside the cell morphology and the β 1AR-expression level of the cell lines, the cellular location of β 1AR fusion proteins was analyzed with fluorescence microscopy as well. As shown in Fig 11, the receptor of interest is expressed consistently on the cell surface, indicating the unimpaired stability and integration of the receptor in the membrane.

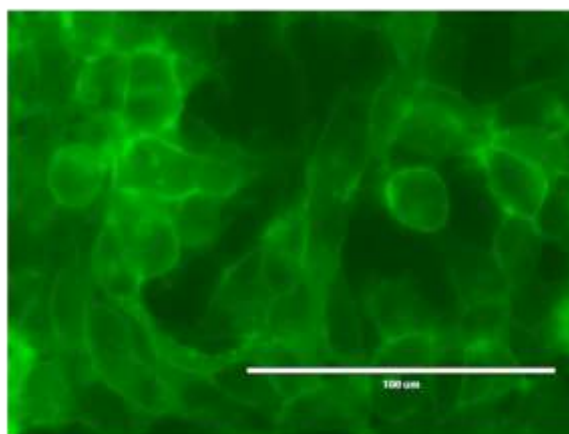


Figure 11: Fluorescence imaging of HEK293 cells overexpressing β 1AR-YFP. Image was taken in GFP channel with 40x objective, scale bar equals 100 μ m.

5.2. Characterization of the generated nanodiscs

The generation procedure of nanodiscs was optimized based on the protocol originally established in the Sligar group, which should be adapted to the HEK293 cell line and optimized for the required functional incorporation of beta-1 adrenergic receptor.

The standard protocol optimized in this thesis was used for nanodisc generation with HEK293 wild type cells, β 1AR-YFP and β 1AR-YFP/CFP overexpression cells as starting material, and used for downstream assays if not stated otherwise.

30 mg Bio-Beads were equilibrated in 800 μ L FPLC Buffer while shaking at RT for at least 2 h in glass tubes. The buffer was then carefully discarded from the pre-incubated Bio-Beads. To enhance the functionality of incorporated β 1AR, the time-consuming membrane isolation step was skipped and the cell pellet was directly incubated in Lysis Buffer for 10 min on ice and centrifuged for 15 min at 4 °C and 16000 x *g*. 20 μ g of cell lysate was mixed with 50 μ g MSP and 40 μ g PEG-PE, filled with Lysis Buffer to a final volume of 60 μ L. The reaction mixture was incubated with Bio-Beads for 3 h at 4 °C under gentle agitation, thereby removing the detergent and inducing the self-assembly of nanodiscs. If a large amount of nanodiscs was needed for downstream experiments, an appropriate number of this standard reaction was prepared and all generated nanodiscs were pooled together after the reaction.

5.2.1. Size exclusion chromatography

Nanodiscs generated with this protocol could be detected at the elution volume of 11.5 mL (Fig 12) in size exclusion chromatography (SEC) with a Superdex 200 10/300 GL column, which clearly differs from the peak of aggregated cell lysate in 1% DDM (elution volume 8.3 mL) and applied MSPs (elution volume 15 mL). Lipids and proteins seem to be completely incorporated spontaneously into nanodiscs, indicated by the absence of an aggregation peak.

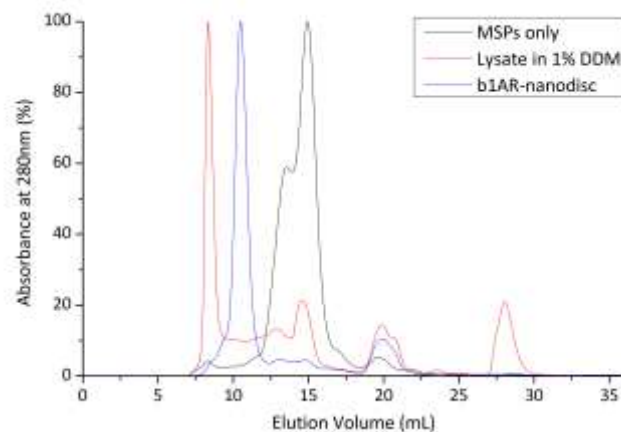


Figure 12: Gel filtration chromatograms of generated nanodiscs (cell lysate in 1% DDM and MSP for comparison). Samples were injected onto a Superdex 200 Increase 10/300 GL column and eluted at 0.75 mL/min with FPLC Buffer while monitoring protein absorbance at 280 nm.

To enable a theoretical estimation of molecular weight of each protein peak based on the elution volume, the column was calibrated with the high molecular weight gel filtration calibration kit. Based on experimentally determined elution volume and known molecular weight (MW) of applied proteins in the calibration kit (chromatograms not shown), the linear correlation of K_{av} and Log_{MW} was calculated (Fig 13) and the theoretical molecular weight of generated nanodiscs was calculated to be about 400 kDa.

Protein	MW (kDa)	Elution Volume (mL)	$K_{av} = (V_e - V_0)/(V_c - V_0)$
Dextran	2000	8.392	0
Ferritin	440	10.674	0.150
Conalbumin	75	14.511	0.403
Aldolase	158	13.072	0.309
Ovalbumin	44	15.431	0.464
Ribonuclease	13.7	17.989	0.633

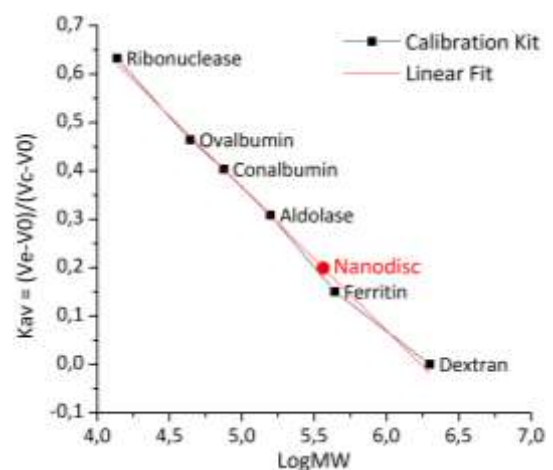


Figure 13: Calibration curve used for MW calculation of nanodiscs. Left: MW, observed elution volume, K_{av} and Log_{MW} of applied proteins from the high molecular weight gel filtration calibration kit. Right: Calibration curve of Superdex 200 Increase 10/300 GL column, based on calculated K_{av} and known MW of applied protein standards.

Nanodiscs generated from one single reaction according to the standard protocol showed a peak in SEC with a height of about 8 mAU at elution volume of 11.5 mL. 1-mL fractions were collected from the elution volume of 7.5 mL, shown in Fig 14. These fractions were concentrated, separated by SDS-PAGE and examined using WB against the membrane protein CD147, which is highly expressed in

HEK293 cells. CD147 was detected mainly in the nanodisc fractions from 9.5 mL to 11.5 mL (corresponding to an estimated molecular weight of about 360 kDa to 1000 kDa), indicating that the 50 kDa protein CD147 was in fact incorporated into larger particles. The likelihood of a coincidental co-elution is low because of the considerable difference in molecular weights. Fractions from 11.5 mL to 12.5 mL (220 kDa to 360 kDa) seem to contain only traces of this protein, this population could consist of nanodiscs with smaller or without incorporated membrane proteins. Intensities of visible WB bands were quantified and normalized to the intensity of CD147 in the respective starting material and indicated in Fig 14. 92% of CD147 was recovered in the collected fractions in the nanodisc peak (9.5 mL to 12.5 mL).

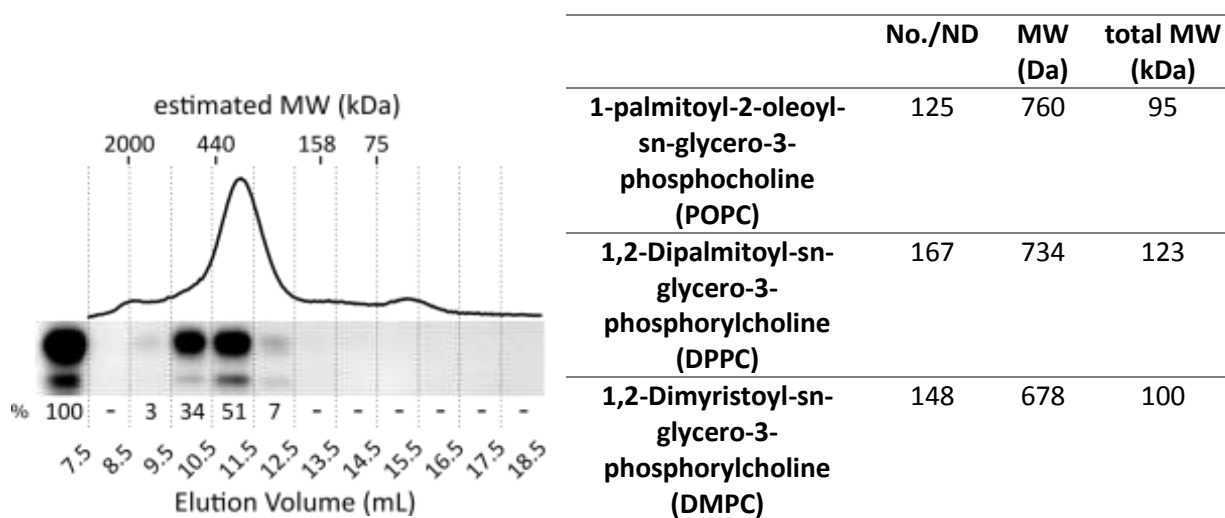


Figure 14: Characterization of nanodiscs generated according to the standard protocol. MW was estimated by calibration with the gel filtration calibration kit (Fig 13). The nanodisc peak was collected in 1-mL fractions and examined by western blot against the membrane protein CD147. All visible WB bands were quantified with background noise correction and normalized to applied cell material. MW of used phospholipids per nanodiscs (generated with MSP1E3D1) was calculated for three kinds of phospholipids, number of phospholipids was taken from Bayburt & Sligar, 2010.

Nanodiscs were assembled of two copies of MSPs (32.6 kDa each for MSP1E3D1), a large number of phospholipids with a total molecular weight of between 95 kDa and 123 kDa (Fig 14, right) as well as membrane proteins inserted. Interestingly, the nanodisc peak of nanodiscs generated with MSP1E3D1 was always observed at an elution volume of 11 mL using the Superdex 200 Increase 10/300 GL column, independent of the mass of incorporated membrane proteins. This observation could be explained by the structural property of nanodiscs, the size of the particle is defined by the length of applied MSP variant (Denisov et al., 2004; Hagn et al., 2013). Nanodiscs with probably different molecular mass were detected in the same SEC peak because the size exclusion chromatography separates proteins and particles by their size and shape.

5.2.2. Electron microscopy

For electron microscopy visualization, nanodiscs were generated from HEK293 wild type cells according to the standard protocol using EM Buffer instead of FPLC Buffer and purified by SEC. Nanodiscs were adsorbed onto carbon-coated grids and stained with uranyl acetate.

The microscopy image was taken at 50000 x magnification by transmission electron microscopy (TEM). The clearly recognizable particles have a round shape and differ slightly in their diameters probably due to the incorporation of membrane proteins with different sizes. According to the manufacturer, the theoretical size of nanodiscs prepared with MSP1E3D1 is about 12.9 nm. The particles observed in this case confirm those results, as they are in a range of about 10 nm to 15 nm.

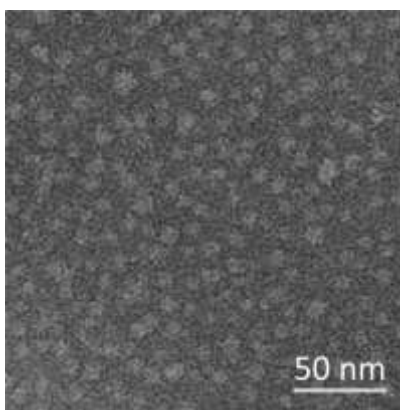


Figure 15: Negative stain TEM image of nanodiscs generated from HEK293 cells. The image was taken at 50000 x magnification, the scale bar equals 50 nm.

The size estimation of nanodiscs based on TEM images (Fig 15) corresponds to observations made by other investigators using imaging methods such as atomic force microscopy and scanning probe microscopy (Timothy H. Bayburt et al., 2002; T. H. Bayburt & Sligar, 2010).

5.2.3. Optimization of the nanodisc generation protocol

The nanodisc generation protocol was optimized and verified upon the choice of detergent, MSP variant, PEG-PE concentration, amount of Bio-Beads and other reaction components, as well as reaction time. The necessity of an extra membrane isolation step is also discussed within this section.

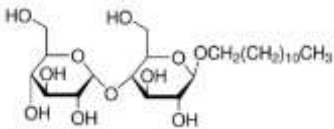
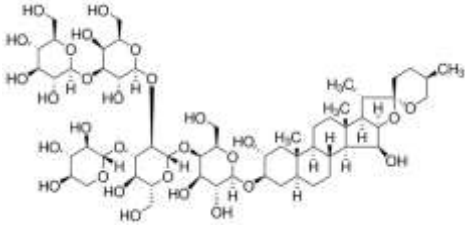
5.2.3.1. Detergent

Since the choice of an optimal detergent is essential for the efficiency of the incorporation as well as the functionality of solubilized β 1AR, for which the nanodisc generation protocol should be optimized, only mild, non-ionic detergents were chosen to be tested for the nanodisc generation.

Nanodiscs were generated according to the standard protocol with cell lysate solubilized with 1% DDM (20 mM) as well as with 1% digitonin (8 mM) (Caron & Lefkowitz, 1976). Even if both detergents differ widely from each other in their molecular weight, chemical formulation and also the critical

micelle concentration (CMC) (detailed comparison in Table 2), generated nanodiscs showed the same size examined by SEC. However, with the same amount of the starting material as well as other reaction components, a higher nanodisc peak (100%) could be observed by using DDM as detergent than by using digitonin (about 70%, Fig 16). Based on this observation, nanodisc generation was performed with DDM in further experiments.

Table 2: Physical and chemical properties of DDM and digitonin.

Detergent	DDM	Digitonin
Molecular weight	511 Da	1229 Da
Micellar average molecular weight	50,000 Da	70,000 Da
CMC at 20-25 °C	0.15 mM	<0.5 mM
Aggregation number	98	60
Structure		

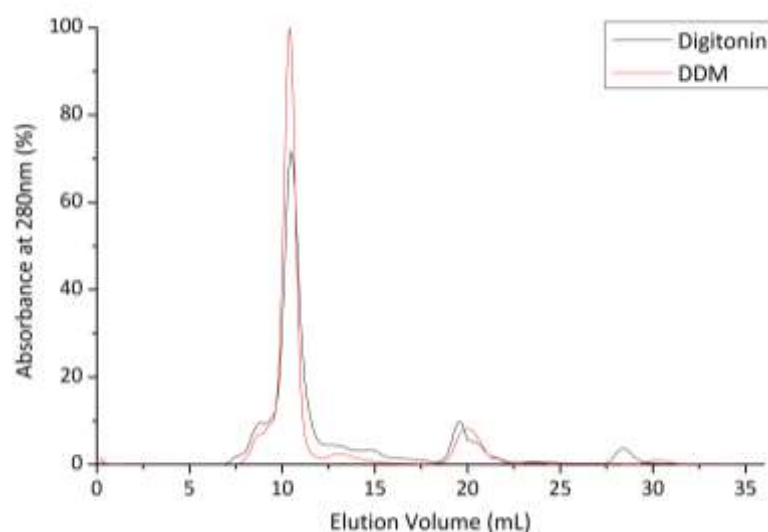


Figure 16: Gel filtration chromatograms of nanodiscs generated with DDM or digitonin.



If this nanodisc generation protocol should be adapted to other more robust membrane proteins or if the folding and functionality of the membrane protein is not required, other detergents could be considered and should be empirically tested for efficiency (Seddon et al., 2004).

5.2.3.2. Membrane Scaffold Protein

The size of nanodiscs depends on the length of applied MSP variant. To compare the sizes of nanodiscs prepared with different MSP variants, SEC was used to separate nanodiscs and their individual components.

MSPs are amphipathic, genetically modified versions of Apolipoprotein A1 (apoA1), the major protein component of HDL particles, which enable the encircling of membrane proteins and phospholipids in nanodiscs. In this thesis, two commercial, common variants of MSPs, the MSP1E3D1 and the MSP1D1, were tested for nanodisc generation according to the same standard protocol. Both MSP variants share the same H2 to H10 helices of apoA1 with additional Histidine-Tag and *Tobacco Etch Virus* (TEV) protease cleavage site at C-terminus. The H1 helix of apoA1 is deleted in both MSP variants, whereas the MSP1E3D1 variant has an additional repeat of H4 to H6 sequences.

Table 3: Physical and chemical properties of MSP1E3D1 and MSP1D1.

MSP	MW (Da)	Deletion	Insertion	No of Amino Acid	Schematic illustration of α -helices
1D1	24662	Helix 1	-	211	
1E3D1	32600	Helix 1	Helix 4-5-6	277	

As shown in Fig 17, the nanodisc generation was successful with both MSP variants. Nanodiscs generated with the smaller MSP variant were shown to have a smaller average particle size than the ones generated with the larger MSP1E3D1. As shown in Fig 17, the nanodisc peak was shifted to a higher retention volume (10.06 mL to 10.73 mL), as expected (n=1).

However, the peak width of MSP1D1 nanodiscs was broader (2.92 mL, signal higher than 5% of the peak height) than of MSP1E3D1 nanodiscs (1.91 mL, signal higher than 5% of the peak height), which indicated a more heterogeneous composition of incorporated proteins in MSP1D1 nanodiscs. At the same time, MSP1E3D1 enabled a larger area of phospholipid double layer in generated nanodiscs, which made the co-incorporation of essential co-factors as well as receptor dimers possible. Therefore, further experiments were performed with MSP1E3D1.

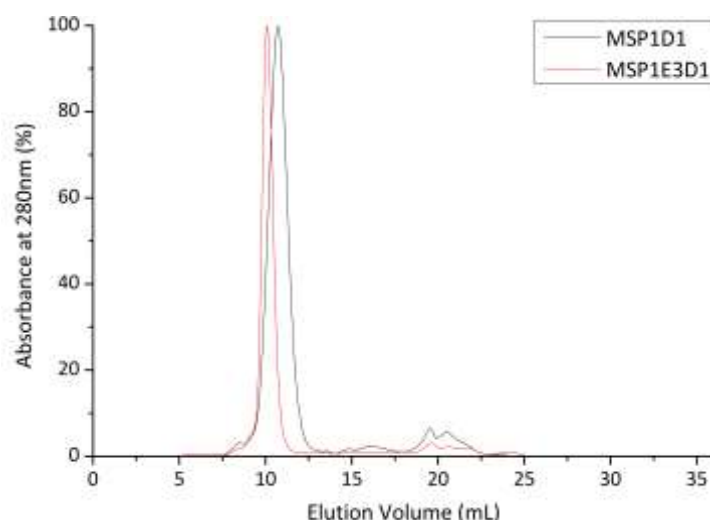


Figure 17: Gel filtration chromatograms of nanodiscs generated using MSP1D1 and MSP1E3D1.

However, if a smaller size of nanodiscs is required to achieve a homogenous population of membrane proteins, truncated MSP variants (Hagn et al., 2013) should be considered.

5.2.3.3. PEG-PE

As the only externally added lipid component, the consideration of PEG-PE (average MW: 2805 Da) in the nanodisc generation was further examined. For the standard protocol, 40 μg (14.3 nmol) of PEG-PE were applied, together with 50 μg MSP1E3D1 (1.5 nmol). Since two copies of MSP1E3D1 were necessary for the self-assembly of one nanodisc particle, the number of inserted PEG-PE molecules could be theoretically calculated as 19 for each nanodisc.

To further verify the importance of PEG-PE in this case, the amount of PEG-PE was varied from 80 μg (37 molecules per nanodisc) to 2 μg (1 molecule per nanodisc) by keeping all the other parameters as the same. One experiment without the addition of PEG-PE was also performed (reaction 0). In general, three different peaks at 11 mL (F1), 12.5 mL (F2) and 14.5 mL (F3) could be clearly observed in SEC chromatograms (Fig 18A). A comparison of SEC runs 37, 19 and 9 showed that the addition of PEG-PE reduced the F2 and F3 peaks, whereas the F1 peak increased and shifted to a lower retention volume. The F1 peak could not be detected in reaction mixture without the addition of PEG-PE (reaction 0). This observation demonstrated that the nanodisc peak at 11 mL could only be formed with additionally added PEG-PE molecules. The F3 peak at 14.5 mL represented excessive MSP1E3D1 molecules, which could not form nanodiscs based on lack of sufficient lipids. Based on the particle size and WB results, the F2 peak contained generated nanodiscs with incorporated membrane proteins and internal lipids without addition of PEG-PE.

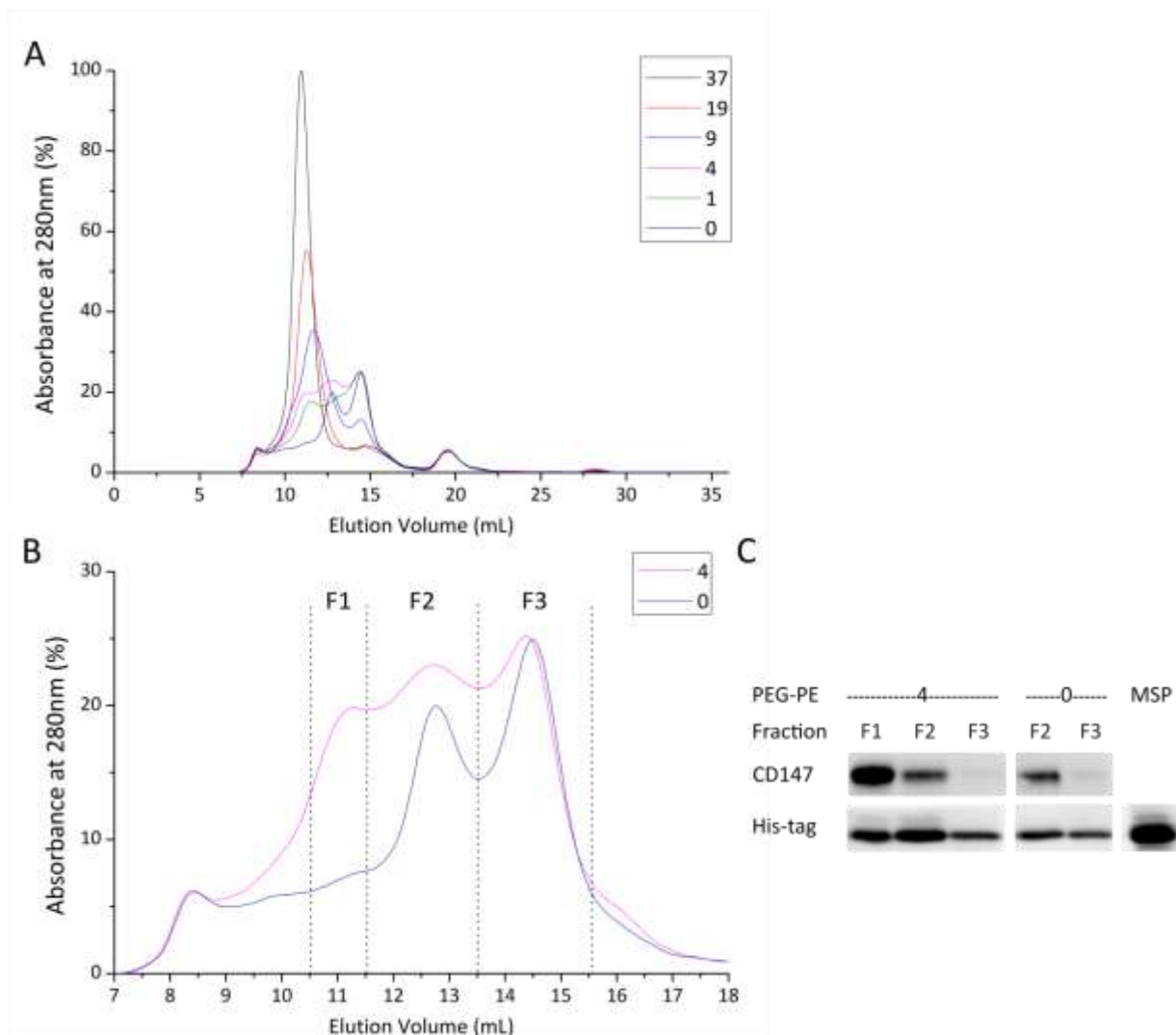


Figure 18: Impact of PEG-PE on nanodisc generation. A: Gel filtration chromatograms of nanodiscs generated with different PEG-PE concentration. The number indicates the quantity of inserted PEG-PE molecules theoretically calculated for each nanodisc. B: Gel filtration chromatograms of nanodiscs with 4 and 0 PEG-PE molecules for each nanodisc. C: Peaks were collected and examined by WB against CD147 and His-Tag.

Runs 4 and 0 were further analyzed (Fig 18B), the peaks (F1, F2 and F3) were collected, concentrated and examined by WB against the His-Tag of MSP, as well as against CD147, which is a highly expressed membrane protein in HEK293 cells and used here as an indicator for the incorporation of membrane proteins into nanodiscs in general (Fig 18C).

As expected, no CD147 signal could be detected in the peak F3, since this peak only contained excessive MSP. The incorporated CD147 could be found in F1 and F2, however, the F1 peak contained more CD147 even the total nanodisc amount was lower than in peak F2.

As already discussed in **section 5.2.1**, the number of phospholipids per nanodisc (generated with MSP1E3D1) is estimated between 125 (for POPC) and 167 (for DPPC). Based on this presumption, a

large portion of lipids incorporated in nanodiscs must be of natural origin, since only 19 PEG-PE molecules were not able to fill the nanodiscs.

Taken together, nanodiscs could be generated without additional PEG-PE molecules. However, the amount of generated nanodiscs was low due to the lack of lipids. And at the same time, the efficiency of membrane protein incorporation was not satisfying in comparison with reactions with PEG-PE addition.

5.2.3.4. Bio-Beads

Bio-Beads SM-2 is composed of macroporous polymeric beads with a high surface area for adsorbing nonpolar substances or surface active agents from aqueous solutions. Based on the standard protocol, the amount of Bio-Beads was varied to optimize the generation of nanodiscs. 15 mg, 30 mg, 60 mg and 120 mg Bio-Beads were pre-incubated and used for nanodisc assembly by keeping all the other reaction components and condition unchanged. Not only the generation efficiency (indicated by the height of nanodisc peak), but also the level of aggregation (indicated by height of aggregation peak) and the level of completeness of the reaction (indicated by free MSP peak) were verified.

In general, the generation efficiency decreased by increased amount of Bio-Beads, indicating unwanted adsorption of assembled nanodiscs on the hydrophobic surface of Bio-Beads. A low amount of Bio-Beads, however, leads to an incomplete self-assembly of nanodiscs, which was indicated by remaining MSP1E3D1 at 15 mL in the reaction with only 15 mg Bio-Beads. Taken together, 30 mg of Bio-Beads were confirmed to lead to the best result, since a high generation efficiency and a high completeness of the nanodisc generation were achieved.

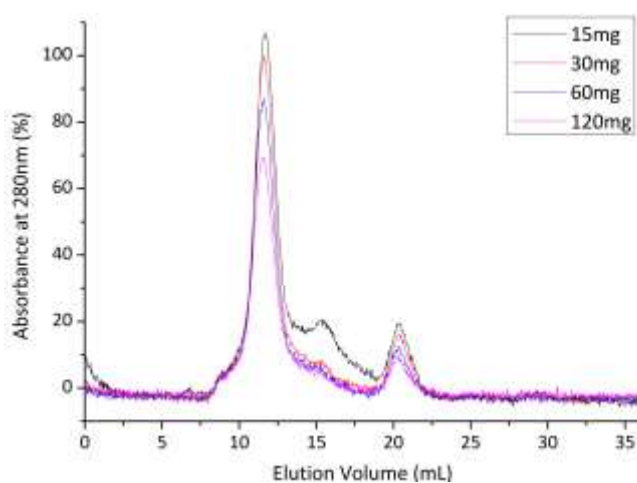


Figure 19: Impact of Bio-Beads amount on nanodisc generation, analyzed by SEC.

5.2.3.5. Component-to-volume ratio

To further examine the impact of component-to-volume ratio on nanodisc generation, four different approaches were verified (Fig 20). Reaction No. 1 equals the standard protocol, the protein absorbance at 280 nm of the nanodisc peak at 11.5 mL was set as 100%. In reaction No. 2, the reaction volume was doubled by keeping the amount of all reaction components as the same as in No. 1. Only 70% of the nanodisc peak height was achieved, indicating an inefficient reaction. The removal of detergent was not complete due to the increased reaction volume. By doubling the amount of reaction components while maintaining the reaction volume (No. 3), the reaction efficiency was as high as the standard reaction, however, the aggregate peak as well as the free MSP peak were increased. If both the reaction component and the reaction volume were doubled (No. 4), resulting the same component-to-volume ratio as in the standard reaction, the nanodisc peak was only increased by 50% and a very high aggregate peak and free MSP peak were observed.

Based on results described above, the component-to-volume ratio of the standard nanodisc generation protocol (No. 1) was optimal and was therefore kept in further experiments. The unexpected observation of experiment No. 4, in which the component-to-volume ratio is the same as in experiment No. 1, was further analyzed in the scale up approach (section 5.2.4.).

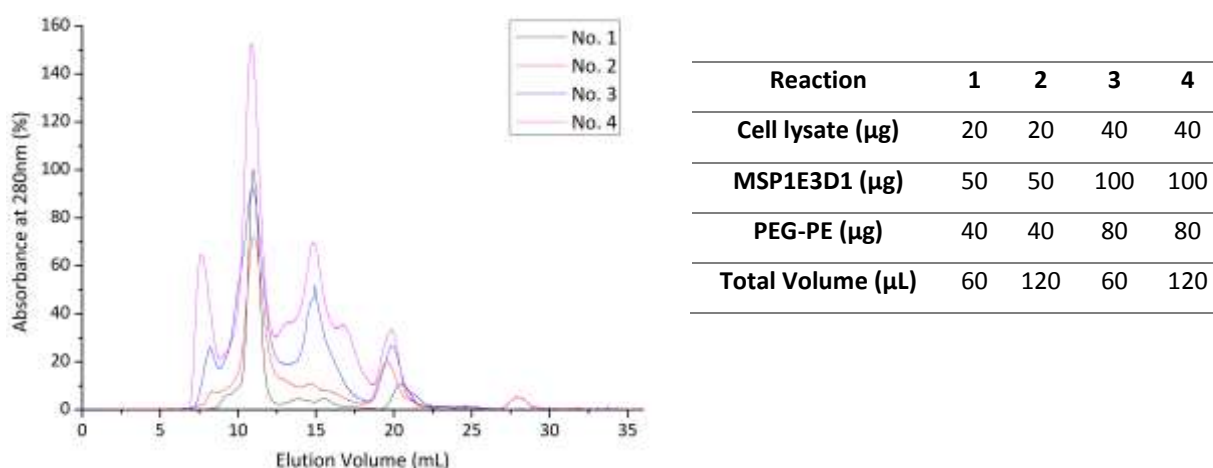


Figure 20: Impact of component-to-volume ratios on nanodisc generation. Left: Gel filtration chromatograms of nanodiscs generated with different component-to-volume ratios. Right: Reaction conditions of different component-to-volume ratios tested.

5.2.3.6. Reaction time

In order to speed up the process of nanodisc generation, experiments were performed to determine the minimum reaction time needed for the successful nanodisc generation as well as for the successful incorporation of membrane proteins.

A 5x standard master mix with all components was generated and spread to five glass tubes with 30 mg pre-incubated Bio-Beads each. One of the reaction mixtures was directly pipetted out of the glass tube afterwards, generating the sample at the time point 0 min. Incubation periods 30 min, 60 min, 90 min and 180 min were tested, all reactions were performed at 4 °C. The generation of nanodiscs was analyzed based the height of the nanodisc peak in SEC, as well as by WB against MSP (via His-Tag). The elution volume of the nanodisc peak, as well as WB intensity of membrane protein β 1AR (via GFP-Tag) was used as indicators to analyze and quantify the incorporation of β 1AR into nanodiscs.

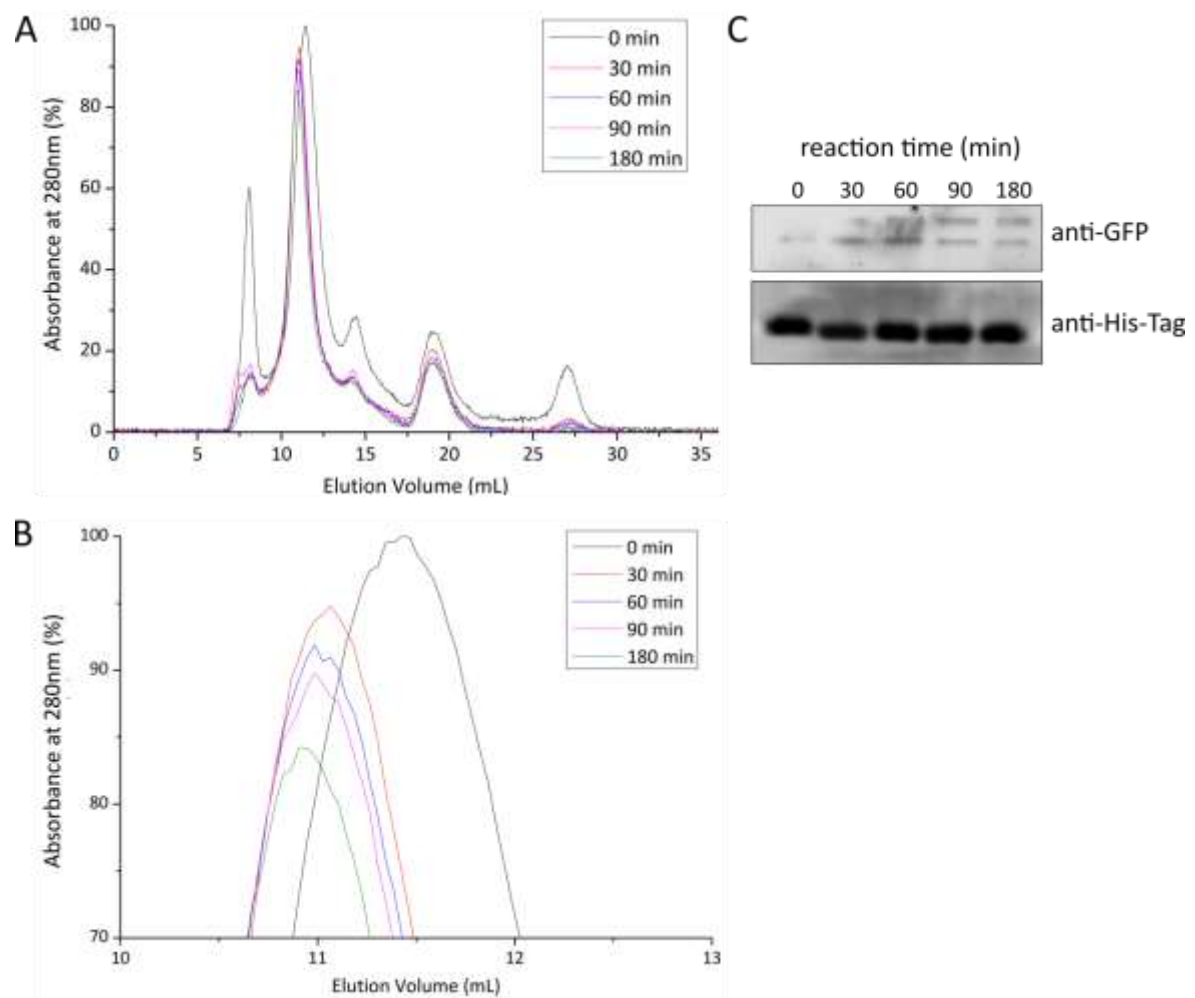


Figure 21: Impact of reaction time on nanodisc generation A and B: Gel filtration chromatogram of nanodiscs generated after different reaction time. C: The nanodisc peak was collected for each reaction and examined by western blot against GFP and His-Tag.

Unexpectedly, the self-assembly process of nanodisc generation seemed to be induced immediately after the reaction components were mixed together. A clear nanodisc peak could be observed even at the time point 0 min (Fig 21A). However, this nanodisc peak is right-shifted in comparison with the nanodisc peak after a longer incubation, indicating a smaller particle size of generated nanodiscs and absence of incorporated membrane protein (Fig 21B). At the same time, a high aggregate peak at

8 mL and a free MSP peak at 15 mL clearly showed the incomplete incorporation of cell material at time point 0. WB results (Fig 21C) further confirmed that nearly no membrane protein was incorporated into nanodiscs at the time point 0 min.

In general, the height of the nanodisc peak decreased by increased reaction time, probably due to the adsorption of nanodiscs on the surface of Bio-Beads over time, comparable with experiments using high amount of Bio-Beads (**section 5.2.3.4.**). A left-shift of the nanodisc peak in SEC was observed after longer incubation time, together with the stronger β 1AR signal in WB. Taken together, it was assumed that even though nanodisc generation is a very quick process, the incorporation of membrane proteins takes more time. Therefore, a minimum incubation time with Bio-Beads of 60 min was required.

5.2.3.7. Membrane preparation

Initially, the nanodisc generation was performed with isolated membrane fraction of HEK293 cells as starting material. According to this protocol, cells were first lysed mechanically by Dounce homogenization. Afterwards, nuclei and non-destroyed cells were pelleted and discarded and the soluble membrane fraction was isolated using ultracentrifugation in a further step. For nanodisc generation, the membrane pellet had to be solubilized again with a suitable detergent. The hands-on time of this procedure lasted over two hours and the loss of membrane protein was over two-third during the membrane isolation (Fig 22).

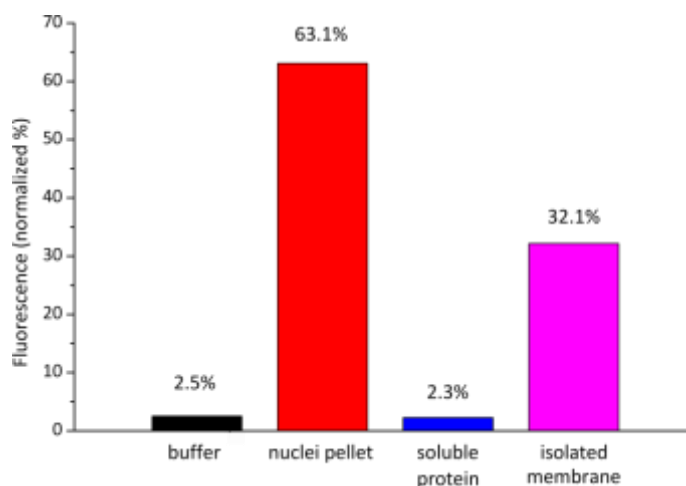


Figure 22: Fluorescence intensity of protein-containing fractions during the membrane isolation process. The sum of all signals was set as 100%, n=1.

Thus, a simplified protocol was required to speed up the process and to improve the recovery of membrane proteins which were used as starting material for nanodisc generation. The optimization and evaluation of the nanodisc generation regarding different starting materials were performed

with CD147 and Mitochondrially Encoded Cytochrome C Oxidase II (MT-CO2) as models for membrane proteins.

Nanodiscs were generated from both lysate of whole HEK293 cells (Fig 23A) and from previously isolated membrane of HEK293 cells (Fig 23B) with the same amount of starting material. The generated nanodiscs were purified by SEC and thereby separated from non-incorporated membrane proteins. The main nanodisc peak was pooled and concentrated, the samples were separated by SDS-PAGE, and selected membrane proteins (CD147 and MT-CO2) were detected by WB (Fig 23C). To compare the amount of membrane proteins reconstituted in nanodiscs with that in the starting material, four samples were prepared from the same amount of cells: in lane 1 (cell lysate), cells were lysed and applied without further processing. From the same amount of cell lysate, nanodiscs were generated according to the standard protocol (lane 2, NDs from cell lysate). Isolated membrane fractions were once applied directly (lane 3, membrane lysate) and once used for nanodisc generation (lane 4, NDs from membrane). In general, the reconstitution of both membrane proteins selected was successful with isolated membrane fraction (lane 4), as well as with directly lysed whole cells (lane 2). The comparison between lane 1 and lane 3 shows a considerable loss of protein over 85% (MT-CO2) as well as over 50% (CD147) during the membrane isolation step. In both cases, the efficiency of incorporation is higher (over 10 fold for MT-CO2) or at least comparable (CD147) with directly lysed whole cells as starting material according to the WB results.

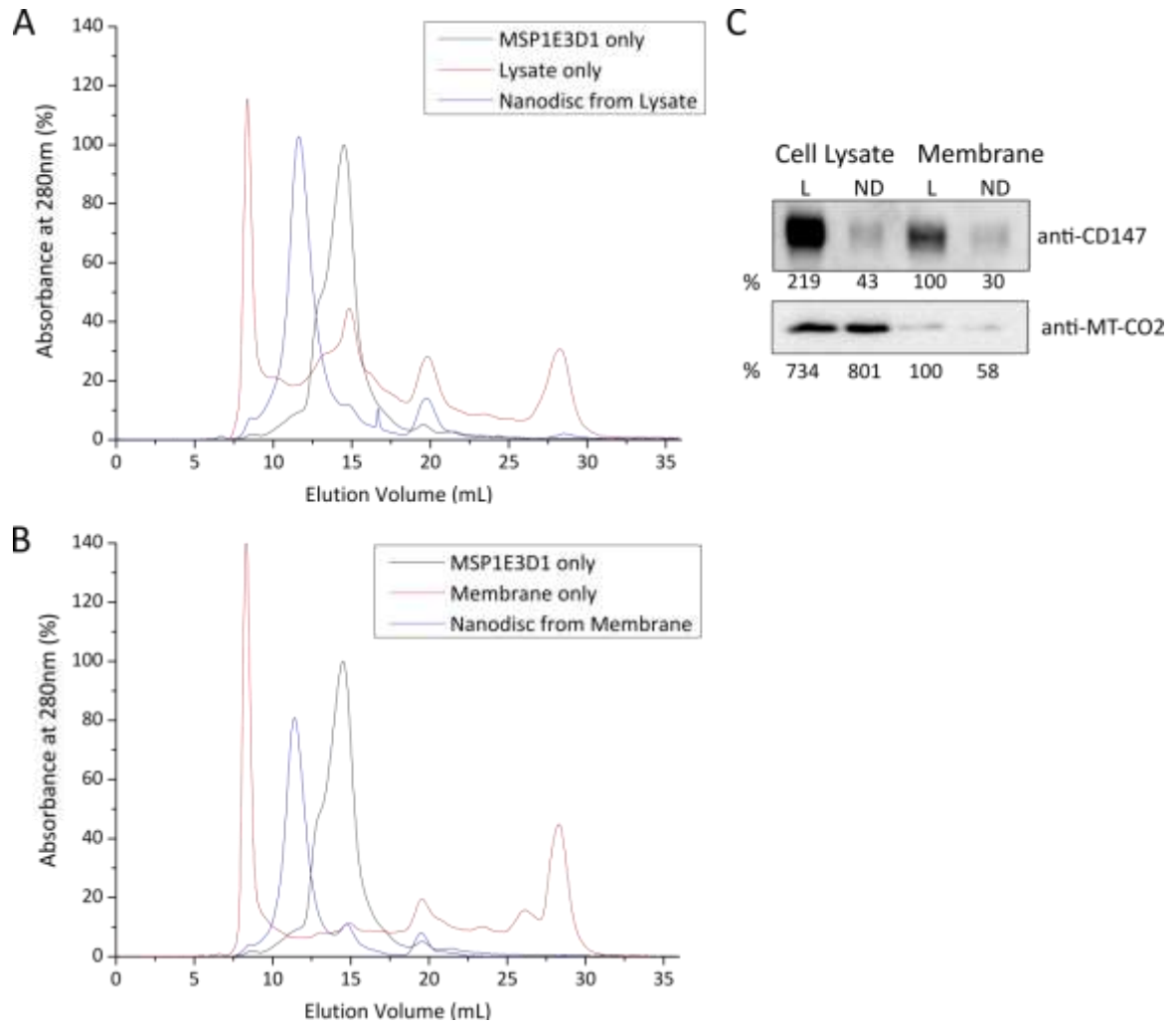


Figure 23: Nanodisc generation from cell lysate and isolated cell membrane. A: Gel filtration chromatograms of cell lysate, MSP1E3D1 and nanodiscs generated directly from cell lysate. B: Gel filtration chromatograms of isolated cell membrane, MSP1E3D1 and nanodiscs generated from isolated membrane. C: Lysate (lane 1), membrane (lane 3) and nanodiscs generated from lysate (lane 2) as well as from membrane (lane 4) were examined by WB against model membrane proteins CD147 and MT-CO2. Intensities of visible WB bands were quantified and normalized to the intensity of membrane protein of interest in membrane.

5.2.4. Scale up approaches

Based on the results described in “component-to-volume ratio” (section 5.2.3.5.), two general approaches were further analyzed for the purpose of a possible scale up of the nanodisc generation:

A: The component-to-volume ratio was doubled compared to the standard protocol.

B: The component-to-volume ratio was kept as the same as in the standard protocol.

In both approaches, the ratio between all reaction components (cell lysate, MSP and PEG-PE) was kept the same as in the standard protocol.

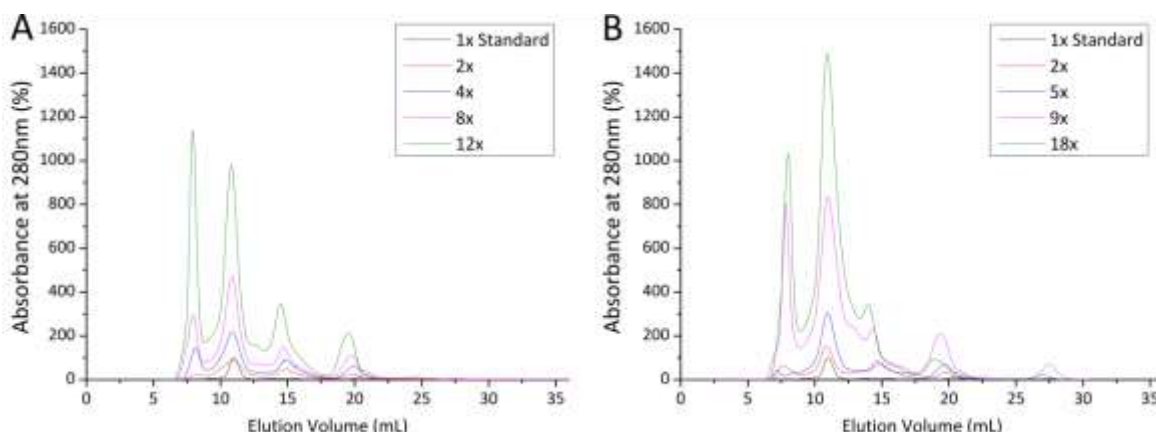


Figure 24: Gel filtration chromatograms of scale up approaches A and B. The nanodisc peak of 1x standard was set as 100%.

To allow a direct comparison of both scale up approaches, protein absorbance at 280 nm was normalized to the nanodisc peak of 1x standard. Not only the nanodisc peak, but also the aggregate peak at 8 mL and the free MSP peak at 15 mL were analyzed as parameters for the goodness of examined scale up approaches. Three additional criteria, the aggregation level, the free MSP level and the scale up efficiency were defined to evaluate the scale up process.

The aggregation level is defined as quotient of the aggregate peak and the nanodisc peak. This parameter should be as low as possible, since it indicates the degree of protein unfolding and aggregation. The aggregation level of the standard procedure was 0%, since no aggregate was obtained. As it could be clearly seen in Table 4, every scale up approach increased the aggregation, the level varied between 14% (approach B, 5x) and 116% (approach A, 12x). In general, a higher scaling factor led to a higher aggregation level.

Similar to the aggregation level, the free MSP level is defined as quotient of the free MSP peak and the nanodisc peak, and should also be as low as possible. Differently to the aggregation level, the free MSP level decreased with increased scaling factor. In approach B, the overall free MSP level was lower than in approach A.

A third parameter, the scale up efficiency was defined as

$$\text{scale up efficiency} = \frac{\text{resulted nanodisc peak}}{\frac{\text{nanodisc peak of 1x standard}}{\text{scaling factor}}}$$

This parameter should be as high as possible, a 100% scale up efficiency implies the same generation efficiency as the optimized standard protocol. In approaches A and B, the efficiency varied between 46% (approach A, 2x) and 93% (approach B, 9x). No approach could achieve the 100% efficiency in comparison to the 1x standard. The overall efficiency of approach B was higher than of approach A.

Table 4: Results of scale up approaches A and B.

Approach		A				B			
Scaling factor	1	2	4	8	12	2	5	9	18
Aggregate peak (mAU)	0	3	19	37	144	8	5	102	131
Nanodisc peak (mAU)	13	12	28	60	124	19	39	106	189
MSP peak (mAU)	1	7	12	19	44	9	11	29	44
Aggregation level	0%	28%	67%	63%	116%	42%	14%	97%	69%
Free MSP level	5%	56%	42%	32%	35%	46%	28%	28%	23%
Scale up efficiency	100%	46%	55%	59%	82%	76%	61%	93%	83%

This observed behavior of scale up reactions differently to 1x standard (aggregation, low reaction efficiency) could be probably explained, that the same kind of 5-mL glass tubes was used as reaction vessels for all experiments and therefore induced a different surface-to-volume relation, which possibly affected the interaction between all reaction components. Taken together, the most promising approach is the approach B, with 9 and 18 fold amount of all reaction components, 8 and 15 fold of nanodiscs could be generated. The aggregate peak with similar height as the nanodisc peak had to be removed using SEC for downstream experiments. For all following experiments in laboratory scale, the 1x standard protocol was used to generate nanodiscs in separate reactions in parallel to avoid the presence of aggregate and free MSP in the final product. If the nanodisc production in industrial scale is required, the nanodisc generation in parallel reactions must be automated. Other expression systems such as cell-free expression or expression in insect cells (e.g. *Sf9* cells) could also be considered in this issue.

5.2.5. Storage conditions

To verify different storage conditions, a standard master mix was generated according to the standard protocol. Generated nanodiscs were distributed in portions of 120 μ L to glass tubes and stored under different conditions for 10 days and 30 days, respectively. The conditions were storage temperatures 4 °C, -20 °C and -80 °C as well as lyophilization with subsequent storage at room temperature, with a final concentration of 3% trehalose (lyo + T) and without additive (lyo). After storage, nanodiscs were tested with SEC (Fig 25A and B) and WB (Fig 25C). A comparative sample was generated by measuring one of the samples directly after nanodisc generation without storage, normalized as 100% (fresh).

When comparing the SEC chromatograms of the samples (Fig 25A and B), a slight left-shift of nanodisc peak was observed for all stored samples, especially for samples stored at 4 °C. The left-

shift increased with increased storage time. This observation could be explained by further incorporation of membrane proteins into nanodiscs, as already seen in the optimization experiments regarding the reaction time (**section 5.2.3.6.**). Upon storage at 4 °C, which equals the incubation temperature of nanodisc generation, it is possible that the dynamic process of protein integration into nanodiscs continues, explaining the left-shift of the nanodisc peak. To further analyze nanodiscs after storage under conditions described above, nanodisc peak of all samples was verified via WB (Fig 25C) against the MSP (via His-Tag) and against the membrane protein β 1AR (via GFP-Tag). The MSP band was observed in all samples and further confirmed the stability of nanodiscs under all storage conditions. The characteristic double bands of β 1AR were observed in all samples except in samples after lyophilization.

Taken together, nanodiscs were very stable upon storage at different temperatures as well as lyophilization. However, a further incorporation of membrane proteins into nanodiscs was proceeded during storage at low temperatures, especially at 4 °C. In addition, lyophilization of nanodiscs destructed the incorporated membrane proteins in nanodiscs and should not be chosen as storage method for nanodiscs.

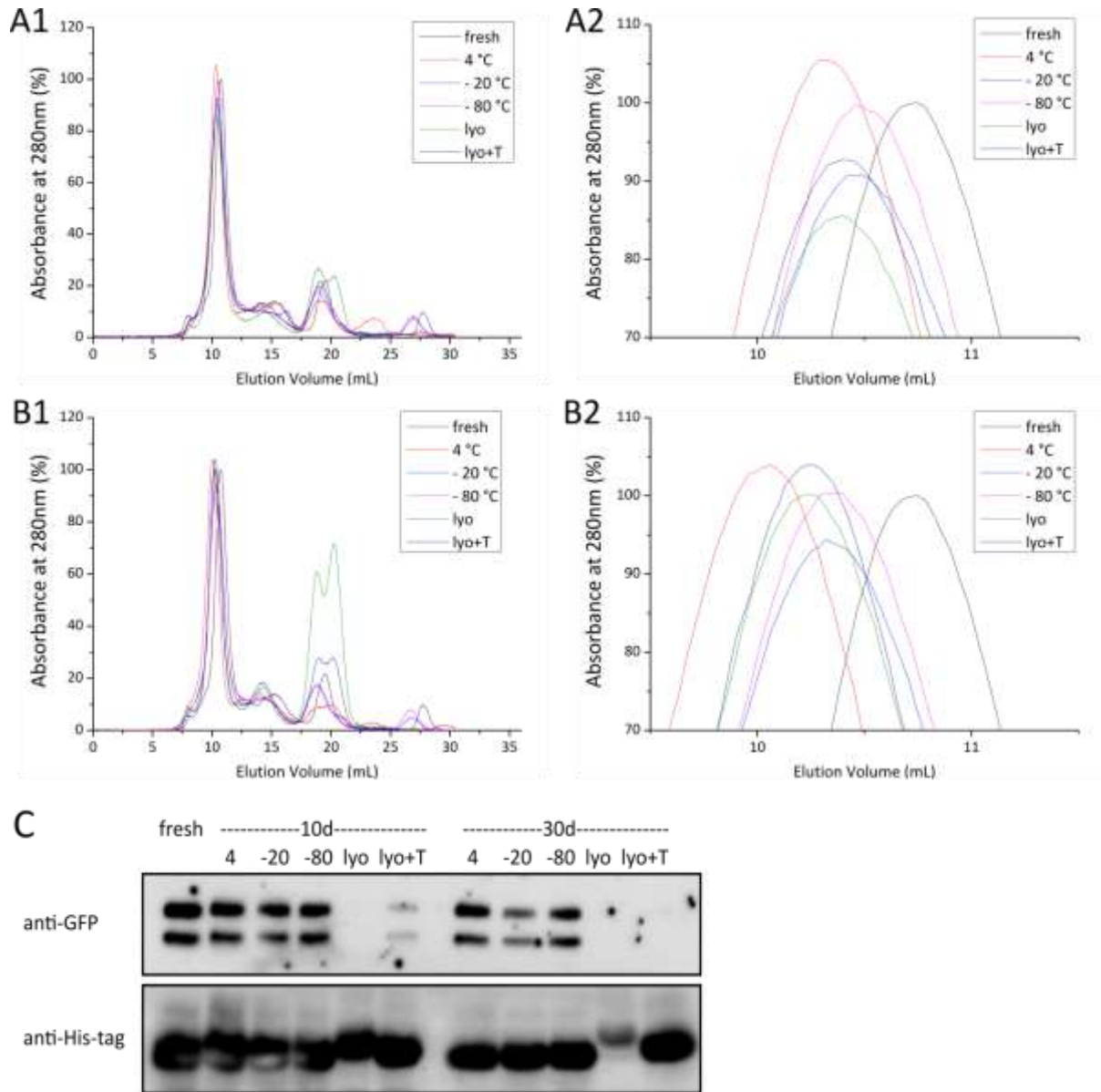


Figure 25: Evaluation of storage conditions for nanodiscs. Gel filtration chromatograms of nanodiscs stored under different conditions for 10 days (A) and 30 days (B), data was normalized to the peak of freshly generated nanodiscs. C: The nanodisc peak was collected and examined by WB against GFP-Tag and His-Tag.

5.3. Verification of β 1AR incorporation in nanodiscs

Nanodiscs incorporating beta-1 adrenergic receptors (β 1AR-ND) were further analyzed and characterized with various analytical methods beside the establishment of an optimized protocol for nanodisc generation with HEK293 cells and the characterization of generated nanodiscs (section 5.2.). The β 1AR receptor used here was genetically modified with an additional YFP-Tag at the intracellular C-terminus of the receptor. This fusion protein (β 1AR-YFP) was stably overexpressed in HEK293 cells which were used as starting material for nanodisc generation according to the optimized standard protocol.

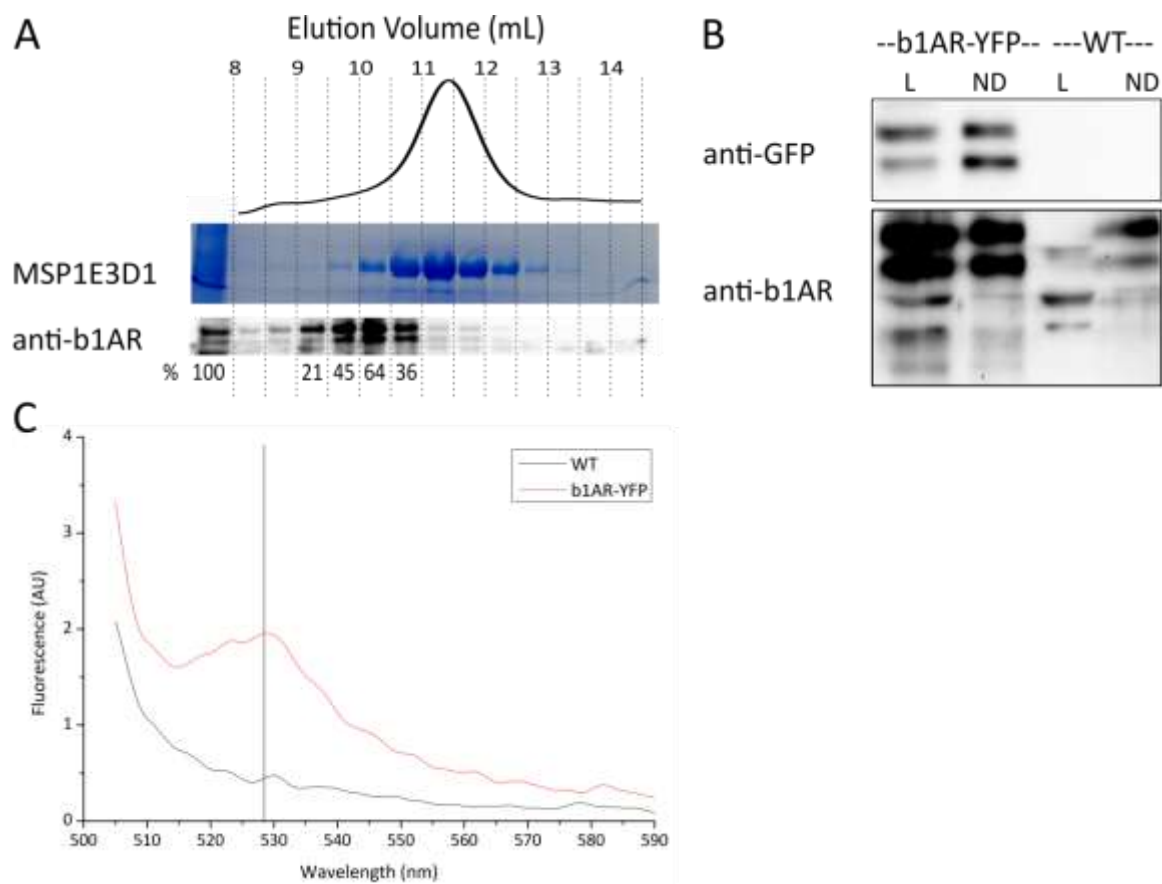


Figure 26: Characterization of β 1AR incorporated in nanodiscs. A: Gel filtration chromatograms of nanodiscs generated from HEK293 cells overexpressing β 1AR-YFP. The eluate was collected in 0.5-mL fractions from 8 mL to 14 mL and examined by WB and SDS-PAGE. All visible WB bands were quantified with background noise correction and normalized to applied cell material. B: WB images of lysates of β 1AR-YFP overexpressing HEK293 cells (lane 1) and of HEK293 wild type cells (lane 3). Nanodiscs were generated with HEK293- β 1AR-YFP cell lysate (lane 2) and with HEK293 wild type cell lysate (lane 4). All samples were examined against the GFP-Tag (upper panel) and β 1AR (lower panel). C: Fluorescence spectroscopy measurements of nanodiscs generated with HEK293 wild type and β 1AR-YFP overexpression cells, the emission maximum of YFP at 527 nm is indicated.

The SEC chromatogram of β 1AR-ND showed no difference to those generated with wild type HEK293 cells (Fig 26A). 0.5-mL fractions were collected from 8 mL to 14 mL and separated by SDS-PAGE, the SDS gel was stained to examine the distribution of nanodiscs based on MSP1E3D1 intensity. At the

same time, proteins were transferred from another SDS gel with the same samples to WB membrane and examined against β 1AR. β 1AR was detected mainly in the nanodisc fractions from 9 mL to 11 mL (corresponding to an estimated molecular mass of approximately 470 – 1300 kDa), indicating that the 78 kDa fusion protein β 1AR-YFP was in fact incorporated into larger particles. Fractions from 11 mL to 12.5 mL (220–470 kDa) seemed to contain only traces of this protein; this population could consist of nanodiscs with smaller or no incorporated membrane proteins. Additionally, SDS-PAGE was performed to detect MSP1E3D1, the intensity of MSP1E3D1 corresponded exactly to the shape of the nanodisc peak in SEC.

To further confirm the incorporation of β 1AR-YFP into nanodiscs, WBs were performed with anti-GFP antibodies against the fused YFP-Tag at C-terminus of the receptor as well as anti- β 1AR antibodies targeting different sequences of β 1AR. As shown in Fig 26B, β 1AR-characteristic double bands could be observed in all lanes with HEK293- β 1AR-YFP lysate and β 1AR-YFP-NDs.

Nanodiscs generated with HEK293 wild type cell lysate and β 1AR-YFP overexpressing cell lysate were analyzed with fluorescence spectroscopy (Fig 26C). For YFP detection, the fluorophore was excited at 485 nm, whereas the emission spectrum between 500 and 600 nm was scanned. Nanodiscs with β 1AR-YFP fusion protein incorporated could be clearly detected in the YFP channel, further confirming the successful incorporation of β 1AR-YFP into nanodiscs. At the same time, the fluorescence signal implied the native folding of the YFP-Tag fused to the receptor of interest and could be used for quantification of generated nanodiscs.

5.3.1. Functional characterization of the β 1AR using Alprenolol Beads

Alprenolol is a non-selective beta blocker and only binds to the correctly folded, native β 1AR. Thus, alprenolol covalently coupled to agarose or magnetic beads can be used to build a ligand-based affinity column to purify and isolate the functional fraction of active beta-1 adrenergic receptors (Caron, Srinivasan, Pitha, Kocielek, & Lefkowitz, 1979; Kelleher, Rashidbaigi, Ruoho, & Johnson, 1983; Kwatra et al., 1995). Here, both agarose and magnetic beads coated with alprenolol via a hydrophilic linker were used to confirm the functionality of β 1ARs incorporated in nanodiscs.

Pre-equilibrated magnetic beads were incubated with nanodiscs without previous SEC purification. Non-bound particles were removed from the beads by magnetic separation (fraction: FT). Afterwards, the beads were washed three times (W1, W2 and W3) and active β 1AR-nanodiscs were eluted twice with Elution Buffer containing higher concentrations of alprenolol (E1 and E2). For the complete removal of particles from the magnetic beads, SDS Loading Buffer was added to the beads and

heated for 10 min at 95 °C (SDS). Collected fractions were analyzed with fluorescence spectroscopy (Fig 27B) and afterwards concentrated and analyzed via SDS-PAGE and WB (Fig 27C).

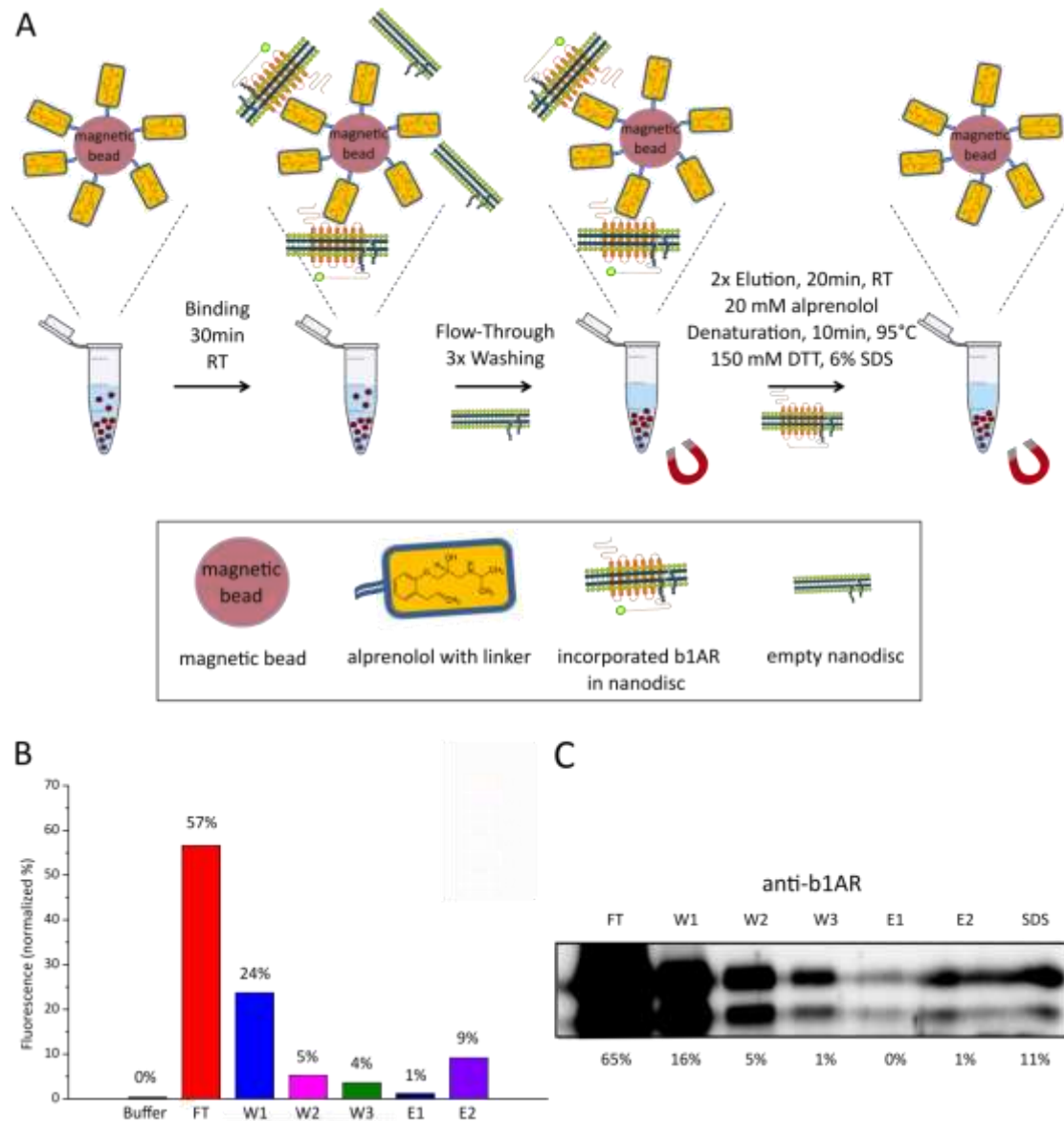


Figure 27: Functional characterization of β 1AR-nanodiscs using alprenolol beads. A: Schematic illustration. B: Fluorescence intensity and C: WB intensity of protein fractions during the affinity purification with magnetic beads coupled with alprenolol. The sum of signal intensity was set as 100%.

Based on results of fluorescence spectroscopy and WB, highest portion of β 1AR-YFP incorporating nanodiscs was found in fractions FT (about 60%) and W1 (about 20%). However, over 10% of all β 1AR-YFP nanodiscs could clearly be found in the eluate (E1, E2 and SDS), confirming the functionality of the receptor was at least partially preserved in these nanodiscs.

5.4. Interaction of AABs and incorporated beta-1 adrenergic receptors in nanodiscs

5.4.1. Interaction assay with GFP-Trap Beads

Although the β 1AR-YFP fusion protein is overexpressed, impurities by other membrane proteins can interfere with the antibody detection. Thus, GFP-Traps coupled to magnetic beads were used to separate nanodiscs incorporating beta-1 adrenergic receptor from other nanodiscs with no or other membrane proteins inserted (Fig 28A). GFP-Trap is a 13 kDa, stable single domain fragment of an alpaca antibody with high binding affinity to fluorescence tags such as GFP, CFP and YFP. GFP-Traps covalently coupled on the surface of magnetic beads were used here to bind the YFP-Tag of incorporated β 1AR-YFP fusion protein in nanodiscs. For affinity purification, β 1AR-YFP nanodiscs were incubated with GFP-Trap Beads for 90 min at 4 °C, nanodiscs with no or with other membrane proteins incorporated were removed from magnetic beads (FT1). The beads were washed three times (W1, W2 and W3) and eluted with 100 μ L Elution Buffer by pipetting up and down for 30 s (E1) and subsequently with 100 μ L SDS Loading Buffer for 10 min at 95 °C (SDS).

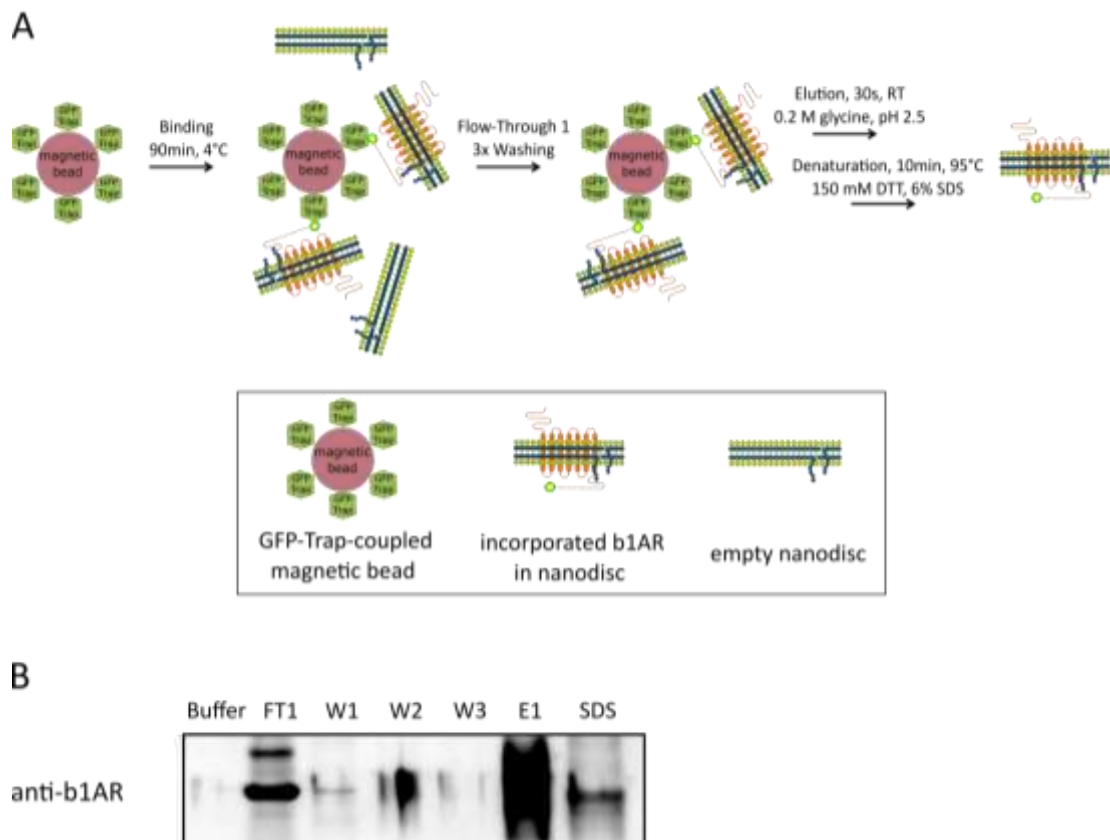
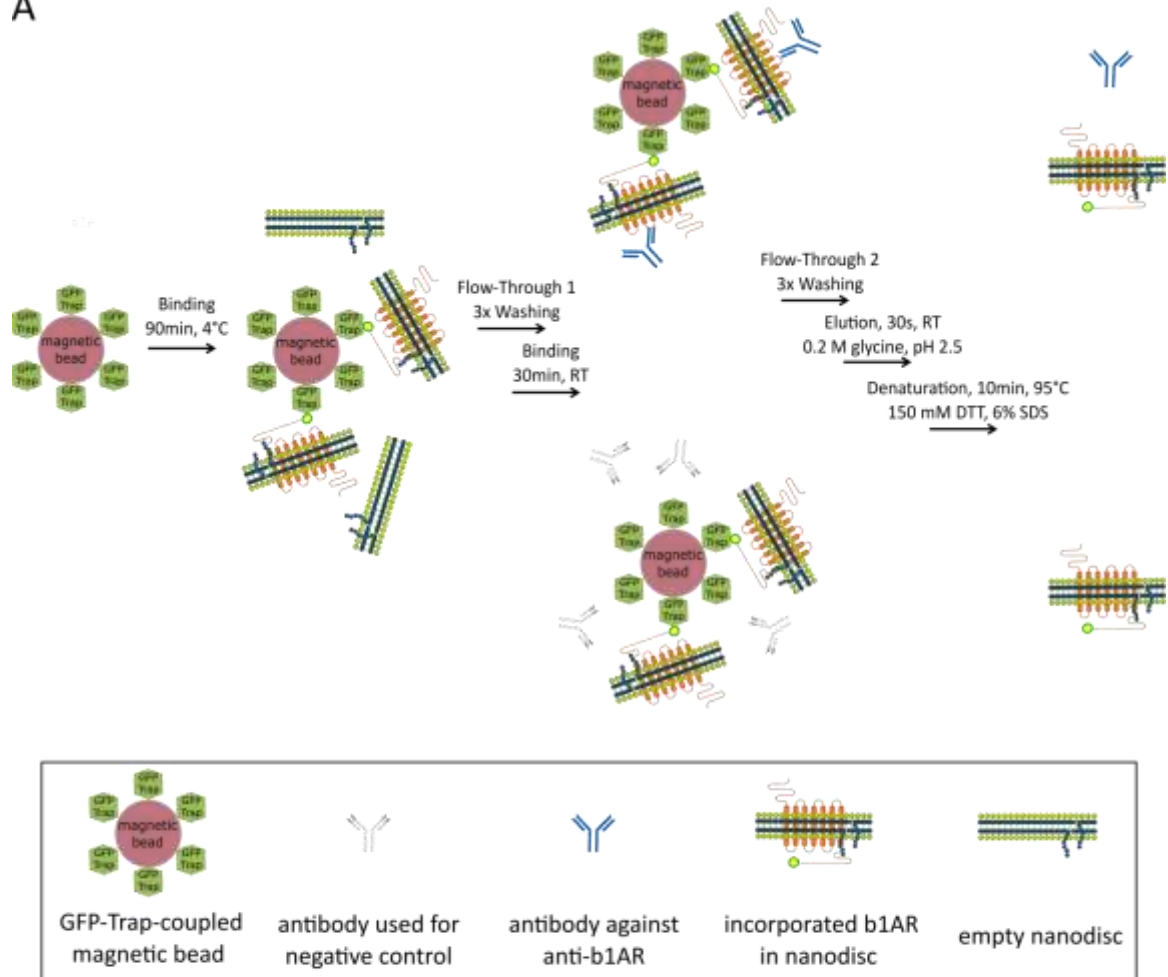


Figure 28: Affinity purification of β 1AR-YFP NDs using magnetic beads coupled with GFP-Trap. A: Schematic illustration. B: WB image targeting β 1AR-YFP during the affinity purification with GFP-Trap Beads.

As it could be clearly seen in WB against β 1AR (Fig 28B), even though a small trace of β 1AR was found in the FT1 fraction, most β 1AR incorporated in nanodiscs was determined in the eluate (E1). Based on this WB result, the affinity purification with GFP-Trap magnetic beads was assumed to be

very efficient and specific. Therefore, the GFP-Trap construct was further used for immunoprecipitation (IP) as well as for surface plasmon resonance spectroscopy (SPR) and enzyme-linked immunosorbent (ELISA) assays.

A



B

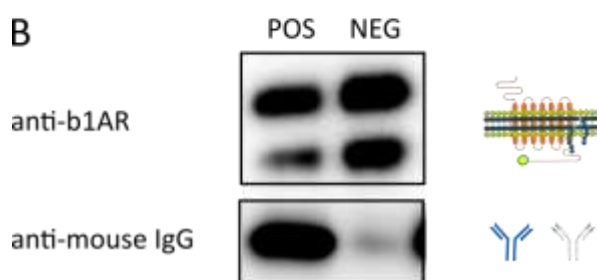


Figure 29: Co-IP of anti-β1AR antibodies using β1AR-YFP NDs coated on GFP-Trap Magnetic Beads. A: Schematic illustration. B: WB image of E1 fraction of experiments with anti-β1AR antibody MAB23-6-7 (POS) and anti-testosterone antibody BM2076 (NEG) as negative control.

To analyze the protein-protein interaction between antibodies and in nanodiscs incorporated β1ARs, co-immunoprecipitation experiments were carried out. For co-immunoprecipitation, isolated antibodies or diluted human serum samples were added to the magnetic beads (Fig 29A), after the

binding of β 1AR-nanodiscs as described for affinity purification above. Non-binding antibodies, as well as other proteins of the human serum, were removed from the beads (FT2). The beads were again washed (W4, W5 and W6) and eluted (E1 and SDS) as described above. To demonstrate the precipitation of antibodies using GFP-Trap Magnetic Beads, mouse monoclonal anti- β 1AR antibody MAB23-6-7, as well as mouse monoclonal anti-testosterone antibody BM2076 as negative control, was applied to the beads in the same concentration. Elution fractions were verified by WB against β 1AR-nanodiscs for loading control and against mouse IgG. The WB images (Fig 29B) showed clearly, that the intensity of β 1AR-YFP is similar for both experiments, implying a similar coating level of β 1AR-nanodiscs on the bead surface. Simultaneously, a much higher signal was detected in the experiment with the anti- β 1AR antibody MAB23-6-7 than with the control antibody BM2076. This observation demonstrated the high specificity of the experimental set-up, which was further adapted for SPR and ELISA assay.

5.4.2. SPR assay

Surface plasmon resonance spectroscopy allows a label-free, real-time monitoring of sequential binding steps and was used here to demonstrate the binding of β 1AR-YFP nanodiscs to immobilized GFP-Trap molecules on the sensor surface, as well as the sequential binding of anti- β 1AR antibodies to β 1AR incorporated in nanodiscs. A large number of optimization steps were performed regarding surface modification of the sensor chip, running buffer, flow rate and concentration of binding partners (data not shown).

GFP-Trap molecules were immobilized (Fig 30) by amine coupling on the sensor surface of CM5 chip with carboxymethylated dextran molecules covalently attached to the gold surface. The surface was firstly activated by injecting EDC/NHS. Afterwards, 50 μ g/mL GFP-Trap was injected to both the reference cell (Fc1) and active flow cell (F2) with a flow rate of 10 μ L/min for 7 min, excess reactive groups were deactivated with ethanolamine in the next step. The immobilization of GFP-Trap on the CM5 sensor surface resulted in a signal increase of about 3000 RU.

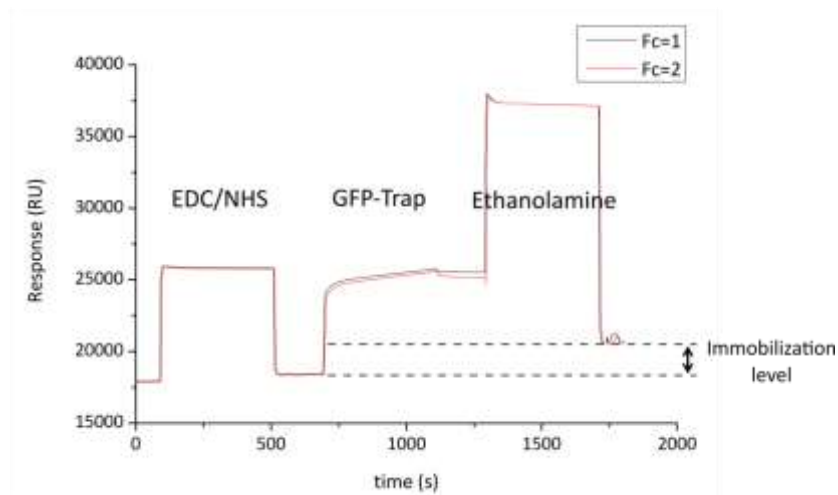


Figure 30: Immobilization of GFP-Trap on the CM5 sensor surface by amine coupling.

After the immobilization, β 1AR-nanodiscs were added to the active flow cell (Fc2) in different concentrations and with different flow rates (5 μ L/min, 10 μ L/min and 30 μ L/min) for different durations considering the aim of each experiment. For determination of binding events, samples (commercial antibodies, MAB23-6-7, huMAB23-6-7, isolated patient IgGs and patient serum samples) in different concentrations were added to the captured β 1AR nanodiscs (schematic illustration in Fig 31A). Fig 31B and 31C show two examples for binding of β 1AR nanodiscs on the CM5 sensor surface (80 s to 380 s) via previously immobilized GFP-Trap molecules, resulting in a signal increase of about 300 RU in sensorgrams. Subsequently binding (580 s to 880 s) of 150 nM anti-His-Tag antibody induced a further signal increase of 400 RU (Fig 31B), whereas 150 nM anti- β 1AR antibody MAB23-6-7 only 100 RU (Fig 31C). This great signal difference was probably caused by different numbers of antigens presented in one nanodisc. Two anti-His-Tag antibodies could theoretically bind to the same nanodisc because there are two copies of MSP carrying two His-Tags, whereas only one binding site is available for the anti- β 1AR antibody in one nanodisc.

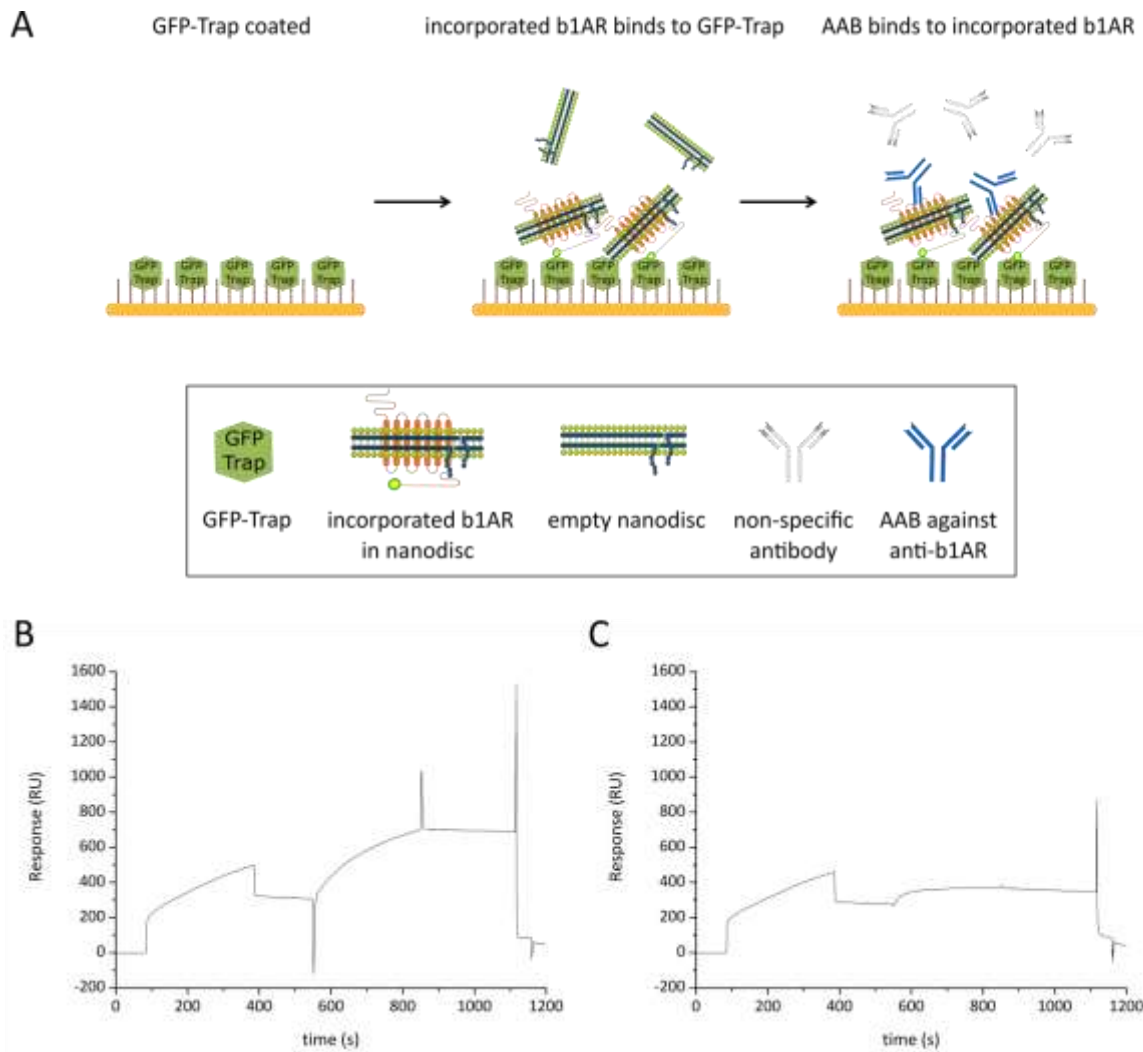


Figure 31: Binding of antibodies to β 1AR-YFP NDs captured on the sensor chip via GFP-Trap. A: Schematic illustration of the standard SPR setup. B: Sensorgram of binding of 150 nM anti-His (Ab34660) antibody. C: Sensorgram of binding of 150 nM anti- β 1AR (MAB23-6-7) antibody.

After the binding event, the sensor surface was regenerated with the Regeneration Solution 1. The sensor surface, as well as immobilized GFP-Trap molecules, was very stable upon regeneration and could be used for over 130 cycles (stability test for 75 cycles shown in Fig 32B). However, a slight signal increase of the baseline was observed after each cycle and must be considered for data interpretation.

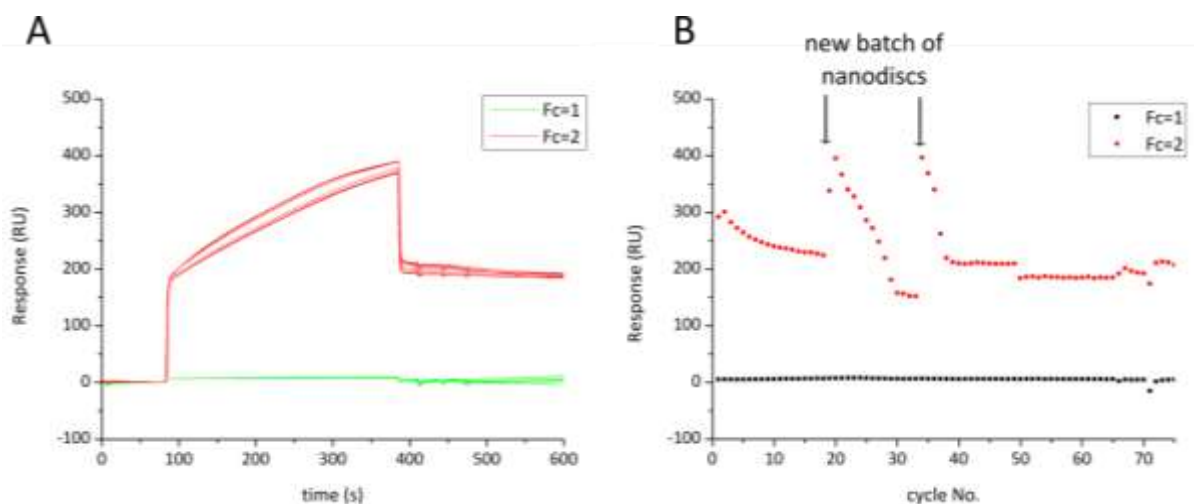


Figure 32: Stability of immobilized GFP-Trap and captured β 1AR-YFP-NDs on the sensor surface. The chip was regenerated with 100 mM glycine (pH 1.5) after the binding of β 1AR-YFP nanodiscs. A: SPR sensorgrams of 8 exemplary cycles. B: Signal level (stability) of reference and active flow cells for 75 cycles.

In addition, SPR experiments were also performed to measure binding affinity and binding kinetics of humanized MAB23-6-7 (huMAB23-6-7), which was generated through immunization against the second extracellular loop of the human β 1AR. Since the second extracellular loop is reported to represent the AAB binding domain of β 1AR (Venkatakrishnan et al., 2013), this monoclonal antibody was used for binding assays as well as in ELISA measurements as standard.

5.4.2.1. Affinity measurements

To further characterize the humanized mouse monoclonal antibody MAB23-6-7 (huMAB23-6-7), affinity measurements were performed with SPR. β 1AR-nanodiscs were captured with a flow rate of 5 μ L/min for 600 s. After the injection, 1200 s were waited to generate a stable baseline for the sequential antibody binding. To reduce the mass transfer effect, huMAB23-6-7 in different concentrations were injected with a high flow rate of 30 μ L/min for 180 s and the dissociation was monitored for further 600 s (Fig 33A). To regenerate the surface efficiently, a two-step regeneration procedure with low (100 mM glycine, pH 1.5) and high pH (50 mM NaOH, 1 M NaCl, pH 13) was performed. The affinity parameters were calculated with the Biacore X100 Evaluation Software using the steady-state affinity model, the sensorgram for zero-concentration sample was used for sensorgram subtraction (Fig 33B). The value of the equilibrium dissociation constant K_D was obtained by fitting a plot of response at equilibrium (R_{eq}) against the concentration (Fig 33C) at the steady-state phase and was determined as being 0.583 nM, which indicates a high binding affinity of huMAB23-6-7 to β 1AR (Fig 33D). This calculated K_D value corresponds well with the reported K_D range of 0.22 nM to 0.43 nM (Holthoff et al., 2012). This range was determined by interaction analysis of MAB23-6-7 to β 1AR overexpressing cells in a cell-based competition ELISA assay. A native-like folding

of $\beta 1ARs$ in nanodiscs can be assumed based on the similar binding behavior of MAB23-6-7 to $\beta 1AR$ incorporated in nanodiscs and overexpressed on the cell membrane.

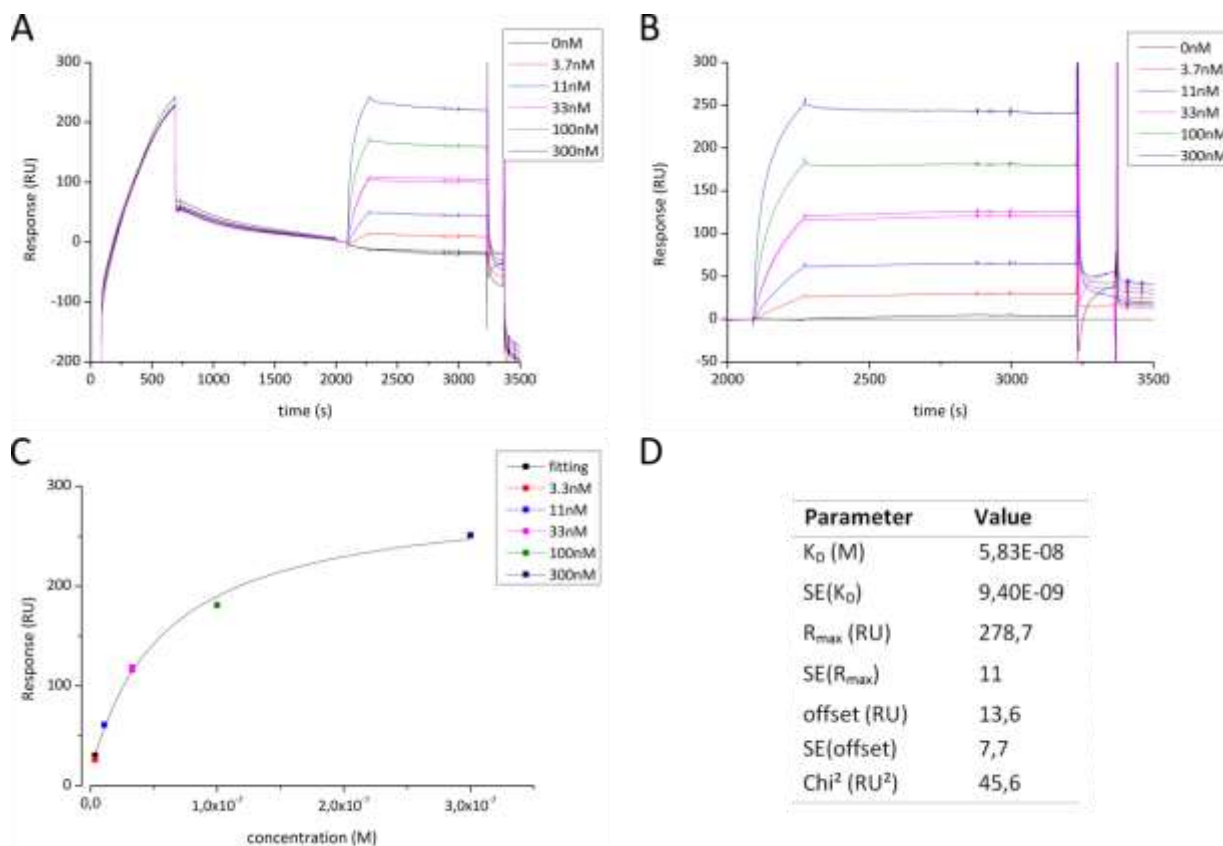


Figure 33: Binding affinity of huMAB23-6-7 to $\beta 1AR$ -YFP nanodisc. A: SPR sensorgrams of nanodisc capture and sequential huMAB23-6-7 binding. B: SPR sensorgrams of huMAB23-6-7 binding to captured nanodiscs, the sensorgrams are subtracted using the 0 nM sample. C: SPR signal level depending on huMAB23-6-7 concentration. D: Calculated affinity parameters.

5.4.2.2. Kinetic measurements

Kinetic parameters were calculated with the Biacore X100 Evaluation Software using the 1:1-binding model (Fig 34A). The calculation was based on the same experimental data analyzed for binding affinity shown in **section 5.4.2.1**. Replicate sensorgrams (33 nM of huMAB23-6-7, green in Fig 34A) showed similar signal levels and behavior, indicating a high reliability of the measurements. The global fitting function was used for the entire set of experimental data with exception of the data point 300 nM due to signal saturation. The residual values of the fit shown in Fig 34A varied between +5 RU and -5 RU (data not shown), the fitted curves correspond reasonably well to the sensorgrams. Estimated kinetic parameters are listed in Fig 34B, the association rate constant k_a , which characterizes the speed of the antibody binding to its target, was determined as $1.84 \times 10^5 \text{ M}^{-1}\text{s}^{-1}$. The dissociation rate constant k_d , characterizing the speed of the antibody dissociation from the target, was determined as $6 \times 10^{-6} \text{ s}^{-1}$.

It is important to highlight the extremely low dissociation rate, which could also be observed directly from the sensorgrams (Fig 33A and B). This property can be very advantageous for the use in ELISA assays, since the antibody-antigen binding will not be strongly influenced or destructed by harsh washing steps.

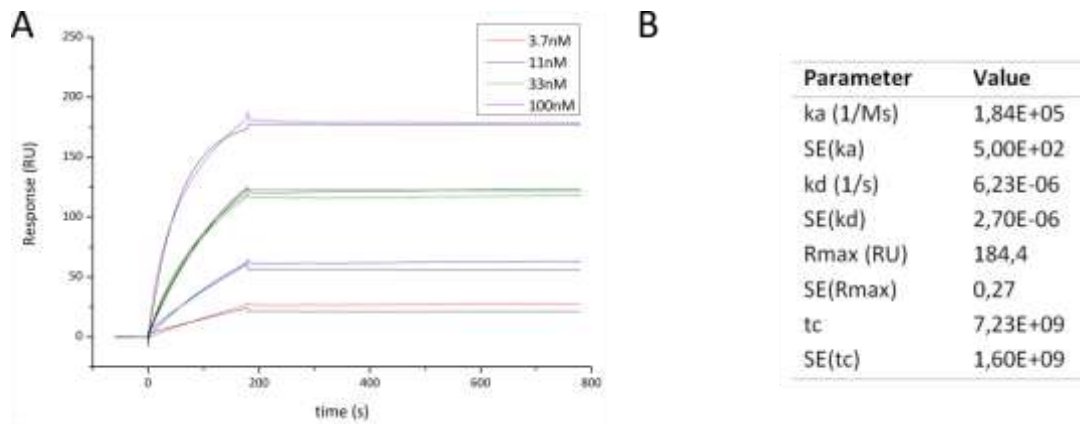


Figure 34: Binding kinetics of huMAB23-6-7 to β 1AR-YFP nanodisc. A: SPR sensorgrams of huMAB23-6-7 binding with fitting based on the 1:1-binding model. B: Calculated kinetic parameters.

5.5. ELISA assay with human serum samples

To establish an ELISA assay set-up for measurements of patient samples, a large number of optimization steps were performed to enhance the specific signal and at the same time to reduce the background noise. Nevertheless, the consumption of materials used was kept as low as possible to minimize the cost.

5.5.1. Optimization

5.5.1.1. Plate, Blocking Solution and Wash Buffer

Two kinds of Nunc-Immuno 96 MicroWell solid plates were verified for immobilization of capture antibodies used in the ELISA assay. Plates with PolySorp surface treatment were designed to have high affinity to molecules of a hydrophobic nature, whereas MaxiSorp plates bind to molecules with mixed hydrophilic/hydrophobic domains with high affinity. No noticeable signal difference could be determined by measuring the concentration of immobilized capture antibody on the surface (data not shown).

In addition, various Blocking Solutions and Wash Buffers were tested to reduce background noise. 5% skim milk, 5% BSA and 10% skim milk, all dissolved in PBS, were used to block the MaxiSorp plate for 2 hours. As control, wells were incubated with PBS for the same duration. After blocking, all wells were washed 4 times with PBS and incubated with THE His-Tag Antibody-HRP in different dilutions for 1 hour. Subsequently, the plate was washed again, incubated with substrate and read at 450 nm. As shown in Fig 35, all three Blocking Solutions were able to reduce the binding of the detection antibody to the ELISA plate remarkably after blocking. However, blocking with 5% BSA showed a higher signal level than blocking with skim milk, especially at high antibody concentration (1:1000). 5% skim milk seemed to be efficient enough to inhibit the binding of detection antibody on the surface, since the use of 10% skim milk didn't further reduce the unspecific signal.

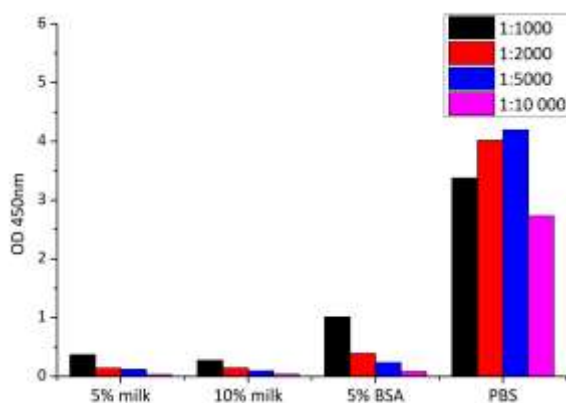


Figure 35: Impact of Blocking Solution on ELISA measurements.

Tween-20 is a widely used detergent in Wash Buffer to reduce unspecific binding in ELISA. The concentration of Tween-20 was carefully tested since assembled nanodiscs coated on the surface should not be destroyed by this detergent. To determine the optimal concentration of Tween-20 in the Wash Buffer, 5%, 0.1%, 0.05% and 0% Tween-20 in PBS were tested (data not shown) and the concentration 0.05% was efficient enough to reduce unspecific binding without destructing nanodiscs.

5.5.1.2. Antibodies and β 1AR nanodiscs

In a “Direct ELISA” set-up, nanodiscs would be immobilized directly on the ELISA plate to bind to autoantibodies from patient samples. In this thesis, the “Sandwich ELISA” variant with an additional capture antibody against β 1AR nanodiscs was preferred compared to the “Direct ELISA”. With the capture antibody targeting β 1AR-nanodiscs, other nanodiscs without or with other membrane proteins incorporated were removed from the ELISA plate and thus, the unspecific binding was reduced.

A large number of antibodies for immobilization of β 1AR-nanodiscs were tested. These could be classified into two groups according to their antigen, the anti- β 1AR antibodies and the anti-nanodiscs antibodies (anti-His-Tag and anti-PEG antibodies). However, the second group was not suitable to eliminate unspecific bindings, since nanodiscs without β 1AR were able to bind as well. By choosing antibodies from the first group, one important criterion must be fulfilled: the antibody should bind to the intracellular domains of β 1AR to allow the optimal presentation of the AAB binding pocket, which is formed by the second extracellular loop of the receptor. Additionally, various anti-GFP antibodies were tested as well since the C-terminal YFP-Tag is located in the intracellular compartment. However, conventional anti- β 1AR antibodies (bs0498 and ab3442 among others) and anti-GFP antibodies (JL-8, ab32146 and ab290 among others) were of murine or rabbit origin and due to cross activity partly recognized by the anti-human antibodies used as detection antibody.

Based on the points mentioned above, the GFP-Trap was chosen to be coated on the ELISA plate surface and to capture the YFP-Tag of incorporated β 1AR-YFP fusion protein in nanodiscs. GFP-Trap is a 13 kDa, stable single domain fragment of alpaca antibody (so-called nanobody) with high binding affinity and very low cross-activity with detection antibodies of human, murine or rabbit origin.

Considering cost reduction as an important factor in development of routine diagnostic assays, the amount of GFP-Trap necessary as capture antibody was empirically determined. Firstly, the absolute amount of GFP-Trap used per well was estimated. 5 μ g, 2.5 μ g, 1.2 μ g as well as 0 μ g of GFP-Trap were coated on a single well of a MaxiSorp plate, incubated with the same amount of nanodiscs as

well as anti-His antibody for detection. As shown in Fig 36A, an amount higher than 1.2 μg per well was unnecessary since the signal was not further increased. Based on this primary observation, the optimal amount of GFP-Trap, in combination with amount of $\beta\text{1AR-NDs}$ per well, was further examined. 1.2 μg , 0.6 μg , 0.3 μg and 0.15 μg GFP-Trap were coated and incubated with 100%, 50%, 25% and 12.5% of $\beta\text{1AR-nanodiscs}$ (100% equals nanodiscs generated from one reaction according the standard protocol). 100 μL of 1 ng/mL anti- β1AR antibody (huMAB23-6-7) were added subsequently to all the wells and detected by anti-mouse antibody (P0214). In relation to GFP-Trap amount, the amount of nanodiscs applied played a stronger role and seemed to be the limiting factor (Fig 36B) in this case. 100% and 50% of nanodiscs, combined with 1.2 μg and 0.6 μg of GFP-Trap, resulted in signal saturation and were therefore abundant for further implementation. 0.3 μg of GFP-Trap in combination with 25% $\beta\text{1AR-nanodiscs}$ were determined to be the best condition and were used in further ELISA experiments with patient serum samples as described in the experimental section (**section 4.2.8.**).

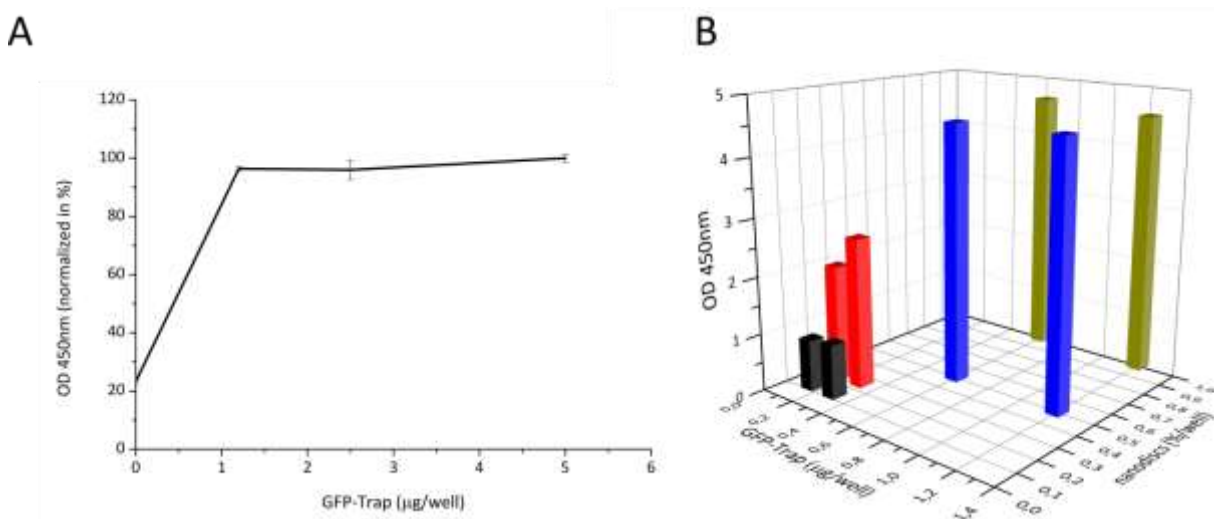


Figure 36: Impact of GFP-Trap amount (A) and combination of GFP-Trap and $\beta\text{1AR-NDs}$ amount (B) on ELISA measurements.

5.5.2. Standard ELISA set-up with GFP-Trap as capture antibody

Based on optimization steps described above, parameters such as assay plate, blocking solution, wash buffer, concentration of antibodies and $\beta\text{1AR-nanodiscs}$ were specified for the ELISA assay set-up, which is described in detail in experimental section (**section 4.2.8.**) and schematically illustrated in Fig 37.

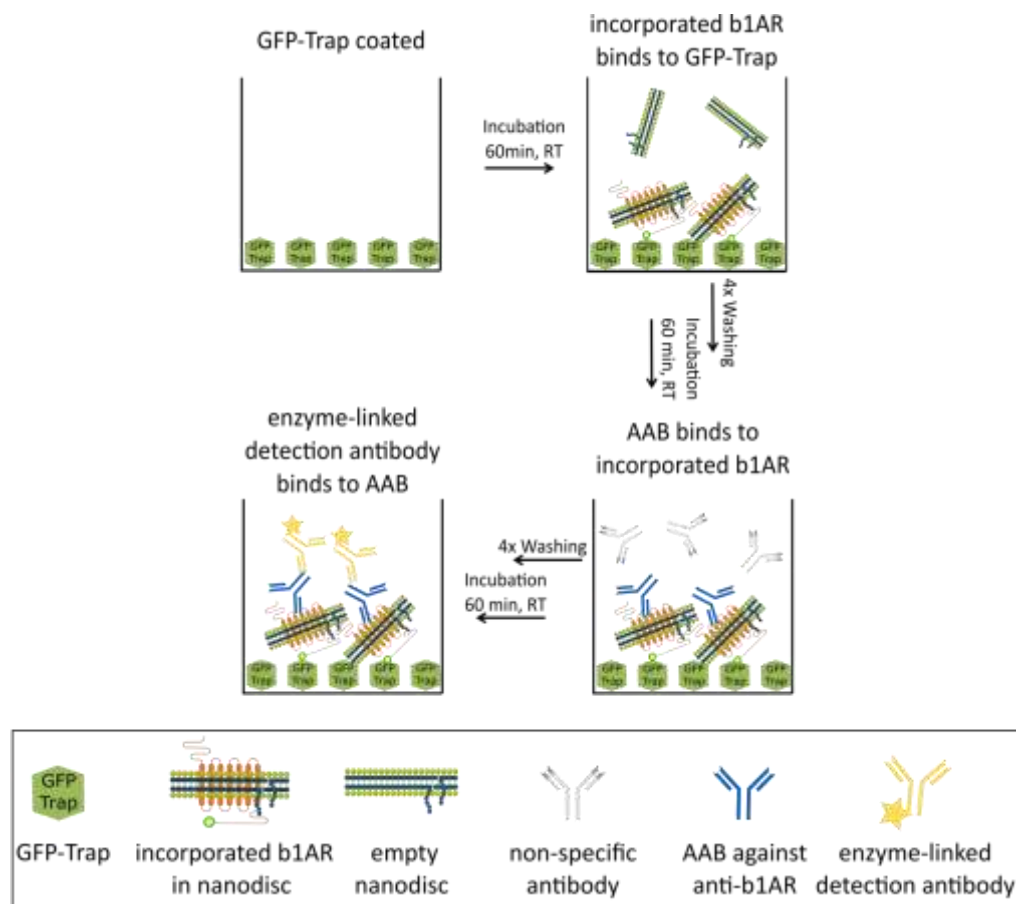


Figure 37: Schematic illustration of the standard ELISA set-up for patient sample measurements.

First of all, control experiments were carried out to determine the signal level of unspecific binding. For this approach, every component of the Sandwich ELISA was removed or replaced by other similar components (Fig 38), and the ELISA signal was compared and normalized pairwise with that of the standard set-up (set as 100%). When the ELISA plate was blocked directly without previous coating of GFP-Trap, an unspecific signal of 23% compared to the standard set-up was detected due to insufficient blocking of the surface and thus unspecific binding of β 1AR-nanodiscs. By replacement of β 1AR-nanodiscs by nanodiscs generated from wild type HEK293 cells, the unspecific ELISA signal was only 3%. Nanodiscs generated from HEK293 wild type cells could neither bind to the coated GFP-Trap nor be recognized by anti- β 1AR antibodies, which explains the very low level of unspecific signal. In the last experiment, antibodies binding to the β 1AR were replaced by a monoclonal antibody against human testosterone (BM2076) in the same concentration. An unspecific signal of 10% compared to the standard set-up was observed.

Taken together, all negative control experiments result in a much lower signal in comparison with the standard set-up. The noise level of about 10% by replacement of antibodies against β 1AR must be considered in measurements with patient samples.

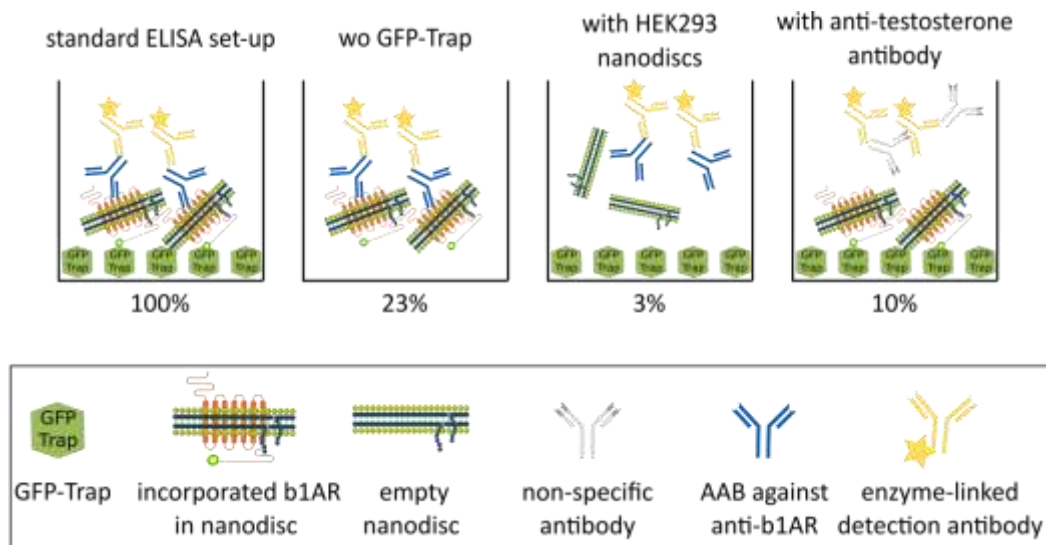


Figure 38: Schematic illustration and normalized ELISA signal of control experiments compared with the standard ELISA set-up.

With this standard set-up, analytical parameters such as limit of detection (LOD) and limit of quantification (LOQ) were estimated with the humanized monoclonal antibody of murine origin against the second extracellular loop of the β 1AR (huMAB23-6-7), which mimics pathological patient autoantibodies. A two-fold serial dilution from 10 μ g/mL to 0.61 ng/mL (14 data points with duplicate measurement) with an additional data point of 0 ng/mL (blank) was prepared with huMAB23-6-7 and measured with the standard ELISA assay (Fig 39A). LOD ($\text{LOD} = \text{mean}_{\text{blank}} + 3\text{SD}_{\text{blank}}$) represents the lowest antibody concentration which can be differentiated from the background noise, calculated from the measured blank value (data point 0 ng/mL). LOQ ($\text{LOQ} = \text{mean}_{\text{blank}} + 10\text{SD}_{\text{blank}}$) is defined as the lowest antibody concentration in a sample that can be quantitatively determined under the stated experimental conditions. To estimate LOD and LOQ, a non-linear growth Logistic5 fitting was applied to data points between 625 ng/mL and 0.61 ng/mL (Fig 39B), other data points with higher antibody concentration were excluded from the fitting due to signal saturation. Based on results of the Logistic5 fitting (data not shown) and the measured blank value (data point 0 ng/mL), the LOD was determined as 0.64 ng/mL and LOQ as 1.26 ng/mL.

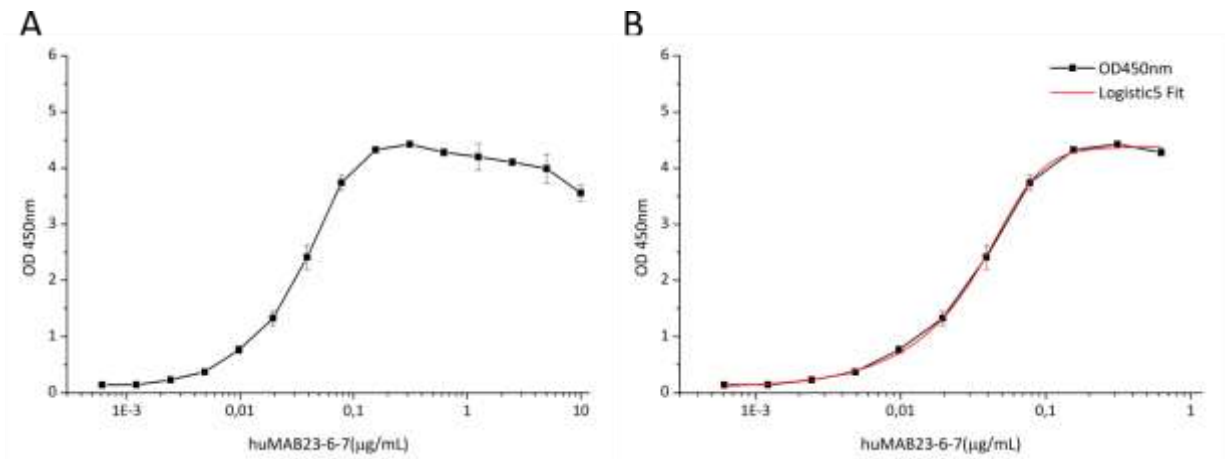


Figure 39: ELISA read-out of huMAB23-6-7 in two-fold serial dilution measured with the standard set-up (A), values under 0.625 µg/mL were fitted with non-linear growth Logistic5 model (B).

Another critical point in the pre-analytical phase is the effect of storage and transport conditions of human samples on analytical methods. Therefore, three serum samples were treated with harsh freeze-thaw cycles to simulate suboptimal storage and transport situation, the ELISA results were compared with those of the same samples measured directly after unfreezing on ice (Fig 40). Three situations were simulated in this case:

0: The aliquoted sample was taken from -80 °C, thawed on ice, measured.

I: The aliquoted sample was taken from -80 °C, unfrozen at RT, frozen at -80 °C, thawed at RT, measured.

II: The aliquoted sample was taken from -80 °C, unfrozen at RT and frozen at -80 °C for 4 times, thawed in water bath at 40 °C and frozen in liquid nitrogen for 5 times, measured.

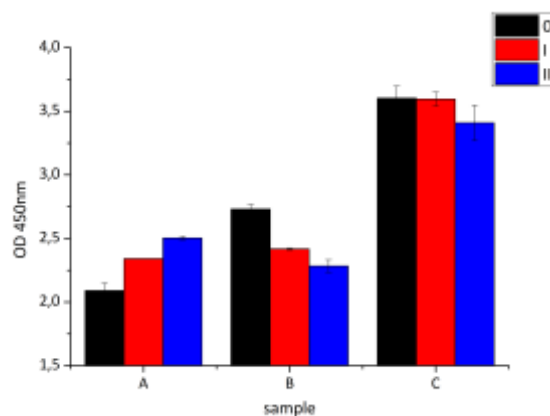


Figure 40: Impact of sample conditions on ELISA measurement. ELISA results of three human serum samples measured freshly after unfreezing on ice (0), one gentle freeze-thaw cycle (I) and nine harsh freeze-thaw cycles (II).

As expected, suboptimal storage and transport conditions affected the results measured with the same experimental set-up. In addition, it was remarkable that the same freeze-thaw condition decreased the signal of samples B and C, while increasing the signal of sample A. The coefficient of variation (CV) varied between 3.1% (sample C) and 9.3% (sample B).

Based on this observation, all patient samples were transported on dry ice and stored at -80 °C upon arrival. For measurement, the samples were thawed on ice, gently mixed after unfreezing and divided into 10 µL aliquots for storage at -80 °C until further use. If the measurement of one sample had to be repeated, a new aliquot was unfrozen on ice, every aliquot was only used once.

For measurements of patient samples, GFP-Trap and anti-human-IgG antibody (P0214) were taken from the same batch and stored in aliquots at 4 °C before use. All buffers used were prepared from the same stock solution. Nanodiscs were generated freshly for each plate using DDM, MSP1E3D1, PEG-PE and Bio-Beads from the same batch. The fluorescence signal of YFP-tag was determined in cell lysate used for nanodisc generation, the ratio of fluorescence intensity to protein concentration indicated the expression level of β 1AR-YFP fusion protein (Fig 41A, black). Generated nanodiscs were analyzed with SEC, the quotient of the height of the nanodisc peak to the volume injected onto the SEC column indicated the nanodisc concentration in the solution (Fig 41A, blue) used in the ELISA assay. Serial dilution of huMAB23-6-7 (3000, 1000, 333, 111, 37 and 0 pg/mL, diluted into PBS) was used to generate the standard curve. Two human serum samples P71 and K37 (diluted 1:250 into PBS) were measured in all ELISA plates to enable the calculation of inter-assay variability (Fig 41B and C). All standards as well as samples were measured in duplicate and the intra-assay variability was determined.

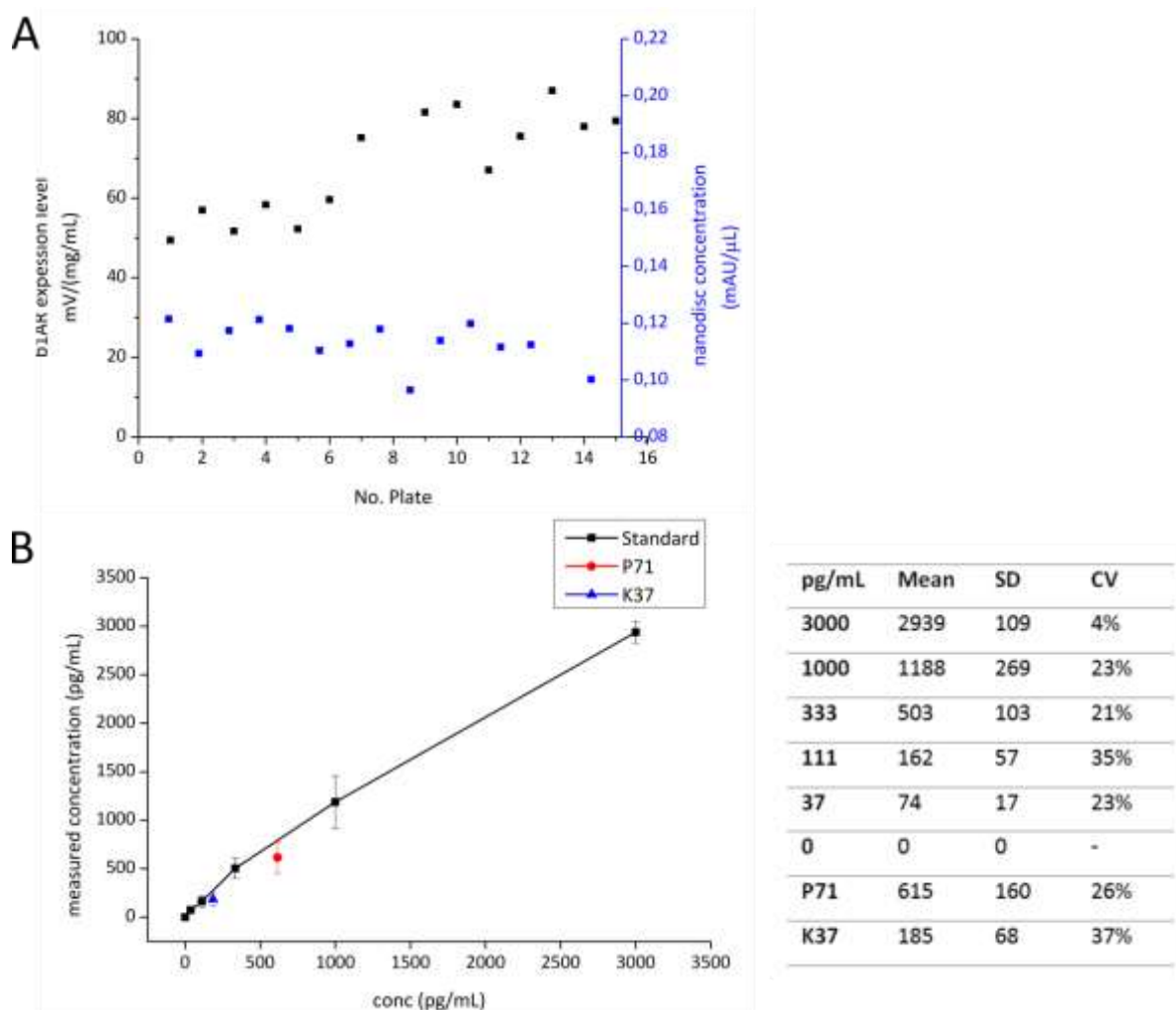


Figure 41: Inter-assay variance of applied standards and human serum samples, as well as β 1AR expression level and nanodisc concentration in 15 ELISA plates measured. A: The expression level of β 1AR-YFP fusion protein and the nanodisc concentration were monitored to determine the inter-assay difference between each nanodisc batch. B: Estimated anti- β 1AR-AAB concentration with standard deviation (SD) and coefficient of variation (CV).

As shown in Fig 41B, the SD remained similar in the absolute value, which implied a higher CV for standards and samples with low anti- β 1AR-AAB concentration.

Since the analytical cut-offs for pathological values are in the higher concentration range (2000 pg/mL and 3000 pg/mL), the impact of the high variation in lower concentration range is insignificant for measurements and classification of cardiomyopathy patient samples. Considering the complexity of the cell culture-based production of each nanodisc batch, reproducible expression levels of β 1AR-YFP fusion protein and nanodisc concentration were achieved (Fig 41A). The inter-assay CV is 24%, calculated based on values of the standards and two samples which were used in all 15 plates. Regarding the fact, that every plate was measured on another day and with the use of different batches of nanodiscs, the inter-assay CV could be further reduced if the nanodisc production is carried out in large-scale and a large number of ELISA plates are coated and stored before use.

5.5.2.1. Characterization of subjects measured with nanodisc ELISA

435 samples taken at different time points from 207 patients with cardiomyopathy as well as 90 samples from 90 healthy blood donors were measured in 15 ELISA plates with the standard set-up. The age distribution of cardiomyopathy patients measured is shown in Fig 42, it varied from 18 to 88 years with a mean of 56 years and median of 57 years. Over 80% of all patients were male (N=168). The control group is formed by healthy blood donors provided by Bayerisches Rotes Kreuz (BRK) with no detailed information about the age and sex distribution. According to the blood donation guideline of BRK, the donors must be from the age of 18 to the age of 72. They should be healthy and there should be no reason for exclusion based on the results of the questionnaire and the on-site medical examination. According to statistics published by the Robert Koch Institute, the gender distribution of blood donors is equal between male and female in Germany (Ritter, Willand, Reinhard, Offergeld, & Hamouda, 2008). The impact of different sex and age distributions between cardiomyopathy patients and healthy controls should be taken into account for further interpretation of the results.

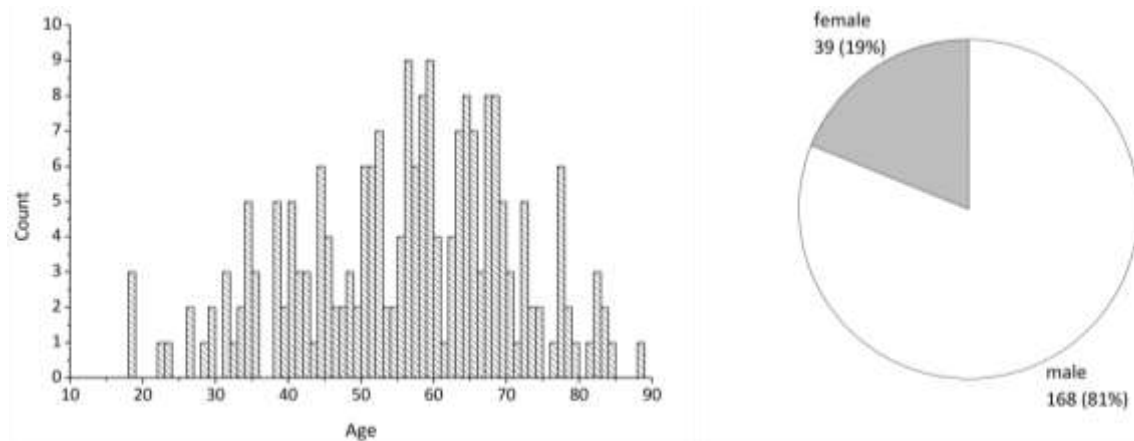


Figure 42: Age and sex distribution of cardiomyopathy patients measured with the ELISA assay.

Within the 207 cardiomyopathy patients measured, 110 were diagnosed with DCM, 84 with ICM and 13 with other types of cardiomyopathy (Fig 43A). The sex distribution inside subgroups DCM (Fig 43B1) and ICM (Fig 43B2) corresponds to the overall distribution. In the subgroup built of patients with other types of cardiomyopathy (Fig 43B3), the female proportion is much higher (54%) than in the total population (19%), however, the impact of the low patient number (N=13) in this subgroup must be considered. The age distribution within three subgroups is shown in Fig 43C1 and Fig 43C2. It should be noted that the average age of patients in the subgroup ICM is over 10 years higher than of patients in the other two subgroups.

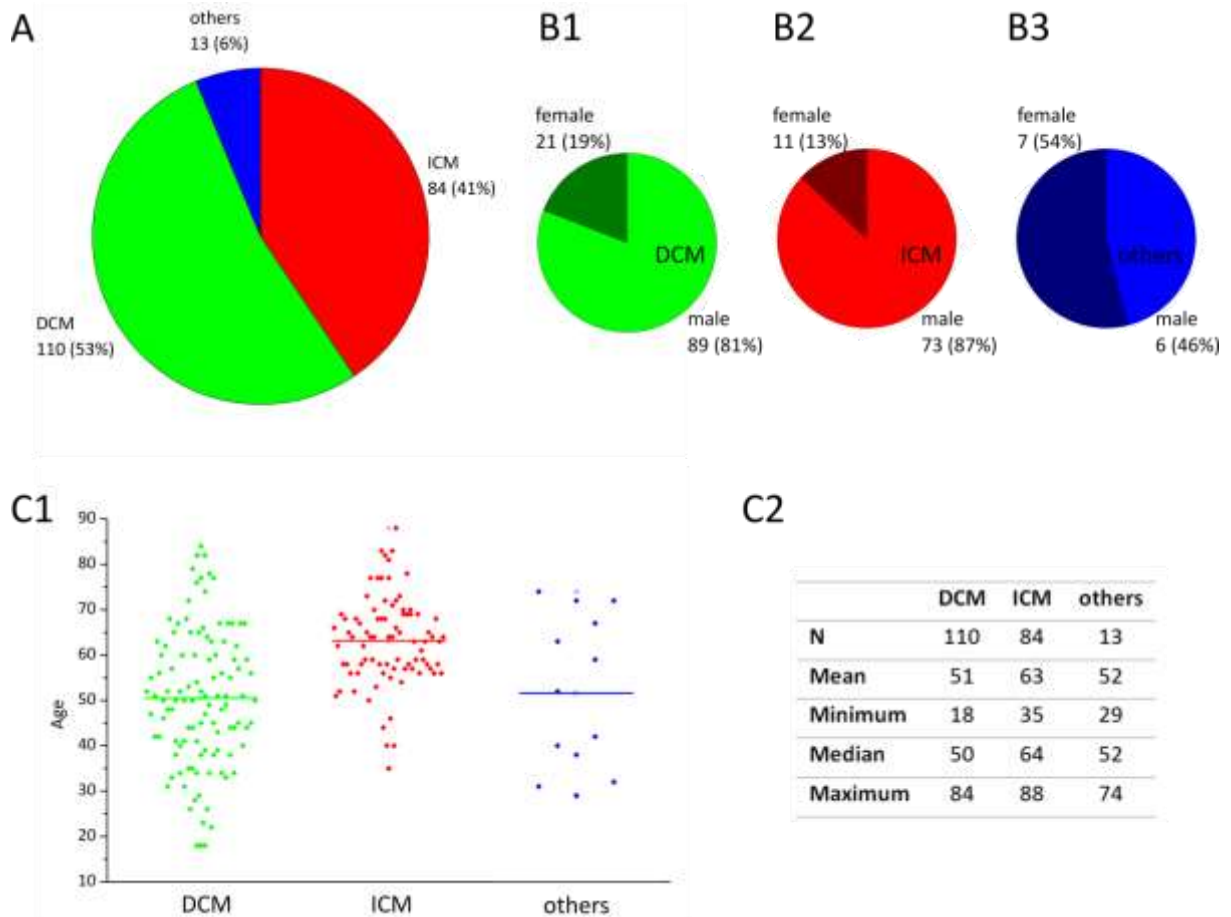


Figure 43: Patients splitted into subgroups based on diagnosis of cardiomyopathy (A), DCM in green, ICM in red and other types in blue. Sex (B1-B3) and age (C1 and C2) distributions within the subgroups differed from these in the total population.

From most of the cardiomyopathy patients only one sample was taken, the frequency of sampling at different time points is shown in Fig 44. If not stated otherwise, the antibody concentration in patient samples measured with nanodisc ELISA is given as mean of all samples from the same patient.

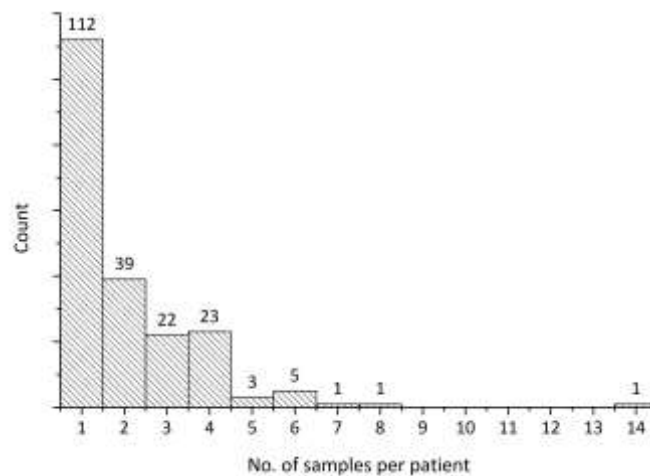


Figure 44: Frequency of sampling at different time points.

Information about duration of the disease is given for 133 of 207 cardiomyopathy patients, the average duration is 7 years, the shortest 1 year, the longest 40 years.

5.5.2.2. Statistical analysis of IgG concentration determined with the nanodisc ELISA

All samples were measured in duplicate with the standard ELISA set-up. The coefficient of variation (CV) of all tested single values with an absolute optical density of at least 1 at 450 nm was lower than 10%, the average intra-assay CV (as mean of all measured samples) was only 5%.

The calculated concentration of anti- β 1AR antibodies in measured samples from cardiomyopathy patients and healthy controls are shown in Fig 45A. The highest 12% in the healthy population corresponded to the literature reporting a 10% prevalence of anti- β 1AR antibodies in healthy controls (Dandel et al., 2012). A cut-off of 480 ng/mL could be set and two different subpopulations within healthy controls could be clearly separated. With this cut-off, 19% of cardiomyopathy samples are defined as positive, which is slightly lower than the percentage reported in publications (Dandel et al., 2012). If the proportion of positives in healthy controls is set as zero, an antibody concentration of 780 ng/mL could be seen as cut-off. In this case, 9% of cardiomyopathy samples will be defined as positive.

Since more than one sample was taken from some patients at different time points, the average concentration (mean) of all samples from the same patient was calculated (Fig 45B). If the same cut-off of 480 ng/mL is applied to the mean patient concentration, 21% of cardiomyopathy patients are defined as positive. Again, with the higher cut-off of 780 ng/mL, 0% of healthy controls and 6% of cardiomyopathy patients would be defined as positive.

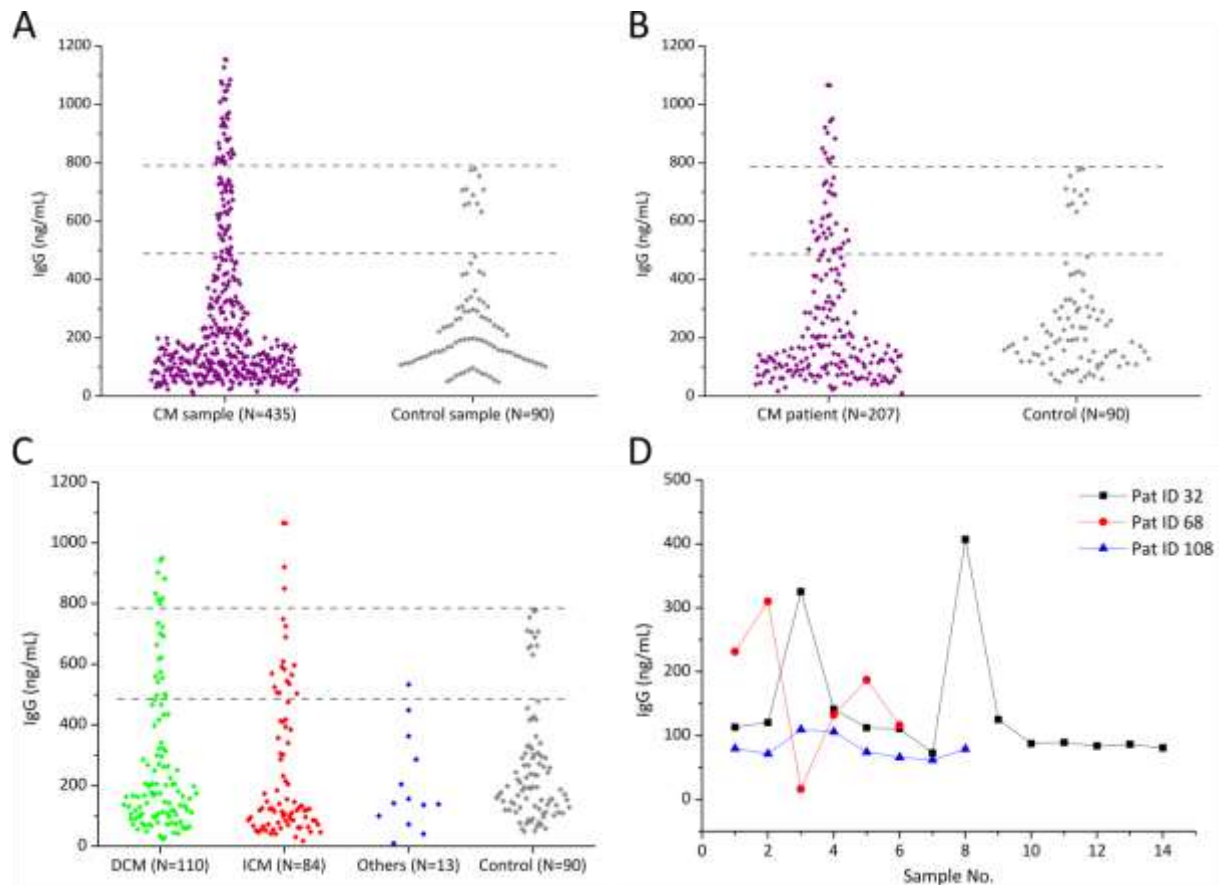


Figure 45: Calculated concentration of anti- β 1AR antibodies in human samples measured with the standard ELISA set-up. **A:** Calculated IgG concentration in samples from cardiomyopathy patients and healthy controls. **B:** Average IgG concentration determined for cardiomyopathy patients (mean) and healthy controls. **C:** Average IgG concentration determined for patients diagnosed with DCM, ICM and other types of cardiomyopathy and healthy controls. **D:** Calculated IgG concentration for three representative cardiomyopathy patients, from whom samples were taken at more than 6 time points.

To further analyze the difference between each subgroup, the average concentration (mean) of anti- β 1AR antibodies was calculated for each cardiomyopathy patient and categorized to the types of cardiomyopathy (Fig 45C, Table 5). Again, regarding the cut-off of 480 ng/mL, it could be shown clearly that the proportion of anti- β 1AR antibody-positive subjects within the subgroup “Others” remains similar as in the subgroup “Control”. Similar distribution between subgroups “DCM” and “ICM” was observed, which is two times higher than the control group. Considering the higher cut-off of 780 ng/mL, 7% of DCM patients and 5% ICM patients were classified as positive, while in subgroups “Others” and “Control” no subject was defined as positive. More importantly, the percentage of anti- β 1AR antibody-positive subjects found in DCM patients was over 50% higher than in ICM patients.

Table 5: Proportion of anti- β 1AR antibody-positive subjects in each subgroup considering defined cut-offs of 480 ng/mL and 780 ng/mL.

Cut-off	DCM (N=110)	ICM (N=84)	Others (N=13)	Control (N=90)
780 ng/mL	7.3%	4.8%	0%	0%
480 ng/mL	20.9%	22.6%	7.7%	12.2%

Comparing Fig 45A and Fig 45B, it could be clearly seen that some data points of very high antibody concentration decreased in their value while calculating the average mean by assignment of samples to patients. The impact of the assignment of samples to patients is further analyzed in Fig 45D. Measured concentrations of anti- β 1AR antibodies from three patients, from whom more than 6 samples at different time points were taken, showed different behavior in their changes over time. While the measured IgG value of patient 108 (blue) showed a very constant level over 8 sampling time points, the IgG level of patient 68 (red) varied strongly over 6 time points. 14 samples taken at different time points are assigned to patient 32 (black), while 12 of the 14 samples showed a similar level of measured IgG concentrations, two data points (time points 3 and 8) varied strongly from the others. Since the coefficient of variation of the nanodisc ELISA is very low, this effect was not caused by the measurement. A closer look into the disease description of the patients, especially in combination with the treatment and disease progression would give more insights into this interesting finding.

There is no significant correlation between antibody concentrations measured with nanodisc ELISA and age or disease duration of subjects using Pearson correlation analysis. Based on the results of the one-way analysis of variance (ANOVA), the means of male and female populations are not significantly different. There is also no significant correlation between antibody concentration measured with nanodisc ELISA and parameters such as Diabetes mellitus, hypertension or the level of ejection fraction of the heart (ANOVA).

Taken together, with the anti- β 1AR antibody concentration determined with the nanodisc ELISA, it was possible to set two cut-offs to differ analyzed subjects in anti- β 1AR antibody positive and negative populations. To further analyze the autoantibody concentration predicted by nanodisc ELISA, a smaller collective of patients and healthy controls will be measured in the future with the bioassay recording the contraction frequency of rat neonatal cardiomyocytes (Wenzel et al., 2017) as well as the functional cell-based FACS assay (Bornholz, Benninghaus, et al., 2016).

6. Conclusion and Outlook

Within the scope of this thesis, the nanodisc generation protocol with purified, recombinant proteins overexpressed in *E. coli* originally developed by Sligar and colleagues was adapted and optimized for cell lysate from human HEK293 cell lines without membrane isolation or further purification steps. Generated nanodiscs were analyzed with size exclusion chromatography. The incorporation of model membrane proteins was confirmed by western blotting, while the shape and size of nanodiscs were imaged with electron microscopy. The protocol optimization was verified upon choice of detergent, MSP variant, PEG-PE concentration, amount of Bio-Beads and other reaction components, as well as reaction time. First scale up and storage experiments were also successfully carried out. However, toward large-scale production of nanodiscs, other expression systems such as cell-free expression (Proverbio et al., 2013) or protein expression in insect cells should be considered to increase the amount of protein of interest in the first instance. The scale up approach should be further pursued and the process should be automated to achieve a higher yield and improve the quality, accuracy and precision of nanodisc production, if required.

In the second part of the thesis, nanodiscs incorporating beta-1 adrenergic receptor were characterized with size exclusion chromatography, western blotting and fluorescence spectroscopy. The biological functionality of reconstituted β 1ARs was examined with pull-down assay using magnetic beads covalently conjugated with alprenolol. Again, to enable the production of β 1AR-nanodiscs in industrial scale, the nanodisc generation process, as well as the affinity purification process, should be further improved and automated.

For detection of pathological autoantibodies in DCM patients, nanodiscs incorporating beta-1 adrenergic receptor were applied for stable antigen presentation of the conformational epitope. This construct was verified in pull-down assays with GFP-Trap covalently coated on magnetic beads, as well as in SPR and ELISA experiments using the monoclonal antibody huMAB23-6-7. Moreover, the binding affinity and kinetics of the humanized MAB23-6-7 antibody (huMAB23-6-7), which binds to the same conformational epitope as autoantibodies from patients, were characterized with SPR. The final ELISA set-up for measurements of human serum samples was optimized regarding choice, concentration and properties of consumables and reagents applied. The impact of sample stability in terms of transport and storage conditions was analyzed. In addition, the possibility of storage and transport of pre-coated ELISA plates with GFP-Trap and β 1AR-nanodiscs is also given.

Since the ELISA assay was purposed to be implemented into routine diagnostics, a cost calculation (Table 6) was performed based on list prices according to manufacturers in 2017. The material cost for one ELISA plate amounts to 190 €. If the ELISA plate is used for 40 patient samples (measurement in duplicate), the material cost for one sample is less than 5 €, which is lower than the legitimate fee of 19.44 € for antibody detection with qualitative test methods according the German physicians' fee schedule (Gebührenordnung für Ärzte GOÄ, M III. 8. Antikörper gegen körpereigene Antigene oder Haptene, 3812.H2 Untersuchung auf Antikörper gegen Herzmuskulatur mittels qualitativer Immunfluoreszenzuntersuchung oder ähnlicher Untersuchungsmethoden).

Table 6: Cost calculation for ELISA assay with β 1AR-YFP nanodiscs. Costs are calculated for one ELISA plate and for one patient, price in EUR, VAT 19%. Only costs for consumables and reagents are considered, the final price with additional staff costs and eventual discounts has to be adjusted accordingly.

Item	Price in € (one plate)	Price in € (one patient)
Nunc MaxiSorp 96 well plate	1.95	0.05
GFP-Trap	27.00	0.68
Bio-Beads	7.12	0.18
MSP1E3D1	143.19	3.58
PEG-PE	1.32	0.03
Chemical for buffers	2.00	0.05
anti-human IgG antibody (detection)	2.33	0.06
huMAB23-6-7 as standard	5.00	0.13
Sum	189.90	4.75

Parameters indicating the analytical performance of the nanodisc ELISA assay were determined and assessed. Measurements with the standard ELISA set-up showed a high intra- and inter-assay precision. The coefficient of variation (CV) of all tested single values (two technical replicates each) was lower than 10%, the average intra-assay CV (as mean of all measured samples) was only 5%. The average inter-assay CV was 24%, calculated based on values of standards and samples measured in all 15 plates. Inter-day and inter-nanodisc batch aspects were also assessed in the determination of inter-assay CV, therefore, it could be further reduced by large-scale production of nanodiscs and preparation of the ELISA plates prior to measurements. By the use of the humanized monoclonal murine antibody huMAB23-6-7, the limit of determination (LOD) was determined as 0.64 ng/mL and the limit of quantification (LOQ) as 1.26 ng/mL. Taken together, the nanodisc ELISA with β 1AR-nanodiscs as target antigen for the detection and quantification of anti- β 1AR autoantibody in human samples fulfilled requirements of standardization and reliability for a possible adaptation into clinical diagnostic testing. In addition, the possibility of high-throughput analysis given by the ELISA assay circumvents the disadvantage of a limited sample throughput of the bioassay detecting the impact of autoantibodies on cardiomyocyte contraction (Wenzel et al., 2017).

Samples from 90 healthy blood donors and 207 cardiomyopathy patients were measured with the established ELISA assay. It was possible to differ samples with binding AABs from controls and autoimmune-negative patients based on measured ELISA results. Our results match the distribution of AAB-positive individuals described by Patel et al 2013 (Patel & Hernandez, 2013). Measurements in the frame of this work were performed with the humanized monoclonal murine antibody huMAB23-6-7 against the second extracellular loop of β 1AR as standard. Alternatively, a well-characterized human sample with a high concentration of anti- β 1AR autoantibodies could be used as standard and should be further investigated and validated in the future.

Regarding the recruitment of DCM patient samples, a larger population with well-defined donors will help for a better understanding of the disease progression. Patient samples prior and after immunoglobulin apheresis or other kinds of treatments, together with information on physiological states and symptoms of the patients, would be helpful to interpret the ELISA result. The control group used in this thesis was formed by healthy blood donors of the BRK with unknown characteristics. Due to the unequal distribution of analyzed DCM patients, a sex- and age-matched control group would be more suitable.

In general, the nanodisc generation protocol for the reconstitution of β 1AR could be easily adapted for other membrane proteins of interest, which are overexpressed in HEK293 or other comparable human cell lines. For the ELISA assay in this study, the protein construct with a single fluorescence tag (β 1AR-YFP) was used. A possible functional assay could be developed with the β 1AR-FRET construct with both YFP- and CFP-Tags for optical detection of the FRET event induced by conformational change of the receptor upon AAB binding. Beside the diagnostic approach, nanodiscs incorporating β 1AR could also be used for treatment of autoimmune-induced DCM (immunoabsorption, neutralization) as well as for vaccination in the preventive healthcare.

7. References

- Ahles, A., & Engelhardt, S. (2014). Polymorphic variants of adrenoceptors: pharmacology, physiology, and role in disease. *Pharmacol Rev*, *66*(3), 598-637. doi: 10.1124/pr.113.008219
- Akkaladevi, N., Mukherjee, S., Katayama, H., Janowiak, B., Patel, D., Gogol, E. P., . . . Fisher, M. T. (2015). Following Nature's Lead: On the Construction of Membrane-Inserted Toxins in Lipid Bilayer Nanodiscs. *J Membr Biol*, *248*(3), 595-607. doi: 10.1007/s00232-014-9768-3
- Alami, M., Dalal, K., Lelj-Garolla, B., Sligar, S. G., & Duong, F. (2007). Nanodiscs unravel the interaction between the SecYEG channel and its cytosolic partner SecA. *EMBO J*, *26*(8), 1995-2004. doi: 10.1038/sj.emboj.7601661
- Arinaminpathy, Y., Khurana, E., Engelman, D. M., & Gerstein, M. B. (2009). Computational analysis of membrane proteins: the largest class of drug targets. *Drug Discov Today*, *14*(23-24), 1130-1135. doi: 10.1016/j.drudis.2009.08.006
- Baas, B. J., Denisov, I. G., & Sligar, S. G. (2004). Homotropic cooperativity of monomeric cytochrome P450 3A4 in a nanoscale native bilayer environment. *Arch Biochem Biophys*, *430*(2), 218-228. doi: 10.1016/j.abb.2004.07.003
- Bayburt, T. H., Carlson, J. W., & Sligar, S. G. (1998). Reconstitution and imaging of a membrane protein in a nanometer-size phospholipid bilayer. *J Struct Biol*, *123*(1), 37-44. doi: 10.1006/jsbi.1998.4007
- Bayburt, T. H., Grinkova, Y. V., & Sligar, S. G. (2002). Self-Assembly of Discoidal Phospholipid Bilayer Nanoparticles with Membrane Scaffold Proteins. *Nano Lett*, *2*(8), 853-856. doi: 10.1021/nl025623k
- Bayburt, T. H., & Sligar, S. G. (2010). Membrane protein assembly into Nanodiscs. *FEBS Lett*, *584*(9), 1721-1727. doi: 10.1016/j.febslet.2009.10.024
- Benjamin, E. J., Blaha, M. J., Chiuve, S. E., Cushman, M., Das, S. R., Deo, R., . . . Muntner, P. (2017). Heart Disease and Stroke Statistics-2017 Update: A Report From the American Heart Association. *Circulation*, *135*(10), e146-e603. doi: 10.1161/CIR.0000000000000485
- Bisognano, J. D., Weinberger, H. D., Bohlmeier, T. J., Pende, A., Reynolds, M. V., Sastravaha, A., . . . Port, D. J. (2000). Myocardial-directed overexpression of the human beta(1)-adrenergic receptor in transgenic mice. *J Mol Cell Cardiol*, *32*(5), 817-830. doi: 10.1006/jmcc.2000.1123
- Blois, T. M., & Bowie, J. U. (2009). G-protein-coupled receptor structures were not built in a day. *Protein Sci*, *18*(7), 1335-1342. doi: 10.1002/pro.165
- Bocquet, N., Kohler, J., Hug, M. N., Kuszniur, E. A., Rufer, A. C., Dawson, R. J., . . . Huber, S. (2015). Real-time monitoring of binding events on a thermostabilized human A2A receptor embedded in a lipid bilayer by surface plasmon resonance. *Biochim Biophys Acta*, *1848*(5), 1224-1233. doi: 10.1016/j.bbamem.2015.02.014
- Borch, J., Torta, F., Sligar, S. G., & Roepstorff, P. (2008). Nanodiscs for immobilization of lipid bilayers and membrane receptors: kinetic analysis of cholera toxin binding to a glycolipid receptor. *Anal Chem*, *80*(16), 6245-6252. doi: 10.1021/ac8000644
- Bornholz, B., Benninghaus, T., Reinke, Y., Felix, S. B., Roggenbuck, D., Jahns-Boivin, V., . . . Boege, F. (2016). A standardised FACS assay based on native, receptor transfected cells for the clinical diagnosis and monitoring of beta1-adrenergic receptor autoantibodies in human heart disease. *Clin Chem Lab Med*, *54*(4), 683-691. doi: 10.1515/cclm-2015-0603
- Bornholz, B., Hanzen, B., Reinke, Y., Felix, S. B., Jahns, R., Schimke, I., . . . Boege, F. (2016). Detection of DCM-associated beta1-adrenergic receptor autoantibodies requires functional readouts or native human beta1-receptors as targets. *Int J Cardiol*, *202*, 728-730. doi: 10.1016/j.ijcard.2015.10.068

- Bornholz, B., Roggenbuck, D., Jahns, R., & Boege, F. (2014). Diagnostic and therapeutic aspects of beta1-adrenergic receptor autoantibodies in human heart disease. *Autoimmun Rev*, *13*(9), 954-962. doi: 10.1016/j.autrev.2014.08.021
- Bornholz, B., Weidtkamp-Peters, S., Schmitmeier, S., Seidel, C. A., Herda, L. R., Felix, S. B., . . . Boege, F. (2013). Impact of human autoantibodies on beta1-adrenergic receptor conformation, activity, and internalization. *Cardiovasc Res*, *97*(3), 472-480. doi: 10.1093/cvr/cvs350
- Bristow, M. R., Kantrowitz, N. E., Ginsburg, R., & Fowler, M. B. (1985). Beta-adrenergic function in heart muscle disease and heart failure. *J Mol Cell Cardiol*, *17 Suppl 2*, 41-52.
- Buvall, L., Tang, M. S., Isic, A., Andersson, B., & Fu, M. (2007). Antibodies against the beta1-adrenergic receptor induce progressive development of cardiomyopathy. *J Mol Cell Cardiol*, *42*(5), 1001-1007. doi: 10.1016/j.yjmcc.2007.02.007
- Carlson, J. W., Jonas, A., & Sligar, S. G. (1997). Imaging and manipulation of high-density lipoproteins. *Biophys J*, *73*(3), 1184-1189. doi: 10.1016/S0006-3495(97)78150-5
- Caron, M. G., & Lefkowitz, R. J. (1976). Solubilization and characterization of the beta-adrenergic receptor binding sites of frog erythrocytes. *J Biol Chem*, *251*(8), 2374-2384.
- Caron, M. G., Srinivasan, Y., Pitha, J., Kocielek, K., & Lefkowitz, R. J. (1979). Affinity chromatography of the beta-adrenergic receptor. *J Biol Chem*, *254*(8), 2923-2927.
- Chang, H. R., Tsao, D. A., Yu, H. S., & Ho, C. K. (2005). The change of beta-adrenergic system after cessation of lead exposure. *Toxicology*, *207*(1), 73-80. doi: 10.1016/j.tox.2004.08.018
- Chattopadhyay, A., Rao, B. D., & Jafurulla, M. (2015). Solubilization of G protein-coupled receptors: a convenient strategy to explore lipid-receptor interaction. *Methods Enzymol*, *557*, 117-134. doi: 10.1016/bs.mie.2015.01.001
- Christopher, J. A., Brown, J., Dore, A. S., Errey, J. C., Koglin, M., Marshall, F. H., . . . Congreve, M. (2013). Biophysical fragment screening of the beta1-adrenergic receptor: identification of high affinity arylpiperazine leads using structure-based drug design. *J Med Chem*, *56*(9), 3446-3455. doi: 10.1021/jm400140q
- Cruickshank, J. M. (2010). Beta blockers in hypertension. *Lancet*, *376*(9739), 415. doi: 10.1016/S0140-6736(10)61217-2
- Dandel, M., Englert, A., Wallukat, G., Riese, A., Knosalla, C., Stein, J., & Hetzer, R. (2015). Immunoabsorption can improve cardiac function in transplant candidates with non-ischemic dilated cardiomyopathy associated with diabetes mellitus. *Atheroscler Suppl*, *18*, 124-133. doi: 10.1016/j.atherosclerosissup.2015.02.023
- Dandel, M., Wallukat, G., Englert, A., & Hetzer, R. (2013). Immunoabsorption therapy for dilated cardiomyopathy and pulmonary arterial hypertension. *Atheroscler Suppl*, *14*(1), 203-211. doi: 10.1016/j.atherosclerosissup.2012.10.029
- Dandel, M., Wallukat, G., Potapov, E., & Hetzer, R. (2012). Role of beta(1)-adrenoceptor autoantibodies in the pathogenesis of dilated cardiomyopathy. *Immunobiology*, *217*(5), 511-520. doi: 10.1016/j.imbio.2011.07.012
- Das, A., Zhao, J., Schatz, G. C., Sligar, S. G., & Van Duyne, R. P. (2009). Screening of type I and II drug binding to human cytochrome P450-3A4 in nanodiscs by localized surface plasmon resonance spectroscopy. *Anal Chem*, *81*(10), 3754-3759. doi: 10.1021/ac802612z
- Denisov, I. G., Grinkova, Y. V., Lazarides, A. A., & Sligar, S. G. (2004). Directed self-assembly of monodisperse phospholipid bilayer Nanodiscs with controlled size. *J Am Chem Soc*, *126*(11), 3477-3487. doi: 10.1021/ja0393574
- Deubner, N., Berliner, D., Schlipp, A., Gelbrich, G., Caforio, A. L., Felix, S. B., . . . Survival-Study, G. (2010). Cardiac beta1-adrenoceptor autoantibodies in human heart disease: rationale and design of the Etiology, Titre-Course, and Survival (ETiCS) Study. *Eur J Heart Fail*, *12*(7), 753-762. doi: 10.1093/eurjhf/hfq072
- Dorsch, S., Klotz, K. N., Engelhardt, S., Lohse, M. J., & Bunemann, M. (2009). Analysis of receptor oligomerization by FRAP microscopy. *Nat Methods*, *6*(3), 225-230. doi: 10.1038/nmeth.1304

- Engelhardt, S., Hein, L., Wiesmann, F., & Lohse, M. J. (1999). Progressive hypertrophy and heart failure in beta1-adrenergic receptor transgenic mice. *Proc Natl Acad Sci U S A*, *96*(12), 7059-7064.
- Felix, S. B., Staudt, A., Landsberger, M., Grosse, Y., Stangl, V., Spielhagen, T., . . . Stangl, K. (2002). Removal of cardiodepressant antibodies in dilated cardiomyopathy by immunoadsorption. *J Am Coll Cardiol*, *39*(4), 646-652. doi: 10.1016/S0735-1097(01)01794-6
- Ferre, S., & Franco, R. (2010). Oligomerization of G-protein-coupled receptors: a reality. *Curr Opin Pharmacol*, *10*(1), 1-5. doi: 10.1016/j.coph.2009.11.002
- Fredriksson, R., Lagerstrom, M. C., Lundin, L. G., & Schioth, H. B. (2003). The G-protein-coupled receptors in the human genome form five main families. Phylogenetic analysis, paralagon groups, and fingerprints. *Mol Pharmacol*, *63*(6), 1256-1272. doi: 10.1124/mol.63.6.1256
- Freedman, N. J., & Lefkowitz, R. J. (2004). Anti-beta(1)-adrenergic receptor antibodies and heart failure: causation, not just correlation. *J Clin Invest*, *113*(10), 1379-1382. doi: 10.1172/JCI21748
- Freemantle, N., Cleland, J., Young, P., Mason, J., & Harrison, J. (1999). beta Blockade after myocardial infarction: systematic review and meta regression analysis. *BMJ*, *318*(7200), 1730-1737. doi: 10.1136/bmj.318.7200.1730
- Gao, Y., Cao, E., Julius, D., & Cheng, Y. (2016). TRPV1 structures in nanodiscs reveal mechanisms of ligand and lipid action. *Nature*, *534*(7607), 347-351. doi: 10.1038/nature17964
- Garavito, R. M., & Ferguson-Miller, S. (2001). Detergents as tools in membrane biochemistry. *J Biol Chem*, *276*(35), 32403-32406. doi: 10.1074/jbc.R100031200
- Gluck, J. M., Koenig, B. W., & Willbold, D. (2011). Nanodiscs allow the use of integral membrane proteins as analytes in surface plasmon resonance studies. *Anal Biochem*, *408*(1), 46-52. doi: 10.1016/j.ab.2010.08.028
- Goddard, A. D., Dijkman, P. M., Adamson, R. J., dos Reis, R. I., & Watts, A. (2015). Reconstitution of membrane proteins: a GPCR as an example. *Methods Enzymol*, *556*, 405-424. doi: 10.1016/bs.mie.2015.01.004
- Haberland, A., Wallukat, G., Dahmen, C., Kage, A., & Schimke, I. (2011). Aptamer neutralization of beta1-adrenoceptor autoantibodies isolated from patients with cardiomyopathies. *Circ Res*, *109*(9), 986-992. doi: 10.1161/circresaha.111.253849
- Hagn, F., Etzkorn, M., Raschle, T., & Wagner, G. (2013). Optimized phospholipid bilayer nanodiscs facilitate high-resolution structure determination of membrane proteins. *J Am Chem Soc*, *135*(5), 1919-1925. doi: 10.1021/ja310901f
- Holthoff, H. P., Zeibig, S., Jahns-Boivin, V., Bauer, J., Lohse, M. J., Kaab, S., . . . Ungerer, M. (2012). Detection of anti-beta1-AR autoantibodies in heart failure by a cell-based competition ELISA. *Circ Res*, *111*(6), 675-684. doi: 10.1161/CIRCRESAHA.112.272682
- Huang, J., Chen, S., Zhang, J. J., & Huang, X. Y. (2013). Crystal structure of oligomeric beta1-adrenergic G protein-coupled receptors in ligand-free basal state. *Nat Struct Mol Biol*, *20*(4), 419-425. doi: 10.1038/nsmb.2504
- Inagaki, S., Ghirlando, R., & Grisshammer, R. (2013). Biophysical characterization of membrane proteins in nanodiscs. *Methods*, *59*(3), 287-300. doi: 10.1016/j.ymeth.2012.11.006
- Iwata, M., Yoshikawa, T., Baba, A., Anzai, T., Mitamura, H., & Ogawa, S. (2001). Autoantibodies against the second extracellular loop of beta1-adrenergic receptors predict ventricular tachycardia and sudden death in patients with idiopathic dilated cardiomyopathy. *J Am Coll Cardiol*, *37*(2), 418-424. doi: 10.1016/S0735-1097(00)01109-8
- Jahns, R., Boivin, V., & Lohse, M. J. (2006). Beta 1-adrenergic receptor-directed autoimmunity as a cause of dilated cardiomyopathy in rats. *Int J Cardiol*, *112*(1), 7-14. doi: 10.1016/j.ijcard.2006.05.008
- Jahns, R., Boivin, V., Siegmund, C., Inselmann, G., Lohse, M. J., & Boege, F. (1999). Autoantibodies activating human beta1-adrenergic receptors are associated with reduced cardiac function in chronic heart failure. *Circulation*, *99*(5), 649-654. doi: 10.1161/01.CIR.99.5.649

- Jane-wit, D., Altuntas, C. Z., Johnson, J. M., Yong, S., Wickley, P. J., Clark, P., . . . Tuohy, V. K. (2007). Beta 1-adrenergic receptor autoantibodies mediate dilated cardiomyopathy by agonistically inducing cardiomyocyte apoptosis. *Circulation*, *116*(4), 399-410. doi: 10.1161/CIRCULATIONAHA.106.683193
- Jin, P., Bulkley, D., Guo, Y., Zhang, W., Guo, Z., Huynh, W., . . . Cheng, Y. (2017). Electron cryo-microscopy structure of the mechanotransduction channel NOMPC. *Nature*, *547*(7661), 118-122. doi: 10.1038/nature22981
- Kelleher, D. J., Rashidbaigi, A., Ruoho, A. E., & Johnson, G. L. (1983). Rapid vesicle reconstitution of alprenolol-Sepharose-purified beta 1-adrenergic receptors. *J Biol Chem*, *258*(21), 12881-12885.
- Kuai, R., Ochyl, L. J., Bahjat, K. S., Schwendeman, A., & Moon, J. J. (2017). Designer vaccine nanodiscs for personalized cancer immunotherapy. *Nat Mater*, *16*(4), 489-496. doi: 10.1038/nmat4822
- Kwatra, M. M., Schreurs, J., Schwinn, D. A., Innis, M. A., Caron, M. G., & Lefkowitz, R. J. (1995). Immunoaffinity purification of epitope-tagged human beta 2-adrenergic receptor to homogeneity. *Protein Expr Purif*, *6*(6), 717-721. doi: 10.1006/prep.1995.0001
- Leitz, A., Bayburt, T., Barnakov, A., Springer, B., & Sligar, S. (2006). Functional reconstitution of β 2-adrenergic receptors utilizing self-assembling Nanodisc technology. *Biotechniques*, *40*(5), 601-612. doi: 10.2144/000112169
- Leslie, A. G., Warne, T., & Tate, C. G. (2015). Ligand occupancy in crystal structure of beta1-adrenergic G protein-coupled receptor. *Nat Struct Mol Biol*, *22*(12), 941-942. doi: 10.1038/nsmb.3130
- Li, Y., Kijac, A. Z., Sligar, S. G., & Rienstra, C. M. (2006). Structural analysis of nanoscale self-assembled discoidal lipid bilayers by solid-state NMR spectroscopy. *Biophys J*, *91*(10), 3819-3828. doi: 10.1529/biophysj.106.087072
- Lohse, M. J. (2010). Dimerization in GPCR mobility and signaling. *Curr Opin Pharmacol*, *10*(1), 53-58. doi: 10.1016/j.coph.2009.10.007
- Lohse, M. J., Engelhardt, S., Danner, S., & Bohm, M. (1996). Mechanisms of beta-adrenergic receptor desensitization: from molecular biology to heart failure. *Basic Res Cardiol*, *91 Suppl 2*, 29-34. doi: doi.org/10.1007/BF00795359
- Lohse, M. J., Engelhardt, S., & Eschenhagen, T. (2003). What is the role of beta-adrenergic signaling in heart failure? *Circ Res*, *93*(10), 896-906. doi: 10.1161/01.RES.0000102042.83024.CA
- Lyukmanova, E. N., Shenkarev, Z. O., Khabibullina, N. F., Kopeina, G. S., Shulepko, M. A., Paramonov, A. S., . . . Kirpichnikov, M. P. (2012). Lipid-protein nanodiscs for cell-free production of integral membrane proteins in a soluble and folded state: comparison with detergent micelles, bicelles and liposomes. *Biochim Biophys Acta*, *1818*(3), 349-358. doi: 10.1016/j.bbamem.2011.10.020
- Machuki, J. O., Zhang, H. Y., Harding, S. E., & Sun, H. (2017). Molecular pathways of oestrogen receptors and beta-adrenergic receptors in cardiac cells: Recognition of their similarities, interactions and therapeutic value. *Acta Physiol (Oxf)*. doi: 10.1111/apha.12978
- Mak, S., Sun, R., Schmalenberg, M., Peters, C., & Luppa, P. B. (2017). Express incorporation of membrane proteins from various human cell types into phospholipid bilayer nanodiscs. *Biochem J*, *474*(8), 1361-1371. doi: 10.1042/BCJ20161110
- Maron, B. J., Towbin, J. A., Thiene, G., Antzelevitch, C., Corrado, D., Arnett, D., . . . Young, J. B. (2006). Contemporary definitions and classification of the cardiomyopathies: an American Heart Association Scientific Statement from the Council on Clinical Cardiology, Heart Failure and Transplantation Committee; Quality of Care and Outcomes Research and Functional Genomics and Translational Biology Interdisciplinary Working Groups; and Council on Epidemiology and Prevention. *Circulation*, *113*(14), 1807-1816. doi: 10.1161/CIRCULATIONAHA.106.174287

- Marty, M. T., Wilcox, K. C., Klein, W. L., & Sligar, S. G. (2013). Nanodisc-solubilized membrane protein library reflects the membrane proteome. *Anal Bioanal Chem*, *405*(12), 4009-4016. doi: 10.1007/s00216-013-6790-8
- Masuo, K. (2010). Roles of beta2- and beta3-adrenoceptor polymorphisms in hypertension and metabolic syndrome. *Int J Hypertens*, *2010*, 832821. doi: 10.4061/2010/832821
- Millar, R. P., & Newton, C. L. (2010). The year in G protein-coupled receptor research. *Mol Endocrinol*, *24*(1), 261-274. doi: 10.1210/me.2009-0473
- Miller-Gallacher, J. L., Nehme, R., Warne, T., Edwards, P. C., Schertler, G. F., Leslie, A. G., & Tate, C. G. (2014). The 2.1 Å resolution structure of cyanopindolol-bound beta1-adrenoceptor identifies an intramembrane Na⁺ ion that stabilises the ligand-free receptor. *PLoS One*, *9*(3), e92727. doi: 10.1371/journal.pone.0092727
- Mitra, N., Liu, Y., Liu, J., Serebryany, E., Mooney, V., DeVree, B. T., . . . Yan, E. C. (2013). Calcium-dependent ligand binding and G-protein signaling of family B GPCR parathyroid hormone 1 receptor purified in nanodiscs. *ACS Chem Biol*, *8*(3), 617-625. doi: 10.1021/cb300466n
- Mobini, R., Staudt, A., Felix, S. B., Baumann, G., Wallukat, G., Deinum, J., . . . Fu, M. (2003). Hemodynamic improvement and removal of autoantibodies against beta1-adrenergic receptor by immunoadsorption therapy in dilated cardiomyopathy. *J Autoimmun*, *20*(4), 345-350. doi: 10.2174/157340308785160534
- Morgan, C. R., Hebling, C. M., Rand, K. D., Stafford, D. W., Jorgenson, J. W., & Engen, J. R. (2011). Conformational transitions in the membrane scaffold protein of phospholipid bilayer nanodiscs. *Mol Cell Proteomics*, *10*(9), M111.010876. doi: 10.1074/mcp.M111.010876
- Mors, K., Roos, C., Scholz, F., Wachtveitl, J., Dotsch, V., Bernhard, F., & Glaubitz, C. (2013). Modified lipid and protein dynamics in nanodiscs. *Biochim Biophys Acta*, *1828*(4), 1222-1229. doi: 10.1016/j.bbamem.2012.12.011
- Münch, G., Boivin-Jahns, V., Holthoff, H.-P., Adler, K., Lappo, M., Truöl, S., . . . Ungerer, M. (2012). Administration of the cyclic peptide COR-1 in humans (phase I study): ex vivo measurements of anti-β1-adrenergic receptor antibody neutralization and of immune parameters. *Eur J Heart Fail*, *14*(11), 1230-1239. doi: 10.1093/eurjhf/hfs118
- Nath, A., Atkins, W. M., & Sligar, S. G. (2007). Applications of phospholipid bilayer nanodiscs in the study of membranes and membrane proteins. *Biochemistry*, *46*(8), 2059-2069. doi: 10.1021/bi602371n
- Nath, A., Koo, P. K., Rhoades, E., & Atkins, W. M. (2008). Allosteric effects on substrate dissociation from cytochrome P450 3A4 in nanodiscs observed by ensemble and single-molecule fluorescence spectroscopy. *J Am Chem Soc*, *130*(47), 15746-15747. doi: 10.1021/ja805772r
- Nikolaev, V. O., Boivin, V., Stork, S., Angermann, C. E., Ertl, G., Lohse, M. J., & Jahns, R. (2007). A novel fluorescence method for the rapid detection of functional beta1-adrenergic receptor autoantibodies in heart failure. *J Am Coll Cardiol*, *50*(5), 423-431. doi: 10.1016/j.jacc.2007.03.051
- Orwick-Rydmark, M., Lovett, J. E., Graziadei, A., Lindholm, L., Hicks, M. R., & Watts, A. (2012). Detergent-free incorporation of a seven-transmembrane receptor protein into nanosized bilayer Lipodisq particles for functional and biophysical studies. *Nano Lett*, *12*(9), 4687-4692. doi: 10.1021/nl3020395
- Overington, J. P., Al-Lazikani, B., & Hopkins, A. L. (2006). How many drug targets are there? *Nat Rev Drug Discov*, *5*(12), 993-996. doi: 10.1038/nrd2199
- Pandit, A., Shirzad-Wasei, N., Wlodarczyk, L. M., van Roon, H., Boekema, E. J., Dekker, J. P., & de Grip, W. J. (2011). Assembly of the major light-harvesting complex II in lipid nanodiscs. *Biophys J*, *101*(10), 2507-2515. doi: 10.1016/j.bpj.2011.09.055
- Patel, P. A., & Hernandez, A. F. (2013). Targeting anti-beta-1-adrenergic receptor antibodies for dilated cardiomyopathy. *Eur J Heart Fail*, *15*(7), 724-729. doi: 10.1093/eurjhf/hft065
- Pierce, K. L., Premont, R. T., & Lefkowitz, R. J. (2002). Seven-transmembrane receptors. *Nat Rev Mol Cell Biol*, *3*(9), 639-650. doi: 10.1038/nrm908

- Proverbio, D., Roos, C., Beyermann, M., Orban, E., Dotsch, V., & Bernhard, F. (2013). Functional properties of cell-free expressed human endothelin A and endothelin B receptors in artificial membrane environments. *Biochim Biophys Acta*, *1828*(9), 2182-2192. doi: 10.1016/j.bbamem.2013.05.031
- Reihnsaus, E., Innis, M., MacIntyre, N., & Liggett, S. B. (1993). Mutations in the gene encoding for the beta 2-adrenergic receptor in normal and asthmatic subjects. *Am J Respir Cell Mol Biol*, *8*(3), 334-339. doi: 10.1165/ajrcmb/8.3.334
- Ritchie, T. K., Grinkova, Y. V., Bayburt, T. H., Denisov, I. G., Zolnerciks, J. K., Atkins, W. M., & Sligar, S. G. (2009). Chapter 11 - Reconstitution of membrane proteins in phospholipid bilayer nanodiscs. *Methods Enzymol*, *464*, 211-231. doi: 10.1016/S0076-6879(09)64011-8
- Ritter, S., Willand, L., Reinhard, B., Offergeld, R., & Hamouda, O. (2008). Demography and donation frequencies of blood and plasma donor populations in Germany. *Bundesgesundheitsblatt Gesundheitsforschung Gesundheitsschutz*, *51*(8), 915-925. doi: 10.1007/s00103-008-0613-7
- Rosenbaum, D. M., Rasmussen, S. G., & Kobilka, B. K. (2009). The structure and function of G-protein-coupled receptors. *Nature*, *459*(7245), 356-363. doi: 10.1038/nature08144
- Roy, J., Pondenis, H., Fan, T. M., & Das, A. (2015). Direct Capture of Functional Proteins from Mammalian Plasma Membranes into Nanodiscs. *Biochemistry*, *54*(41), 6299-6302. doi: 10.1021/acs.biochem.5b00954
- San Martín, M. A., García, Á., Rodríguez, F. J., & Terol, I. (2002). Dilated Cardiomyopathy and Autoimmunity: an Overview of Current Knowledge and Perspectives. *Revista Española de Cardiología (English Edition)*, *55*(05), 514-524.
- Sato, T., Baker, J., Warne, T., Brown, G. A., Leslie, A. G., Congreve, M., & Tate, C. G. (2015). Pharmacological Analysis and Structure Determination of 7-Methylcyanopindolol-Bound beta1-Adrenergic Receptor. *Mol Pharmacol*, *88*(6), 1024-1034. doi: 10.1124/mol.115.101030
- Schafer, M., Frischkopf, K., Taimor, G., Piper, H. M., & Schluter, K. D. (2000). Hypertrophic effect of selective beta(1)-adrenoceptor stimulation on ventricular cardiomyocytes from adult rat. *Am J Physiol Cell Physiol*, *279*(2), C495-C503. doi: 10.1152/ajpcell.2000.279.2.C495
- Schonberger, J., & Seidman, C. E. (2001). Many roads lead to a broken heart: the genetics of dilated cardiomyopathy. *Am J Hum Genet*, *69*(2), 249-260. doi: 10.1086/321978
- Scognamiglio, R., Avogaro, A., Casara, D., Crepaldi, C., Marin, M., Palisi, M., . . . Dalla Volta, S. (1998). Myocardial dysfunction and adrenergic cardiac innervation in patients with insulin-dependent diabetes mellitus. *J Am Coll Cardiol*, *31*(2), 404-412. doi: 10.1016/S0735-1097(97)00516-0
- Seddon, A. M., Curnow, P., & Booth, P. J. (2004). Membrane proteins, lipids and detergents: not just a soap opera. *Biochim Biophys Acta*, *1666*(1-2), 105-117. doi: 10.1016/j.bbamem.2004.04.011
- Serrano-Vega, M. J., & Tate, C. G. (2009). Transferability of thermostabilizing mutations between beta-adrenergic receptors. *Mol Membr Biol*, *26*(8), 385-396. doi: 10.3109/09687680903208239
- Sheng, J. R., Grimme, S., Bhattacharya, P., Stowell, M. H., Artinger, M., Prabahakar, B. S., & Meriggioli, M. N. (2010). In vivo adsorption of autoantibodies in myasthenia gravis using Nanodisc-incorporated acetylcholine receptor. *Exp Neurol*, *225*(2), 320-327. doi: 10.1016/j.expneurol.2010.07.003
- Shirzad-Wasei, N., Oostrum, J. V., Bovee-Geurts, P. H., Kusters, L. J., Bosman, G. J., & DeGrip, W. J. (2015). Rapid transfer of overexpressed integral membrane protein from the host membrane into soluble lipid nanodiscs without previous purification. *Biol Chem*, *396*(8), 903-915. doi: 10.1515/hsz-2015-0100
- Sondek, J., & Siderovski, D. P. (2001). Ggamma-like (GGL) domains: new frontiers in G-protein signaling and beta-propeller scaffolding. *Biochem Pharmacol*, *61*(11), 1329-1337. doi: 10.1016/S0006-2952(01)00633-5

- Stork, S., Boivin, V., Horf, R., Hein, L., Lohse, M. J., Angermann, C. E., & Jahns, R. (2006). Stimulating autoantibodies directed against the cardiac beta1-adrenergic receptor predict increased mortality in idiopathic cardiomyopathy. *Am Heart J*, *152*(4), 697-704. doi: 10.1016/j.ahj.2006.05.004
- Störk, S., Plotnikov, A. N., Peters, G., Davies, B. E., Nnane, I., Rivas, D., . . . Ertl, G. (2016). Effects of JNJ-54452840, an Anti- β 1 Receptor Antibody Cyclopeptide in Heart Failure Patients: A Randomized, Double-blind, Parallel-group, Phase-2 Pilot Study. *Cardiovasc Pharm Open Access*, *5*(190). doi: 10.4172/2329-6607.1000190
- Strader, C. D., Sigal, I. S., Candelore, M. R., Rands, E., Hill, W. S., & Dixon, R. A. (1988). Conserved aspartic acid residues 79 and 113 of the beta-adrenergic receptor have different roles in receptor function. *J Biol Chem*, *263*(21), 10267-10271.
- Tang, C. M., & Insel, P. A. (2004). GPCR expression in the heart; "new" receptors in myocytes and fibroblasts. *Trends Cardiovasc Med*, *14*(3), 94-99. doi: 10.1016/j.tcm.2003.12.007
- Taylor, M. R., & Bristow, M. R. (2004). The emerging pharmacogenomics of the beta-adrenergic receptors. *Congest Heart Fail*, *10*(6), 281-288. doi: 10.1111/j.1527-5299.2004.02019.x
- Timothy H. Bayburt, Yelena V. Grinkova, & Sligar, a. S. G. (2002). Self-Assembly of Discoidal Phospholipid Bilayer Nanoparticles with Membrane Scaffold Proteins. *NanoLett*, *2*(8), 853-856. doi: 10.1021/nl025623k
- Trimpert, C., Herda, L. R., Eckerle, L. G., Pohle, S., Muller, C., Landsberger, M., . . . Staudt, A. (2010). Immunoabsorption in dilated cardiomyopathy: long-term reduction of cardiodepressant antibodies. *Eur J Clin Invest*, *40*(8), 685-691. doi: 10.1111/j.1365-2362.2010.02314.x
- Venkatakrishnan, A. J., Deupi, X., Lebon, G., Tate, C. G., Schertler, G. F., & Babu, M. M. (2013). Molecular signatures of G-protein-coupled receptors. *Nature*, *494*(7436), 185-194. doi: 10.1038/nature11896
- Vernier, G., Wang, J., Jennings, L. D., Sun, J., Fischer, A., Song, L., & Collier, R. J. (2009). Solubilization and characterization of the anthrax toxin pore in detergent micelles. *Protein Sci*, *18*(9), 1882-1895. doi: 10.1002/pro.199
- Wallin, E., & von Heijne, G. (1998). Genome-wide analysis of integral membrane proteins from eubacterial, archaean, and eukaryotic organisms. *Protein Sci*, *7*(4), 1029-1038. doi: 10.1002/pro.5560070420
- Wallukat, G. (2002). The beta-adrenergic receptors. *Herz*, *27*(7), 683-690. doi: 10.1007/s00059-002-2434-z
- Wallukat, G., Haberland, A., & Schimke, I. (2014). A vision of future treatment in chagas heart disease. *J Am Coll Cardiol*, *63*(10), 1027. doi: 10.1016/j.jacc.2013.08.1660
- Wallukat, G., Muller, J., Haberland, A., Berg, S., Schulz, A., Freyse, E. J., . . . Schimke, I. (2016). Aptamer BC007 for neutralization of pathogenic autoantibodies directed against G-protein coupled receptors: A vision of future treatment of patients with cardiomyopathies and positivity for those autoantibodies. *Atherosclerosis*, *244*, 44-47. doi: 10.1016/j.atherosclerosis.2015.11.001
- Wallukat, G., & Nissen, E. (2001). Anti beta1-adrenoceptor autoantibodies analyzed in spontaneously beating neonatal rat heart myocyte cultures-comparison of methods. *In Vitro Cell Dev Biol Anim*, *37*(3), 175-176. doi: 10.1290/1071-2690(2001)037<0175:AAAAIS>2.0.CO;2
- Wallukat, G., & Schimke, I. (2014). Agonistic autoantibodies directed against G-protein-coupled receptors and their relationship to cardiovascular diseases. *Semin Immunopathol*, *36*(3), 351-363. doi: 10.1007/s00281-014-0425-9
- Warne, T., Moukhametzianov, R., Baker, J. G., Nehme, R., Edwards, P. C., Leslie, A. G., . . . Tate, C. G. (2011). The structural basis for agonist and partial agonist action on a beta(1)-adrenergic receptor. *Nature*, *469*(7329), 241-244. doi: 10.1038/nature09746
- Warne, T., Serrano-Vega, M. J., Baker, J. G., Moukhametzianov, R., Edwards, P. C., Henderson, R., . . . Schertler, G. F. (2008). Structure of a beta1-adrenergic G-protein-coupled receptor. *Nature*, *454*(7203), 486-491. doi: 10.1038/nature07101

- Wenzel, K., Schulze-Rothe, S., Haberland, A., Muller, J., Wallukat, G., & Davideit, H. (2017). Performance and in-house validation of a bioassay for the determination of beta1-autoantibodies found in patients with cardiomyopathy. *Heliyon*, 3(7), e00362. doi: 10.1016/j.heliyon.2017.e00362
- Whorton, M. R., Bokoch, M. P., Rasmussen, S. G., Huang, B., Zare, R. N., Kobilka, B., & Sunahara, R. K. (2007). A monomeric G protein-coupled receptor isolated in a high-density lipoprotein particle efficiently activates its G protein. *Proc Natl Acad Sci USA*, 104(18), 7682-7687. doi: 10.1073/pnas.0611448104
- Zocher, M., Roos, C., Wegmann, S., Bosshart, P. D., Dotsch, V., Bernhard, F., & Muller, D. J. (2012). Single-molecule force spectroscopy from nanodiscs: an assay to quantify folding, stability, and interactions of native membrane proteins. *ACS Nano*, 6(1), 961-971. doi: 10.1021/nn204624p